THE USE OF MECHANICAL REDUNDANCY FOR FAULT DETECTION IN NON-STATIONARY MACHINERY

by

Mohamed H. ElMaghraby

A thesis submitted in partial fulfillment
of the requirements for the degree of
Masters of Applied Science (MASc) in
Natural Resources Engineering

The Faculty of Graduate Studies
Laurentian University
Sudbury, Ontario, Canada

THESIS DEFENCE COMMITTEE/COMITÉ DE SOUTENANCE DE THÈSE

Laurentian Université/Université Laurentienne
Faculty of Graduate Studies/Faculté des études supérieures

Title of Thesis Titre de la thèse	The Use of Mechanical Redundancy for Fault Detection in Non-stationary Machinery
Name of Candidate Nom du candidat	ElMaghraby, Mohamed H.
Degree Diplôme	Master of Applied Science
Department/Program Département/Programme	Natural Resources Engineering
Date of Defence Date de la soutenance	October 17, 2014

APPROVED/APPROUVÉ

Thesis Examiners/Examinateurs de thèse:

Dr. Markus Timusk
(Supervisor/Directeur de thèse)

Dr. Marc Arsenault
(Committee member/Membre du comité)

Dr. Brent Lievers
(Committee member/Membre du comité)

Dr. Amr Abdel-Dayem
(Committee member/Membre du comité)

Dr. Wilson Wang
(External Examiner/Examinateur externe)

Approved for the Faculty of Graduate Studies
Approuvé pour la Faculté des études supérieures
Dr. David Lesbarrères
M. David Lesbarrères
Acting Dean, Faculty of Graduate Studies
Doyen intérimaire, Faculté des études supérieures

ACCESSIBILITY CLAUSE AND PERMISSION TO USE

Abstract

The classical approach to machinery fault detection is one where a machinery's condition is constantly compared to an established baseline with deviations indicating the occurrence of a fault. With the absence of a well-established baseline, fault detection for variable duty machinery requires the use of complex machine learning and signal processing tools. These tools require extensive data collection and expert knowledge which limits their use for industrial applications.

The thesis at hand investigates the problem of fault detection for a specific class of variable duty machinery; parallel machines with simultaneously loaded subsystems. As an industrial case study, the parallel drive stations of a novel material haulage system have been instrumented to confirm the mechanical response similarity between simultaneously loaded machines. Using a table-top fault simulator, a preliminary statistical algorithm was then developed for fault detection in bearings under non-stationary operation. Unlike other state of the art fault detection techniques used in monitoring variable duty machinery, the proposed algorithm avoided the need for complex machine learning tools and required no previous training.

The limitations of the initial experimental setup necessitated the development of a new machinery fault simulator to expand the investigation to include transmission systems. The design, manufacturing and setup of the various subsystems within the new simulator are covered in this manuscript including the mechanical, hydraulic and control subsystems. To ensure that the new simulator has successfully met its design objectives, extensive data collection and analysis has been completed and is presented in this thesis.

The results confirmed that the developed machine truly represents the operation of a simultaneously loaded machine and as such would serve as a research tool for investigating the application of classical fault detection techniques to parallel machines in non-stationary operation.

Acknowledgements

I would like to express my genuine appreciation to my dear supervisor Dr. Markus A. Timusk for being a tremendous mentor. His continued support, encouragement and guidance have been instrumental throughout my research. Leading by example, Dr. Timusk's professionalsim and work ethic have been an excellent opportunity for me to learn and grow as an engineer. It was a pleasure working with you sir and I look forward for future collaboration.

I am greatly thankful to the Centre for Excellence in Mining Innovation for their financial support and to Mr. Allan Akerman for his encouragement and trust. His expertise in mining automation has been influential and allowed me to appreciate maintenance and reliability applications to mining.

I was lucky to get the chance to work with Mr. Greg Lakanen from the Engineering Department. Through his trust and guidance, I was able to complete a long and tedious fabrication and installation stage successfully. I also want to thank him for all the technical discussions we had, thank you Greg.

I would also like to thank Rail-Veyor® Technologies for their industrial partnership and technical support during the field instrumentation.

Finally, I want to thank my family and loved ones for all the moral support for the past years.

To my late father, may he rest in peace.

Table of Contents

List of Figures

List of Tables

Chapter 1

1 Introduction

With ever-increasing market globalization and corporate consolidations, every company's survival in the mining industry depends on its ability to compete. As it has always been, the customer is always on the lookout for the lowest prices for a given product quality. To meet this lowest price, without affecting the profit margin, industry turns to minimizing the production and operation costs. With less money available for capital investments, existing machinery are driven to their limits to sustain the required production levels leaving no room for error or delay associated with machinery breakdown.

A properly applied maintenance strategy aims to maximize machinery availability and minimize unplanned breakdowns. Such a strategy would not only improve existing machinery availability, but would also improve reliability, product quality and delivery performance while reducing direct operation and maintenance costs. Given the direct maintenance can cost up to 40% of the operational budget of large-scale plant-based industries [1], continued improvements in the maintenance department would provide a significant competitive advantage.

1.1 Measuring the Success of a Maintenance Plan

A quick indicator of the effectiveness of plant equipment is the Overall Equipment Effectiveness index (OEE). This index represents the effective utilization of the machinery and thus is negatively affected by the six big machinery losses depicted in Figure 1-1.

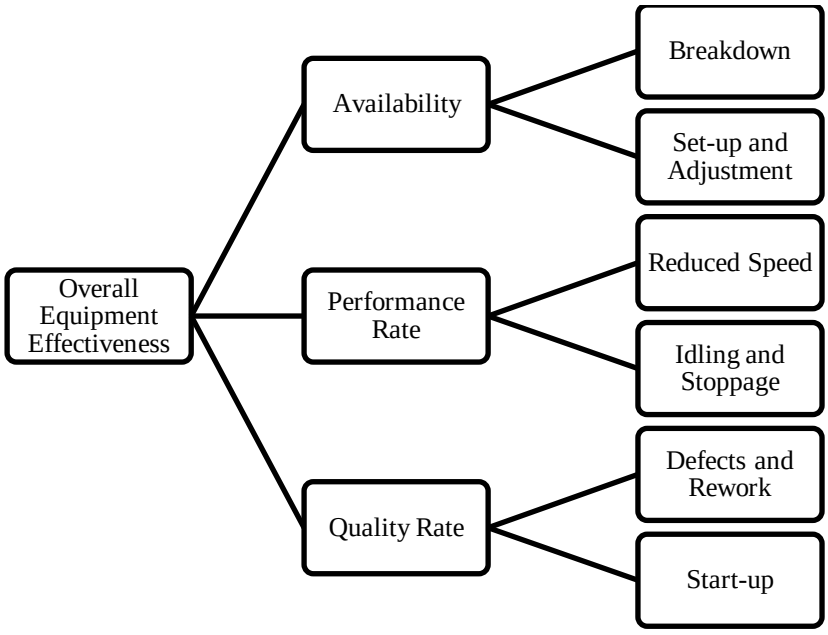

Figure 1-1: Six Big Machinery Losses (adapted from [1])

As shown in the previous figure, all six losses can be grouped into three major categories; losses that affect machinery availability such as breakdown and setup time, losses affecting performance rate such as reduced speed operation, idling and stoppage, and finally losses that affect product quality such as defects and start-up. It is imperative that all three losses should be considered together rather than separately. For instance, the availability index could be improved by running the machines at a lower speed; however this would worsen the performance rate. Alternatively, performance rate could be improved at the expense of a lower product quality where a significant portion of the production output would not meet the required specifications.

Using the aforementioned metrics, the success of a maintenance strategy can be quantitatively measured. A maintenance policy that increases the OEE and Mean Time Between Repair (MTBR) while reducing the Mean Time to Repair (MTTR) ensures that maintenance expenses

are minimized while production availability and yield are improved thus representing a step towards maintenance excellence.

1.2 Maintenance in the Context of the Mining Industry

Compared to the international best practice standard of 85% OEE found across industries, the typical OEE in the mining industry ranges between 40-60% [1]. Such shortcoming is mainly attributed to the difficulty encountered in fully utilizing the large scale machinery and to the demanding operational environment.

Figure 1-2: Sandvik Bucket Wheel Excavator (taken from [2])

The common open-pit mine site will usually employ a single bucket-wheel excavator like the one shown in Figure 1-2 for rock breaking. Any compromise to the availability, performance rate or product quality of such critical machine could bring the whole operation to a halt. The same scenario is applicable to the rock crusher, conveyor system and other critical machinery used on

the mine site. Direct maintenance costs can range up to 50% of a mine site operation budget; more than any other industry [1]. With such significant expenses, maintenance has to be treated as a strategic function that is a value adding activity rather than just an act of containing costs.

The best way to see how adopting a proper maintenance strategy can affect a company's economic position is to view the machinery as a profit centre. In this context, profit is the difference between revenue and cost where revenue for a machine is represented as the throughput times the added value, with the throughput as availability multiplied by production hours. Cost, on the other hand, is the sum of energy, operating expenses and maintenance and capital expenses. From this point of view, profit then becomes a function of machine availability, capacity utilization, efficiency and maintenance cost.

As with other industries, the maintenance strategy used in the mining domain is driven by balancing the availability of resources and the criticality of a given machine in the production chain. Depending on those two factors, there are four major strategies used as follows.

1.2.1 Run-to-Failure (RTF)

The original maintenance policy; fix it if it breaks. Initially, the cost of an RTF maintenance program is zero and the policy's simplicity can be attractive, however costs and problems balloon when the breakdown eventually happens. First of all, in the absence of regular inspections, small easily fixable machinery faults can grow into catastrophic breakdowns. Secondly, if the required spare parts are not in stock, the associated lead times will increase the downtime. Other than the fact that such breakdown can affect downstream machinery, the disastrous failure can be potentially life threatening to plant personnel; especially with high

inertia machinery. Still, RTF policy can be a good choice for machines of low-criticality to plant operation; especially if the cost of maintenance would be more than the price of a new machine.

1.2.2 Periodic Maintenance

The obvious pitfalls of using RTF for maintenance of critical machinery can be avoided by switching to a periodic maintenance program where machinery components are serviced at pre-determined intervals. The proactive aspect of periodic maintenance represents a definite improvement over RTF especially for equipment subject to wear out type of failure.

The success of periodic maintenance depends on the proper selection of the inspection interval. To successfully determine the appropriate maintenance interval, considerable statistical analysis of machinery operation history is needed to calculate the Mean Time Between Failure (MTBF) for each machine such that the maintenance interval is set to be less than this machine's MTBF. The major challenge is that if the MTBF is overestimated, then there is high probability that the machine will breakdown before next inspection. Conversely, if the MTBF is underestimated, machinery components would be replaced prematurely. Not only would such thing incur added expense to the maintenance program by inflating the maintenance stocking budget, but would certainly introduce "infant mortalities" especially for machinery with a bath-tub failure distribution as shown in Figure 1-3.

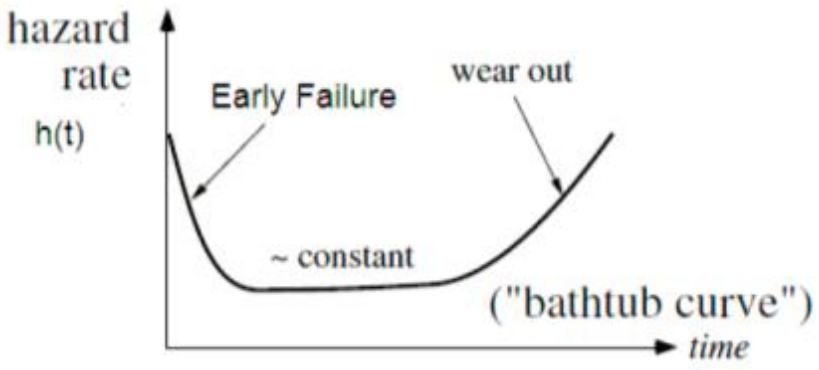

Figure 1-3: Bath-tub Failure Distribution (taken from [3])

1.2.3 Predictive Maintenance

The main goal of predictive maintenance is to reach a level of maintenance excellence where machinery are fixed just before they break thereby eliminating periodic maintenance expenses associated with regular inspections, premature component replacement, and excessive spare part storage. This just-in-time maintenance approach is only achievable through the continuous monitoring and analysis of machinery parameters such that component faults can be diagnosed non-invasively without the need to remove the machine from the production line. A similar form of continuous parameter monitoring is prevalent in process plants through machine performance monitoring and Statistical Process Control techniques (SPC).

Unlike SPC where machine parameters are collected just to ensure product quality, predictive maintenance takes the extra step of actually assimilating the performance measures collected; such as motor speed, pump flow, system pressure, into a maintenance strategy that would analyze this data to infer machinery status. Such use of advanced technologies to analyse collected machine parameters to determine equipment condition, and potentially predict failure is known as Condition Monitoring (CM).

1.2.4 Proactive Maintenance

The main focus of Proactive Maintenance is to eliminate the source of faults right from the start. This might include everything from re-planning machinery utilization to the re-design of certain machinery components. Compared to other maintenance strategies, a proactive approach is used such that continuous reassessment of all machinery installation, operation, and maintenance is completed to ensure that all possible sources of faults are removed even before the occurrence of a fault.

Even though proactive maintenance would represent the ideal case, such policy is only applicable to simplified situations. To further explain the difference between the aforementioned strategies, the following section illustrates the application of each maintenance strategy to a typical mining system; a material haulage system.

1.3 Applications of Maintenance Strategies to a Mining System: Rail-Veyor®

Rail-Veyor® is a novel material haulage system by Rail-Veyor Technologies in Sudbury, Ontario, Canada. In contrast to regular diesel-powered trucking solutions, the Rail-Veyor® system presented in Figure 1-4 uses electrical drive stations to propel a passive rail train through the continuous mesh between the drive station's rubber tires and the train's side plates. More details on the system's operation and construction will be presented in Chapter 5.

This novel material transport solution offers several potential advantages over conventional diesel-powered haulage systems. The smaller physical footprint of this new system minimizes the required drift size for underground applications thus significantly reducing construction and

setup costs. Additionally, the use of an electrical propulsion system reduces the mine site ventilation overhead given the elimination of diesel emissions generated by conventional haulage systems.

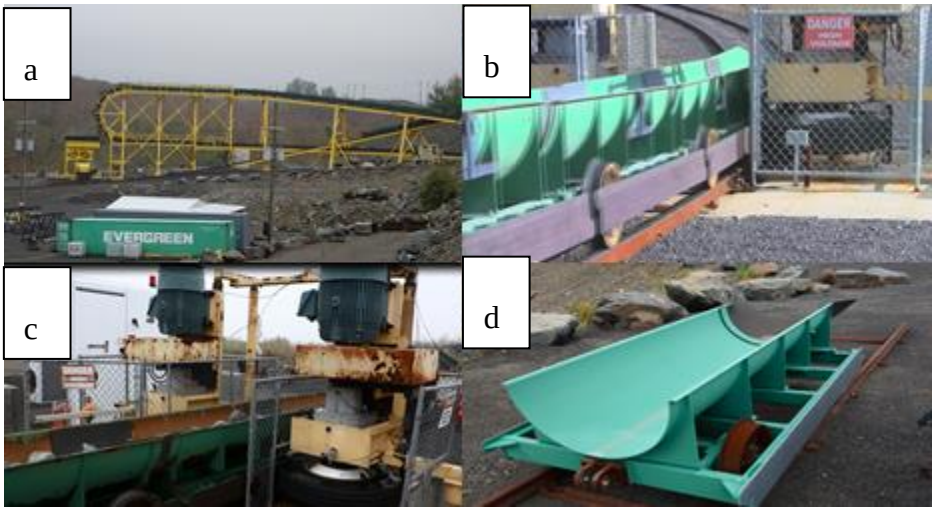

Figure 1-4: Different Components of Rail-Veyor® System; (a) Dump loop, (b) Down-hill Drive station, (c) Mechanical Setup of Drive Station, (d) Rail-cart

As a critical component for mine site operation, a successful maintenance plan is required to ensure the continuous operation of this haulage system to avoid production interruptions. Mechanical components that are prone to wear out have to be regularly inspected to minimize the probability of an unexpected breakdown. For instance, rail-car bearings are continuously greased, the rail tracks are inspected at planned interval, and the oil for the hydraulic brakes is periodically changed. Such regular maintenance chores are part of the periodic maintenance plan followed for the system's mechanical components. Even though the upfront expense of periodic maintenance could initially be unattractive compared to the zero-cost RTF plan, the expenses associated with such periodic maintenance plan are much less significant than the expenses that

would be incurred if an unlubricated rail-car bearing seizes or a hydraulic brake valve fails when contaminated oil is used in the system.

It should be noted however that unlike easily accessed components, the periodic maintenance of totally-enclosed machinery components would be far more expensive. As an example, consider the Rail-Veyor® drive station shown in Figure 1-4(c) where the reduction gearbox used represents a critical subsystem for each station. For Rail-Veyor's(R) passive rail system, the only source of railcar propulsions is the successful operation of each drive station. The criticality of this subsystem makes it an ideal candidate for scheduled maintenance. However the process of uninstalling the gearbox, transporting it to the workshop, and opening it up to replace worn components periodically would be impractical and financially unattractive. This problem is compounded by the fact that numerous drive stations are installed along the railway with some of them installed underground in close-quartered drifts.

It can be seen from the previous discussion that a balance is needed between the upfront costs associated with an exhaustive periodic maintenance policy and the dangers associated with the unforeseen catastrophic equipment failure that might occur when a simple reactive maintenance policy is employed. Such a balance can be attained by employing a predictive maintenance approach such as CM where the continuous monitoring of machinery operation minimizes the possibility of unexpected failure while eliminating the need for unnecessary periodic machine servicing.

1.3.1 Condition Monitoring: The Balance

"Condition monitoring is no longer considered just an engineering tactic; it is a valuable management strategy for coping with changing economic circumstances." [4]. The application

of this maintenance approach has found its way in a range of industries including the processing, manufacturing, and energy industries. Given that machinery condition is under constant monitoring in this approach, the probability of unexpected breakdowns will be reduced. Additionally, the proper application of condition monitoring minimizes the MTTR given that faults are detected and fixed in their infancy. Moreover, the recent technological advance allowed for the implementation of non-invasive monitoring techniques thus eliminating the need for time-consuming physical inspection.

1.3.2 Advantages of Applying a CM Solution to Rail-Veyor Drive Stations

Given the criticality of the drive stations for the operation of the Rail-Veyor material haulage system, it would be ideal to implement a condition-monitoring solution that would non-invasively monitor the operation of the mechanical components of the drive stations including the components of the reduction gearbox such as the bearings and gears. Obvious advantages to such monitoring solution would be:

- Minimizing the spare-parts stocking required for conventional periodic maintenance and the associated premature part replacement;
- Extension of gearbox operating life by detecting and fixing faults in their infancy and thus avoiding secondary damage that could affect other systems in the drive station;
- Better utilization of human resources, especially that a monitoring strategy would be equally applicable to all drive stations on site ultimately minimizing required maintenance expenses.

1.3.3 The Limitations of Current Monitoring Solutions

Given how this novel haulage system is tele-operated, it would be ideal if the monitoring solution is automated such that an alarm is triggered if failure is imminent. The problem however is not trivial given that off the shelf monitoring solutions are not applicable to this case. The main limitation of current monitoring solutions is that their operation assumes constant machinery duty cycle triggering an alarm when a monitored parameter overshoots a pre-set limit. The fact that the material haulage system is operating in a continuously variable duty cycle; hauling different loads at different operating speeds and at different operating environments, means that current monitoring solutions would not be able to separate monitored parameter variations associated with the duty changes from those associated with mechanical faults thus affecting the reliability of commercial off the shelf CM system.

As it will be eluded to in this thesis, the state of the art in condition monitoring for variable duty machinery employs artificial intelligence techniques that require significant data collection and that are highly application specific. Additionally, the use of such techniques requires significant level of expertise and the majority of the solutions would have to be rebuilt in the case of any machinery or operation modifications.

As presented in [5] the author; a senior figure in Australian's CM service providers, have concluded that in the long run, CM solutions will only be sustained if real business needs are successfully addressed. Given the upfront costs of installing a CM solution, the industry expects a reliable, problem-free system that is easy to use. As such, the complexities associated with the application of sophisticated AI algorithms in state of the art CM techniques limit their use in the industrial setting. This can be confirmed by the fact that FFT analyzers are still the preferred

choice for the monitoring of rotating equipment vibration levels in the industry; a technique that has been introduced in 1980's.

1.4 Scope of the Thesis

The thesis at hand proposes a new CM technique that is applicable to a certain class of variable duty machinery; Parallel Machines. This class of machinery is defined by two basic characteristics that preclude it from the application of standard online condition monitoring approaches. The first characteristic is that the machine is in a constant state of transient operation, thus making it difficult to differentiate between changes in transducer measurements that are due to variable duty and those that are due to machine malfunction or fault. The second characteristic is the fact that the machinery involves multiple sub systems that are subject to identical and simultaneous loading, operating environments and duty cycles. An example of such machinery is a system of multiple hydraulic pumps driving a common load. The monitoring strategy presented here employs an anomaly detection scheme together with methods of signal processing and feature extraction that exploit the parallel duty arrangements of this equipment.

Utilizing in-situ data collected at a local material haulage system, the loading similarity between the parallel drives stations was investigated. Additionally, a table top experimental setup was used to verify the validity of exploiting the mechanical redundancy in parallel machines to detect faults in variable duty simultaneously loaded machinery. The investigation also included the design, fabrication and assembly of a new machinery fault simulator to further investigate the proposed fault detection technique. Given the time constraints of a Master's program, the main focus in this thesis is the review of possible monitoring strategies applicable to the aforementioned class of machinery that would eliminate the need for complex artificial

intelligence techniques. More importantly, a great deal of effort was put into the development of the new machinery fault simulator presented in this thesis. The construction of this research tool is of great importance for the research given that intentional faulting of the Rail-Veyor® stations was not practical.

The new simulator would allow the user to fault different subsystems including; gears and bearings for a reduction gearbox, rolling element bearings in passive idlers used in automotive serpentine belt systems and gears and bearings found in a typical side loaded gear pump.

Concepts studied and applied in this research included:

- Maintenance and reliability practices
- Signal Processing, data acquisition, data analysis and instrumentation in the context of fault detection
- In-situ transducer setup and data collection
- Experimental bearing fault simulation
- Mechanical and hydraulic design
- Fabrication, installation, instrumentation and control of test stands

1.5 Organization of Thesis

This thesis investigated the exploitation of mechanical redundancy for fault detection of simultaneously loaded machinery operating in a variable duty cycle. The structure is as follows:

Chapter 1-Introduction

- Introduced the competitive advantage of a proper maintenance strategy with special focus on mining industry.

- Presented the different maintenance strategies used in the industry and provided an illustrative example of the application of each strategy in the context of a material haulage system used in mining.
- Illustrated, with an example, how CM can provide the balance required between reliability and projected maintenance costs.
- Stated the limitations of current industrial monitoring techniques and how the complexities associated with newly developed solutions limit their use in the industry.
- Defined the scope of this research and outlined the organization of the thesis.

Chapter 2-Literature Review

- Presented the three stages of Condition-based Monitoring and Diagnostics including the determination of expected malfunction modes, the parameters to be monitored and the signal processing techniques to be used for fault detection.
- Investigated vibration-based Condition Monitoring for rotating equipment and discussed the failure modes of gearbox components, the resulting vibration signals and the signal processing required to detect the faults in vibration signal.
- Introduced the state of the art in Condition Monitoring in Non-stationary machinery operation including both the pattern recognition and system identification approaches. The discussion involved the presentation of the limitations of currently available monitoring solutions for applications experiencing variable load-speed operation.
- Suggested the utilization of mechanical redundancy for parallel machines as a means for fault detection.

Chapter 3- Simultaneously Loaded Non-stationary Machinery: Parallel Machines

- Introduced several examples of parallel machines commonly seen in different industries.
- Investigated vibration similarity for the parallel drive stations of a novel material haulage system. This investigation encompassed *in-situ* data collection and post processing.
- Presented the details of a preliminary statistical algorithm that utilized the loading similarity of parallel components for fault detection in non-stationary operation. The algorithm development included experimental data collection on a tabletop vibration trainer.
- Discussed how the proposed algorithm was successful in monitoring the condition of rolling element bearings and explained how commercially available standard alarm systems would be affected by the non-stationary operation of variable duty machinery.
- Demonstrated the need for a new transmission system simulator that truly represents the operation of parallel machinery.

Chapter 4-Design and Fabrication of a New Experimental Apparatus

- Discussed the functional requirements for the new machinery simulator.
- Presented the design and fabrication of the different systems within the new simulator including the mechanical, hydraulic, instrumentation and control subsystems.

Chapter 5-Baseline Data Collection and Analysis Using the New Experimental Apparatus

- Discussed the instrumentation and data collection process undertaken to establish vibration baselines for the different subsystems of the new experimental apparatus.
- Presented the time waveform, FFT and Spectrogram of the vibration levels measured for healthy components.

- Applied the Statistical Correlation algorithm discussed in this thesis to validate the loading similarity between parallel subsystems in the newly developed test rig and discussed the results.

Chapter 6- Fault Simulation and Detection using the Newly Developed Fault Simulator

- Demonstrated the fault simulation capabilities of the newly developed test rig. Faults simulated included bearing and gear faults seeded in both the gearbox and the belt drive system.
- Investigated the performance of the Statistical Correlation algorithm using the faulted data sets obtained from the new simulator and discussed the results.

Chapter 7- Conclusions

- Drew conclusions from the study and presented future work.

This concludes the first chapter, in which the relevant maintenance background information has been presented. In the next chapter, the literature founding the basis of vibration-based condition monitoring is presented.

Chapter 2

2 Literature Review

The aim of this chapter is to present the background regarding the foundations of modern CM solutions. Starting with a presentation of the general CM problem, the first section covers the requirements, design and applications of typical CM solutions. The second section focuses on the use of vibration monitoring for machinery health assessment including the various Digital Signal Processing (DSP) techniques used for different rotating machinery components. The following section will discuss some of the major limitations facing current industrial CM affecting their reliability when used to monitor variable duty machinery. This will then be followed by a presentation on the state of the art proposed in the academia to develop fully automated CM geared for machinery operating in non-stationary manner; the discussion will also stress on the challenges facing the practical application of such techniques in the industry.

2.1 The Three Stages of Condition-based Monitoring and Diagnostics

Machinery condition monitoring represents the corner stone of the Condition-Based Maintenance (CBM) strategy adopted for highly critical plant machinery. Historically, the application of CM involved an offline monitoring strategy where the vibration levels of certain machinery were routinely inspected using handheld vibration analyzers. Advances in DSP and computing have led to significantly more advanced monitoring and diagnostic systems to effectively evaluate machinery condition in real-time. This shift to online monitoring has become the standard in CM. A very critical advantage to such remote monitoring capabilities is that it gives the

machinery operator the ability to share the monitored parameters with specialized personnel such as the machine's manufacturer who might not be able to physically inspect the machinery.

A properly implemented CM solution will improve a plant's machinery safety, reliability and efficiency by accomplishing three major tasks; early failure detection, wear monitoring, and efficiency optimization. Through the implementation of trip alarms, a CM solution can warn the operator against an incipient failure. Not only reducing the likelihood of catastrophic failure, trip alarms actually minimize the effect of a component breakdown by catching it early on before affecting downstream machinery, which in effect minimizes the MTTR and associated breakdown costs. Wear monitoring can be achieved through trend analysis of collected data allowing operators to assess the wear level of critical machinery allowing them to quantitatively determine how longer the machine can be operated. This benefit is significantly important in the mining industry where it must be determined if the machine would survive till the next planned shutdown. Finally, the constant monitoring of operational parameters such as speed and pressure provides the operation team with necessary data required to optimize machinery operation and maximize the output.

Implementing a CM solution requires careful planning and execution. For illustration, the three major steps in developing an aircraft pump monitoring [6] strategy will be presented in the following subsections.

2.1.1 Determining malfunction modes

Consider the development of a CM solution to monitor the health of an aircraft's fuel pump like the one shown in Figure 2-1. For such a gear pump, malfunction modes include; blown seals,

sheared pump shaft, broken external gear, and damaged bearings. Given the mechanical nature of the critical pump components, their failure should follow a wear out probability density function; represented by the tail of the bath-tub curve presented in Chapter 1. With the critical application of powering the fuel system in an aircraft, a system is required for early warning of excessive wear. The main source of pump failures is usually attributed to cavitation. At the pressurized side of the pump, the fluid pressure pushes the bearing block against the end face of the pump creating a small clearance leading to wear on the thrust face of the bearings. Such wear can create a thin leak path affecting the pump performance.

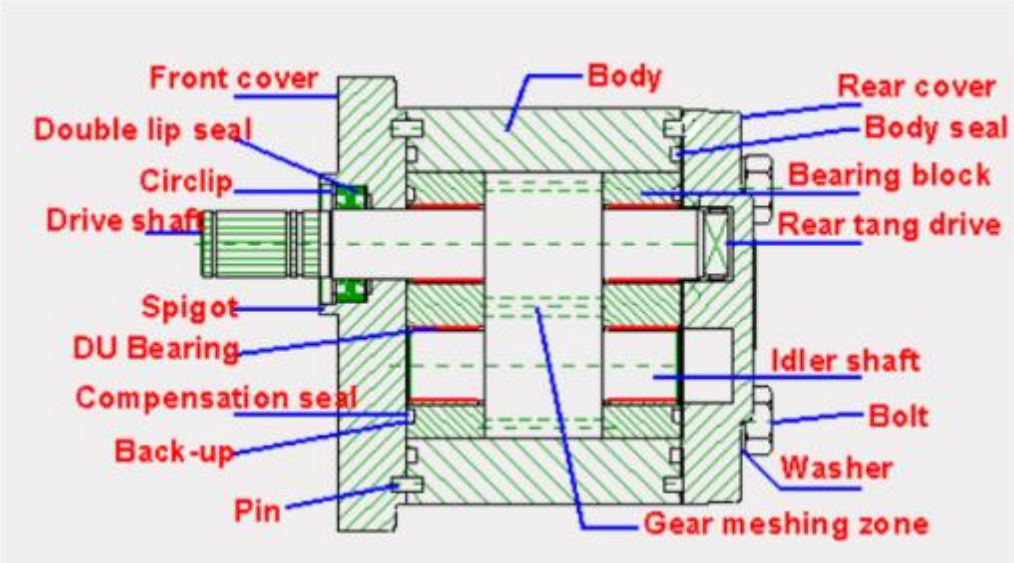

Figure 2-1: Typical Gear Pump Cross-section (taken from [7])

After realizing the wear-out nature of the expected malfunction mode, the next step would be to determine the best suited parameters to be monitored.

2.1.2 Defining parameters to be monitored

Typically, monitored parameters in a CM solution are chosen based on how significantly they are affected by the pre-determined malfunction modes. However, economic and practical considerations also need to be taken into account when selecting the parameter to be monitored. In the context of the example at hand, pressure transducers and flow meters are usually integral parts of an aircraft's fuel system. Moreover, given that pump flow ripple represents a key feature of the operation of a positive displacement pump, circuit pressure and flow can provide useful information about the state of the pump. However, regular flow meters do not have the measurement bandwidth to register the quick nature of the flow ripples [6]. As such, pressure ripple measurements are used to infer the flow ripple.

Defining the monitored parameter is a crucial step in developing a CM solution. Depending on the parameter chosen, the specification of the Data Acquisition (DAQ) system is determined such as the types of transducers, measuring points, and sampling rate, etc.

Figure 2-2: Pressure Transducers Arrangement (taken from [6])

For the example at hand, the arrangement of six piezoresistive pressure transducers shown in Figure 2-2 was used to collect pressure readings at a sample rate of 30 kHz. With data collected, the final step in the CM process is to analyze and interpret the collected data to assess the health of the gear pump.

2.1.3 Data processing and compression

Through processing, the data collected is upgraded into information relating to the pump condition. There are a multitude of DSP techniques that can be used in any CM solution, however all of those technique share a common theme; they allow for the enhancement of important features in the data that otherwise wouldn't be obvious. Additionally, an on-line CM solution such as the one employed for the aircraft pump requires the use of compression techniques to practically transmit the measurements taken by the pressure transducers at a rate of 30 kHz. Care must be taken to ensure that the data compression does not lead to loss of information specifically in regard to the DSP techniques that would be subsequently used to analyze the data.

Important DSP techniques typically employed in the majority of CM solutions include; Fast Fourier Transform (FFT) analysis to distinguish the frequency information in the signal and statistical analysis of the signal to determine the trend in the collected measurements. For the example in hand, FFT was used to determine the frequency and phase angle of the pressure ripples while statistical processing is done to infer the flow ripples that couldn't be measured directly. Finally through trend analysis, the differences in recorded pressure readings are determined for different pump conditions allowing the researchers to assess pump condition from

collected pressure measurements. The exact algorithms employed for this case study can be found in [6].

The previous example presented a brief review of a CM solution that utilized pressure measurements to assess aircraft fuel pump condition to illustrate the three stages of a CM solution design. However, since the type of monitored parameter depends on the anticipated failure modes, it would be expected that the choice of monitored parameters depends on the type of machinery under consideration, Table 2-1 summarizes the different parameters typically monitored for different types of plant machinery.

It is obvious that vibration and oil analysis represent the most common CM techniques used in the industry. The non-invasive nature of vibration analysis makes this type of monitored parameter optimal for on-line CM of various machinery types due to its simple setup and high measurement rate bandwidth. As such, the following subsection will present the prevailing vibration monitoring techniques used in the context of CM of rotating equipment.

Table 2-1: Machine Specific Approaches to Industrial Condition Monitoring Techniques (adapted from [8])

Monitored Components	**Vibration**	**Pressure and Flow**	**Oil Analysis**	**Ultrasonic**	**Thermography**	**Current Analysis**
Reciprocating	✓	✓	✓		✓	
Rotating	✓		✓		✓	
Hydraulic	✓	✓	✓	✓		
Electrical	✓				✓	✓
Piping		✓	✓	✓		

2.2 Vibration Monitoring for Rotating Equipment

Even in standard operating conditions, all machines have a certain vibration signal that is directly related to the components making up the machine. Since the basis of CM is to determine the condition of internal machine components using externally collected data, the use of vibration monitoring allows pinpointing a fault location since the signature is directly linked to the rotational periodicity of the faulted component.

Historically, the relationship between vibration signal and machine condition was initially recognized by Rathbone in his 1939 paper on Vibration Tolerance [9]. In his paper, Rathbone presented a chart relating the vibration amplitude versus frequency for different machinery presenting the vibration severity that would indicate a possible fault. It wasn't until the 1960's that overall machinery vibration level was utilized to assess the health condition. During that period, vibration levels were measured periodically using simple meters and scopes, and the results were scribbled in a clipboard. Permanently installed transducers were featured in the 1980's due to the advancements in sensors and DAQ systems and were used to continuously monitor critical machinery in real-time. During that period, vibration monitoring giants such as SKF, Bently, and Brüel & Kjær's all focused initially on the large market for rotary machinery diagnostics, e.g., turbines, generators, and centrifugal pumps and compressors. Through their efforts, those industry giants provided the foundations of the currently established vibration monitoring techniques.

The following subsections will present the common failure modes of standard rotating equipment components with focus on gearbox monitoring given the widespread application of gearboxes in

industrial power transmission systems. This will be followed by introducing the industry standard DSP techniques that have proven their reliability in the field.

2.2.1 Failure Modes of Gearbox Components

As previously mentioned, the first step in developing a CM solution is determining the possible failure modes typically encountered by the machinery under observation. A common subsystem in most rotating machinery is the transmission system. The gearbox represents the most common power transmission system used in the industry due to its ruggedness, high efficiency, and high torque capacity [10]. In most cases, rolling-element bearings are used to support the gearbox shafts.

The aforementioned components experience wear during the operation of the transmission system and the continuous stresses can deform those components eventually leading to an unexpected failure due to fatigue cracks. Being a prime example of a critical subsystem that would benefit from an online CM system, the following subsections will present the failure modes of the main gearbox components such as shafts, bearings and gears.

Shafts

In a typical gearbox, the function of the shafts is to carry the gear assembly and connect the gearbox to both the driver and driven machinery. There are three different faults that can occur due to improper shaft manufacturing and assembly; imbalance, misalignment and shaft bending.

Imbalance can be caused by the improper installation of the rotor assembly causing a radial Centre of Mass (CoM) eccentricity. Misalignment is another common assembly-related fault that

might occur when the gearbox is coupled to the driven machinery. Whether the misalignment is parallel, angular, vertical, or horizontal as shown in Figure 2-3, such a fault induces shaft bending deflections, stresses and would affect both the meshing of the gears and the radial loading on the support bearings.

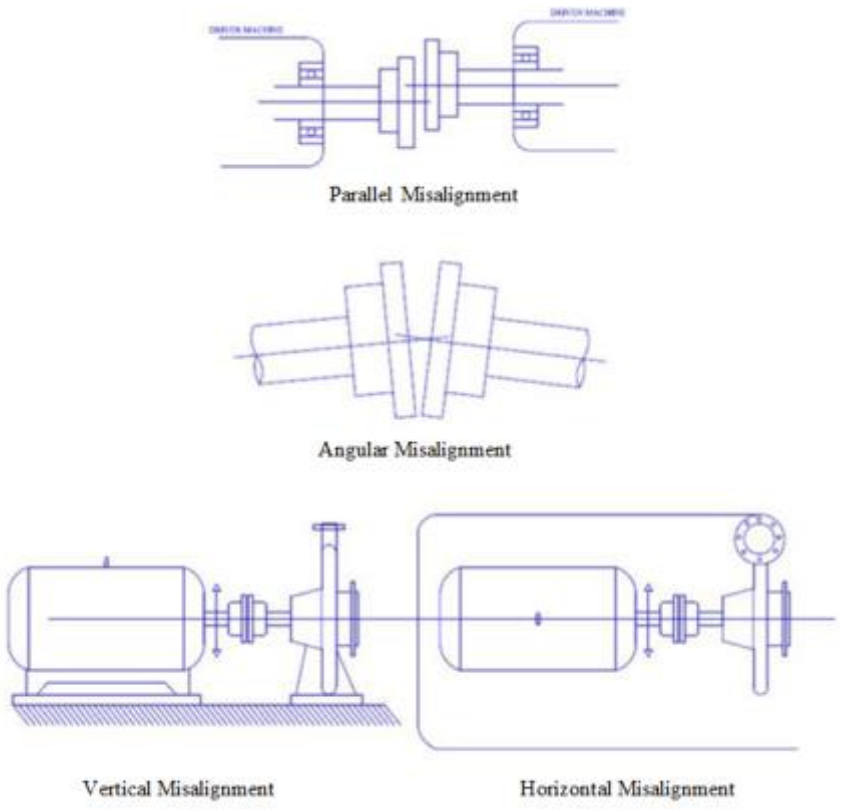

Figure 2-3: Different Types of Misalignment (taken from [11])

Bearings

As one of the most commonly used machine elements, the unexpected failure of rolling-element bearings is a frequent reason for machine breakdown [12]. As shown in Figure 2-4, the four major components of rolling-element bearings are: the outer race, inner race, cage, and rolling elements. With the function of supporting rotating shafts, the roller-elements of the bearings

allow the inner race to rotate freely with the shaft while the outer race sits still in the support structure.

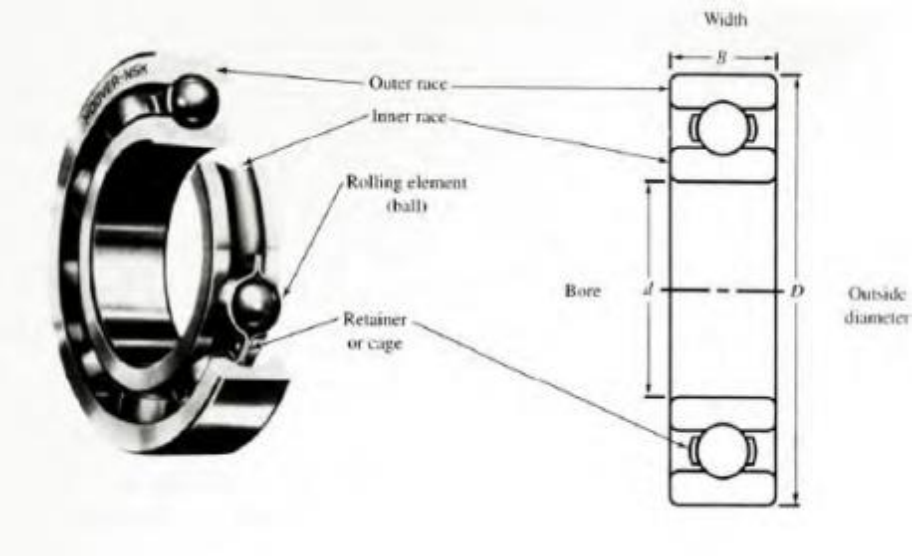

Figure 2-4: Components of a Typical Rolling-element Bearing (taken from [12])

It is obvious that the continuous rolling of the bearing elements will eventually lead to the wear out of the rollers and the raceways. A spall or scratch to the surface of any rolling element can lead to a roller fault as shown in Figure 2-5(c). If the inner or outer race ways are scratched or otherwise damaged, an inner or outer race fault is said to have occurred; as shown in Figures 2-5(a) and 2-5(b), respectively.

Figure 2-5: Different Bearing Faults: (a) outer race fault; (b) inner race fault; (c) roller fault (adapted from [13])

Gears

Gears are also critical components in a gearbox transmission system. The loading stresses on a gear tooth can affect its profile thus increasing the transmission error and reducing the gearbox efficiency. Furthermore, such high stress regions can lead to further wear compromising the involute profile of the gear affecting the meshing process. Depending on the severity of the loading, gear faults can range from a small crack at the base of a gear tooth, to the complete destruction of a tooth affecting the contact ratio and overall function of the gear.

In addition to tooth breakage, surface pitting represents another well documented fault in gears [14]. This surface damage occurs when the contact stress between the two gears is greater than the fatigue tolerance limit of the gear material. In a more serious representation, inadequate lubrication can result in direct metal to metal contact that might lead to local welding of mating surfaces.

As previously explained, the periodicity and amplitude of the vibration signature of different components can be used to determine the overall health of the machine and to distinguish the faulted components. Depending on the component of interest, a range of DSP techniques have been successfully adapted to the context of condition monitoring. The following section will cover the DSP techniques used in vibration analysis and will introduce specific techniques that established their use in analysing the vibration response of bearings and gears.

2.2.2 Vibration Response of Gearbox Components and Appropriate DSP Techniques

The effectiveness of any given DSP technique depends mainly on the type of signal processed. For instance, spectral analysis algorithms are successfully used for the analysis of stationary periodic signals. On the other hand, joint Time-frequency techniques are better suited for time varying (non-stationary) signal analysis. In the case of machinery vibration, the measured signal is directly related to the mechanics of the monitored machine. As such, this subsection aims to explain the physical nature of the vibration response of gearbox components before presenting the appropriate DSP methods used for signal analysis.

The vibration response of a gearbox is physically coupled to the components that make up the transmission system. Measured vibration signals are always a combination of source effects and transmission path effects [12]. For the simple case of unbalance, the forcing function is a pure sinusoid excited at the shaft rotation frequency. At a single measurement point, the contribution of this unbalance to the vibration response is represented by the convolution of the forcing function s_j with the impulse response function (IRF) of the transmission path h_{ij} [12] as shown

in Equation 2-1. Using the Laplace Transform, the convolution operation is converted into the multiplication of the Fourier Transform of both the forcing function and the IRF in Equation 2-2.

$$x_i = \sum_j s_j * h_{ij} \quad \text{Eq. (2-1)}$$

$$X_i = \sum_j S_j * H_{ij} \quad \text{Eq. (2-2)}$$

Presenting the Fourier Transform of both the forcing function and IRF in log scale, the vibration response can be shown to be the sum of the spectral components of both functions as shown in Figure 2-6. In the general case of constant speed machinery, the log amplitude of the forcing function spectra consists of discrete components reflecting the response of machine components. On the other hand, the log amplitude of the IRF will be continuous with peaks representing the natural frequencies of the path.

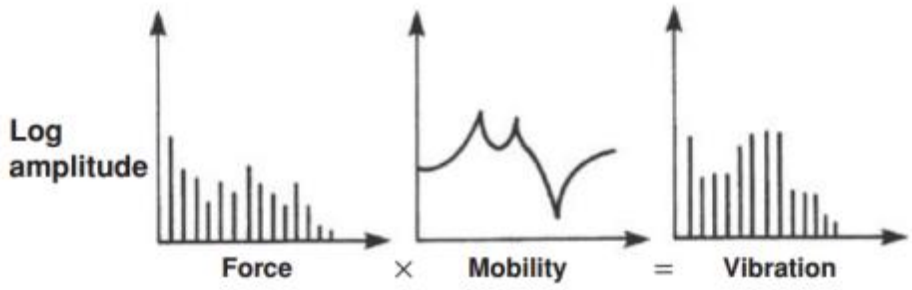

Figure 2-6: Vibration Response as the Product of Force and Path (taken from [12])

The previous paragraphs, presented the simple case of a single source effect. However, for a multi-component gearbox, vibration measurement at one point will be the sum of response from different sources constituting a Multiple Input, Multiple Output (MIMO) system. Still, the

response for such MIMO system will be very similar to the one presented in Figure 2-6. This is mainly because the same discrete components will still be present; yet with different strengths, and the IRF response is mainly governed by the natural frequencies of the paths which are specific to the structure. With this in mind, it is important to understand the physical nature of the forcing function of different gearbox components if we are to develop a CM solution.

Shafts

All three shaft faults discussed exhibit themselves at shaft speed or its first few harmonics. A shaft imbalance results in CoM eccentricity causing a radial excitation force rotating at shaft speed. As for the transmission path, even though shafts are usually axisymmetric with isotropic stiffness in all directions, the support bearings usually have nonlinear stiffness in both vertical and horizontal directions. This leads to the observation that for the simple case where the radial imbalance excites a sinusoidal response, the vibration measured will be distorted to an extent and the spectrum will contain few harmonics of shaft speed. Practically, rotor unbalance represents a more common failure mode in the context of CM of gas turbines rather than industrial gearboxes. This is mainly due to the higher rotor mass and lower flexibility of gas turbine rotor assembly in addition to the fact gas turbine rotor assemblies rotate at near their critical speed. For such high risk applications, permanently fixed proximity probes are used to determine the polar representation of shaft rotation in the form of orbit plots. Using such monitoring technique shaft imbalance would express itself in an elliptical orbit shape rather than circular one.

On the other hand, shaft misalignment is more commonly seen in gearbox applications. This is mainly due to the fact that precision alignment is a very tedious process. To ease the process of connecting two machines, flexible couplings are used to take up the misalignment; of course

only up to their rated capacity. When two shafts are misaligned and coupled they are strained toward each other. When they are rotating, the strain becomes cyclical showing as an increased amplitude at rotating frequency as presented in Figure 2-7(a). As mentioned previously, misalignment introduces a shaft bending deflection which is spatially fixed due to the coupling but is rotating with respect to the shaft as shown in Figure 2-7(b)

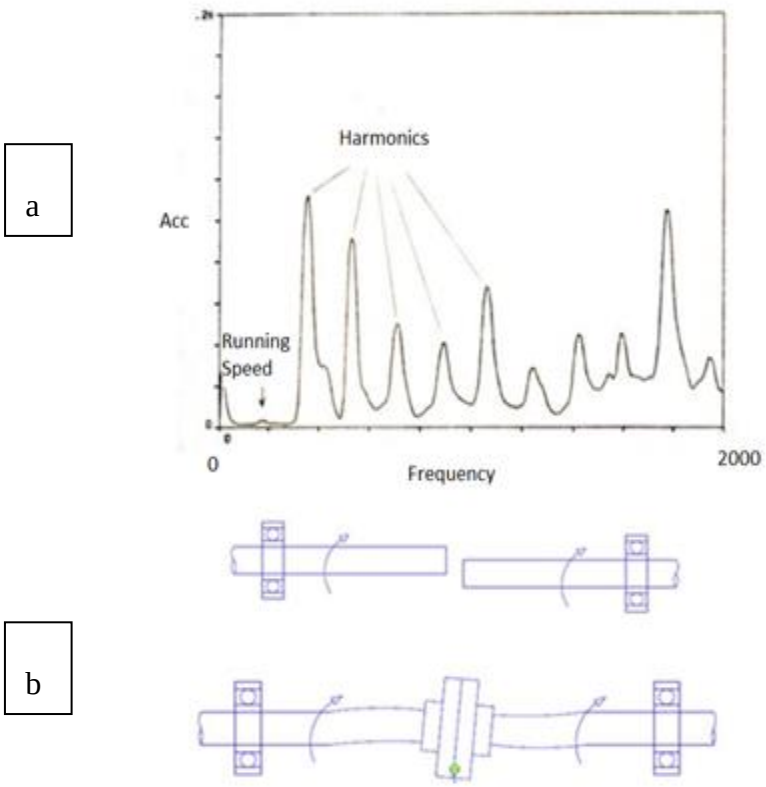

Figure 2-7: Parallel Misalignment: (a) Increased synchronous frequency amplitude; (b) the coupler straining for misaligned shafts [11]

As presented in [12], a common problem is distinguishing between unbalance and misalignment faults, Randall has investigated the measurements of a gas turbine running at 5100 RPM coupled to a generator running at 3000 RPM. Table 2-2 presents the vibration levels before and after the

alignment. From that table, it could be seen that there was a 12 dB improvement in the 2X harmonics of the gas turbine, suggesting that there was a misalignment problem.

Table 2.2: Vibration Levels Before and After Realignment (taken from [12])

Frequency (Hz)	50 (1X)	100 (2X)	85 (1X)	170 (2X)
Level before repair (mm/s)	10	0.5	9	1.4
Level after repair (mm/s)	2	0.5	3.6	0.35
Improvement (dB)	14	0	8	12

Gears

Gears transmit torque and speed between two shafts through the teeth meshing of adjacent gears. This periodic meshing action occurs at the meshing frequency which is equal to the shaft rotational speed multiplied by the number of teeth for a gear. As such, the frequency spectrum of the vibration signal for a greatly simplified gearbox would be mainly dominated by the shaft frequency and the aforementioned gear meshing frequency as seen in Figure 2-8. Of special importance, the distribution of gear meshing sidebands represents an invaluable tool in gear fault detection. It should be noted that those sidebands are present even in healthy gearbox due to the variation in tooth stiffness, changing contact points and deviations from perfect conjugate [16].

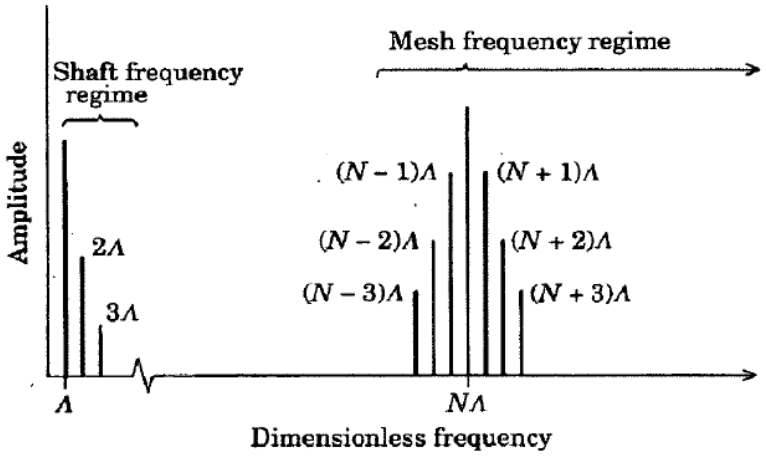

Figure 2-8: Gear Meshing Frequency (taken from [15])

Local faults like spalls and localized pitting give rise to intrusive frequency components over a wider range partly through modulation and partly as additive impulses. Such faults give sidebands that are closely grouped to tooth-meshing harmonics. On the other hand, distributed faults would only show up as a slight increase in the amplitude of meshing frequency and related sidebands. These types of faults are hard to detect as they are already masked by effects of changing tooth stiffness.

Bearings

Different types of bearings represent an integral part of any rotating machinery. Rolling-element bearings however represent the type most encountered in industrial gearboxes and pose one of the most frequent reasons for machinery breakdown. As previously discussed, bearing failure can be caused by inner race, outer race, or rolling element faults. When a local fault is struck, a shock is introduced exciting high-frequency resonance frequencies in the transmission path between the bearing and the accelerometer's point of attachment. As explained in [17] the load supported by

the bearing together with the changing transmission path as the bearing rotates both results in amplitude modulation of the bursts excited by the shocks.

In addition to high frequency resonance, for different local faults, the rotation action of the rollers excites bearing specific frequencies which depend on bearing construction and running speed. The formulae used to calculate the bearing specific frequencies are as follows [17]:

Ball pass frequency, outer race: $$BPFO = \frac{nf_r}{2}\left(1 - \frac{d}{D}cos\emptyset\right)$$ Eq. (2-3)

Ball pass frequency, inner race: $$BPFI = \frac{nf_r}{2}\left(1 + \frac{d}{D}cos\emptyset\right)$$ Eq. (2-4)

Fundamental train frequency: $$FTF = \frac{f_r}{2}\left(1 - \frac{d}{D}cos\emptyset\right)$$ Eq. (2-5)

Ball spin frequency: $$BSF = \frac{D}{2d}\left[1 - \left(\frac{d}{D}cos\emptyset\right)^2\right]$$ Eq. (2-6)

The aforementioned equations (2-3 to 2-6) are based on the kinematics of the bearing where n is the number of rolling elements, d is the diameter of each rolling element, and ∅ is the load angle from the radial plane under the assumption that the inner race is rotating while the outer one is fixed. It should be noted however that this kinematic model assumes no slip. Slip however is inevitable given the load angle variation with the position of each rolling element subsequently

affecting the rolling diameter. The cage however ensures that the mean rolling speed of all elements is the same with a random slip of 1-2% [12].

The resulting slip causes a fundamental change in the nature of the vibration signal observed. Rather than being phase locked to the shaft speed, the minor slip causes the bearing vibration signals to deviate from a deterministic model to a cylostationary model [17] where the nth order statistics are varying periodically. The implication of this is that specialized DSP techniques such as Envelope analysis can extract diagnostic information that otherwise would have remained hidden in the regular vibration spectra. Before getting into the details of those advanced techniques, the following subsection will present the fundamental signal processing approaches used for vibration-based condition monitoring.

2.2.3 Standard DSP Techniques

Signal processing techniques are needed to upgrade the collected data to diagnostic information. Depending on the nature of the signal monitored and available computing power for analysis, the different categories of signal processing used for vibration-based CM are presented in this chapter starting by simple time-waveform statistics up to more complex wavelet analysis.

Time waveform statistics

In the early days of CM, maintenance technicians used oscilloscopes to view the vibration time signal of critical machinery. In [18] the author suggests that the use of time-waveform analysis can simplify the detection of faults that might be possibly missed by spectral analysis. This includes cracked, broken or deformed gear teeth or bearing defects on low speed machinery (<10 RPM).

The diagnostic power of time-waveform analysis is greatly improved through the calculation of statistical indicators such as Peak Value (PV), Root Mean Square (RMS) and Crest Factor (CF). Commonly referred to as condition indices, the aforementioned indicators can be used to process the collected vibration signal returning a single indicator on whether the condition of the machine is within normal operating parameters. Generally, the presence of a fault leads to an increase in the amplitude of these condition indicators. Table 2-3 presents the common condition indices in a summarized form

Table 2-3: Commonly Used Condition Indicators (adapted from [14])

Indicator	**Notes**	**Formulae**
Peak Value	The maximum vibration amplitude	$PV = x_{max}(t)$ Eq. (2-7)
Root Mean Square	The normalized second moment of vibration level Energy in the signal	$RMS = \sqrt{\frac{1}{N}\sum_{n=1}^{N}(x(n) - \bar{x})^2}$ Eq. (2-8)
Crest Factor	A measure of the ratio of peak values to the root mean square	$CF = \frac{PV}{RMS}$ Eq. (2-9)

Kurtosis	A measure of the 'Spikiness' of the signal	$k = \frac{\frac{1}{N}\sum_1^N (x_i - \bar{x})^4}{\left[\frac{1}{N}\sum_1^N (x_i - \bar{x})^2\right]^2}$ Eq. (2-10)

Spectral Analysis

While time-domain signal analysis techniques can be used to detect faults, they are generally incapable of determining the fault source. Spectral analysis is used to break down the complex time-domain vibration signal into its constituting frequency components. As discussed previously, machinery vibration is physically linked to the periodic forcing function dictated by the machine's kinematics. For constant speed machinery, the rotational frequency of each component can be determined; using formulae like the ones previously used to determine characteristic bearing frequencies. Then using the FFT, the vibration signal of a machine is converted into the frequency domain and the vibration level of specific components can be determined using band filters around the component's characteristic frequency.

The practical applications of Fourier transform deviate from the analytic procedure due to the discretization inherent with DSP. In Figure 2-9, Randall [12] described the artifacts due to the three stages in passing from Fourier integral to Discrete Fourier Transform (DFT). The first step is the digitization of the time waveform by convoluting it with a pulse train resulting in 'aliasing'. The second step involves the truncation of the waveform into a finite length resulting in 'leakage'. Finally, discrete sampling of the spectrum results in 'picket fence effect'.

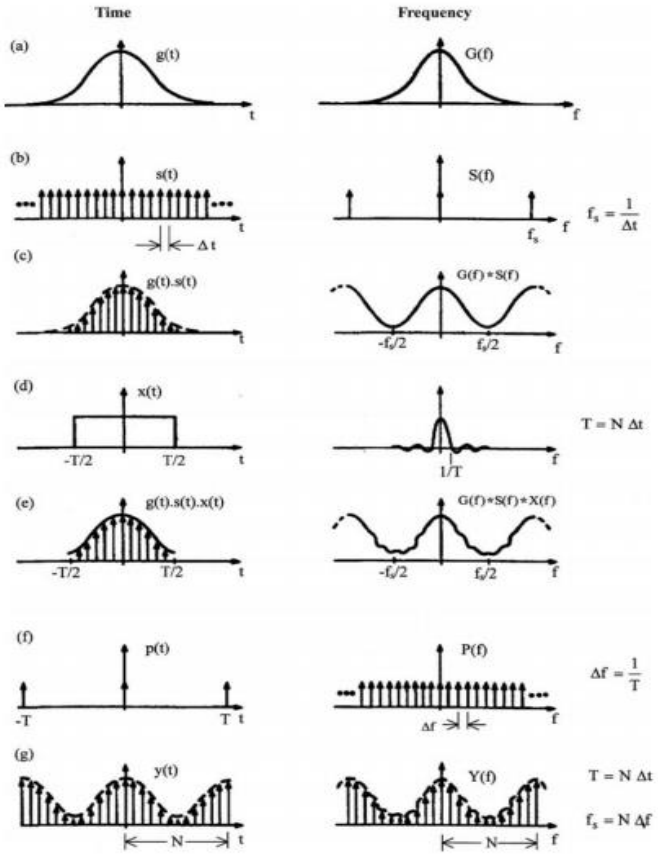

Figure 2-9: The Three Stages of Calculating the DFT: (a-c) time sampling; (d-e) truncation; (f-g) frequency sampling (taken from [3])

To avoid 'aliasing' care must be taken to ensure that the signal contains no frequencies higher than the Nyquist frequency; or half the sampling frequency. As such, a low pass filter is usually used to filter out those high frequency components to avoid aliasing. The 'leakage' phenomenon on the other hand is attributed to the truncation of the time waveform signal, which corresponds to convoluting the signal by a rectangular window. 'Leakage' can be minimized by using windows other than rectangular; such as Hanning and Blackman windows. It must be noted that the Hanning window minimizes the weight of the initial and ending data points in a segment as shown in Figure 2-10, as such it is common practice to break up long data records into smaller overlapping data sets.

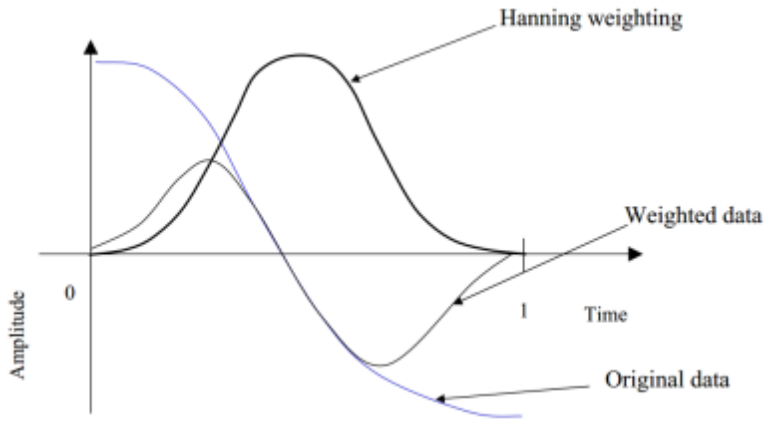

Figure 2-10: The Weighing Effect of Hanning Window (taken from [19])

2.2.4 Specialized Techniques for Bearing and Gears

As mentioned previously, the main goal of DSP techniques used in CM is to enhance specific signal features that could aid in the detection of a component fault. Since the vibration response of each component is physically linked to its construction and dynamics, certain techniques have been devised to enhance important signal features that are prominent in the vibration signal of bearings and gears.

Envelope Analysis

As previously discussed, the random slip experienced by the rolling elements in bearings significantly changes the bearing's vibration signature from being deterministic into cylostationary. Through the use of Envelope Analysis (EA), important diagnostic information concerning bearing vibration can be extracted. The advantage of EA is that it can reveal low power bearing fault impulses that would be typically dominated by instrumentation noise in regular spectral analysis. This is achieved since the spectral analysis is done on the signal's envelope rather than the signal itself. Thus unlike conventional frequency methods that can only

detect bearing faults at late stages, EA can detect faults 100s if not 1000s of hours prior to bearing failure [20].

The envelope of the signal is extracted using amplitude demodulation of the high frequency resonance F_2 associated with rolling element impacts. In presence of a fault, an impact is produced at a modulation rate F_1 corresponding to the bearing specific frequency which is frequency modulated by the high frequency carrier signal (resonant frequency F_2)as shown Equation 2-11 [20]

$$\cos(F_1) * \cos(F_2) = 0.5[\cos(F_1 + F_2) + \cos(F_1 - F_2)] \qquad \text{Eq. (2-11)}$$

In order to enhance the impulsive features in the signal, the time signal is first filtered using a band pass filter. The filter used is usually set such that shaft frequencies are filtered out of the signal. Next, the filtered signal is passed through an enveloper which demodulates the signal to extract the rate of the high energy impulses in the signal. The last step in EA shown in Figure 2-11 is to take the FFT of the enveloped signal such that the end result is a spectrum presenting the bearing characteristic frequencies.

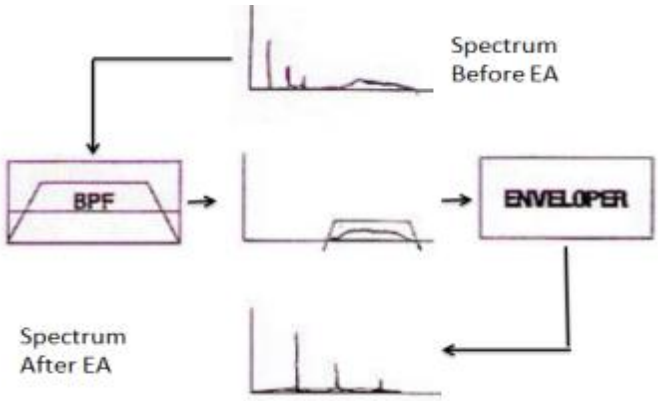

Figure 2-11: Steps in Envelope Analysis (graphically adapted from [61])

Time Synchronous Averaging

Times Synchronous Averaging (TSA) technique is especially suited for gearbox analysis as it is used to separate the vibration response of the gear under analysis from other components and noise sources that are not synchronous with that gear. The underlying logic behind TSA is that all vibration related to gears on the shaft will repeat periodically with shaft rotation [14] and that gear mesh frequencies are dependent on gear kinematics and shaft speed.

In the TSA algorithm, the vibration signal is divided into N equal-sized adjacent segments each representing one complete shaft period T The segments are then averaged together to enhance the vibration signatures that are periodic with shaft rotation as shown in Equation 2-12 [27]. As such, TSA serves to enhance the deterministic components of the vibration signal representing the gear under analysis. This powerful procedure however requires a high resolution encoder signal for shaft angle, which represents an added cost to the instrumentation system.

$$y_a(t) = \frac{1}{N}\sum_{n=0}^{N-1} y(t + nT) \qquad \text{Eq. (2-12)}$$

An additional restriction to the application of TSA is that it is very sensitive to speed variations. Since the averaging effect of TSA reinforces signature features that are phase locked to the shaft rotation, even a 0.1% speed change will cause these features not to line up thus cancelling the benefits of TSA [48].

Discrete Random Separation

In an industrial gearbox, the relatively weak bearing signals are mainly masked by discrete frequency ‘noise’ from gears. It is thus usually advantageous to remove such noise from the

signal before processing it for bearing fault detection. Discrete Random Separation (DRS) aims to remove this noise under the premise that gear vibration is principally different from bearing vibration. As previously mentioned, gear vibration is mainly discrete; on the other hand, the slip in roller element bearing renders the bearing signal as cylostationary. DRS removes the discrete component of the signal by first multiplying the signal with its own delay, thus emphasizing the periodic components. This emphasized signal is then subtracted from the original signal leaving only the random part; which contains bearing diagnostic information as shown in Figure 2-12

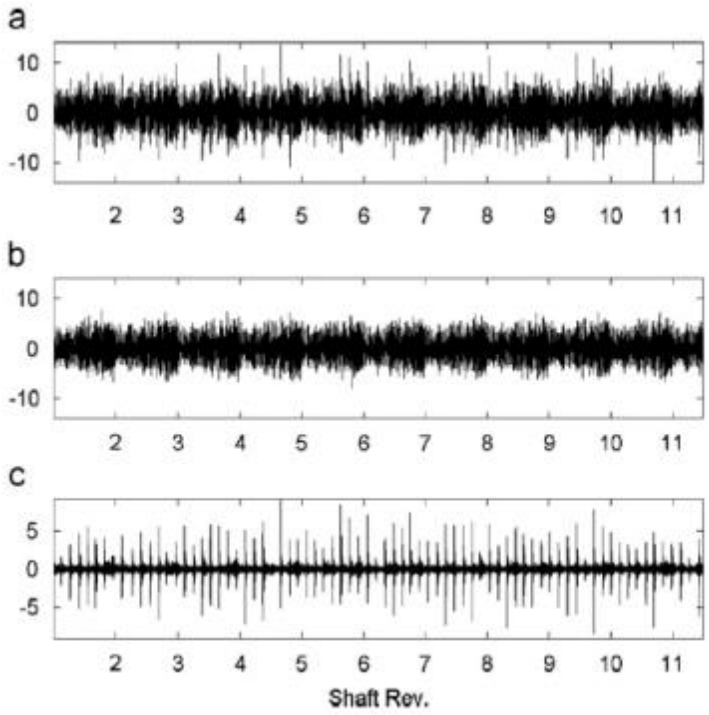

Figure 2-12: DRS Enhancement of an outer-race fault: (a) measured vibration signal; (b) extracted discrete component; (c) extracted non-deterministic component (taken from [17])

Operation condition changes will ultimately affect the vibration response of most machinery. As such, the main goal of a CM solution is to differentiate the vibration changes resulting from operational changes from those due to structural degradation. The following subsection will

present techniques typically used to help CM systems accommodate variations is machinery speed.

2.2.5 Accommodating Changing Speed

The variable speed operation of most machinery can significantly complicate the classical spectral analysis techniques previously presented. This is mainly due to the spectral smearing that occurs when the signal's frequency components are changing position due to rotational speed changes. The following subsection will present different strategies to accommodate varying machinery speed. Order tracking can be used as a preprocessing step to eliminate the smearing effect in spectral analysis. On the other hand, a Time-frequency analysis techniques could be used to extract the spectral content of a signal without losing the time information.

Order-analysis

Order tracking is a typical preprocessing step for transient signals since it corrects the synchronous variability due to operational speed changes. Originally, order tracking was implemented directly in the measurement setup by using a once-per-rotation key phasor through a phase-locked loop to ensure synchronous data sampling [15]. This analog phase loop still had a finite response time and as such was not very successful in resolving segments with varying acceleration rate. Alternatively, digital resampling for order tracking is typically used where a high resolution tachometer is used such that sampling is completed for uniform increments in shaft rotation. Figure 2-13 shows how order tracking can minimize spectral smearing for the vibration signal of a mining shovel's gearbox

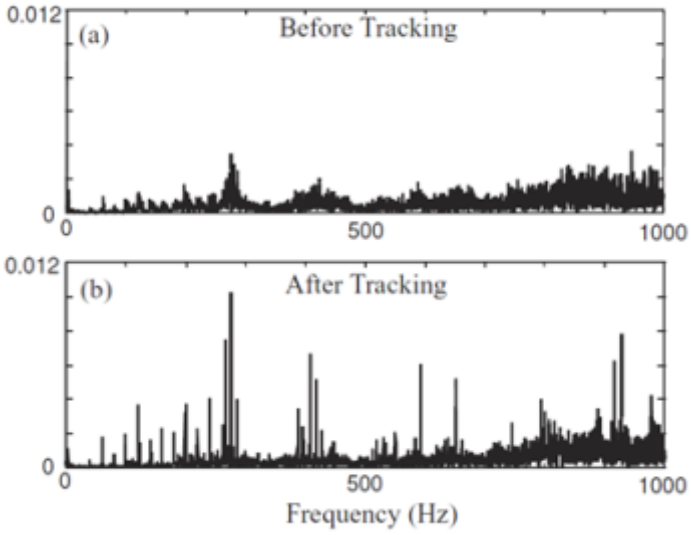

Figure 2-13: Order Analysis (taken from [12])

As mentioned, the varying operating speed for variable speed machinery causes frequency modulation of the resulting vibration signal for the machine's components. Given the integral nature of the FT, converting the vibration time signal into the frequency domain results in the loss of time information. To address the limitations of both frequency and time domain in the analysis of non-stationary signals, joint time-frequency representations have been proposed such as Short Time Fourier Transform (STFT), Wigner-Ville Distribution (WVD) and Wavelet Transform (WT).

Short Time Fourier Transform

Essentially, STFT represents a windowing technique applied to the Fourier Transform of a signal. Utilizing a sliding window $g(t)$ centred at time τ to perform time-localized FT of the signal $x(t)$ as in Figure 2-14. As such the STFT can achieve both frequency and time localization required for the analysis of non-stationary signals.

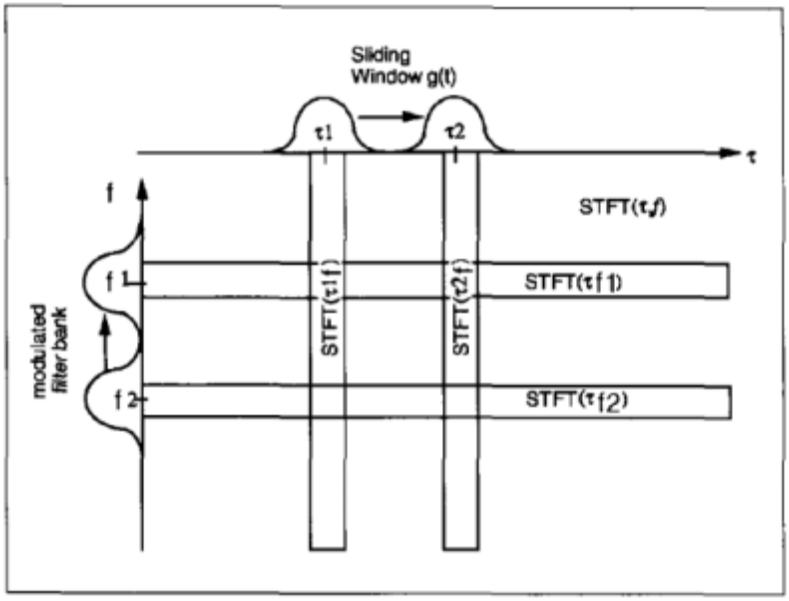

Figure 2-14: Short Time Fourier Transform (taken from [49])

Still, STFT suffers from the fact that the addition of the windowing function affects the resolution of the frequency domain. Additionally, since the time-bandwidth product is lower bounded by $\pi/4$ as stated by the Heisenberg inequality, a trade-off is always encountered between time and frequency resolutions [21] [22]. Moreover, once the window is selected, it cannot be changed during the transform.

Wigner-Ville Distribution

Compared to the STFT, Wigner-Ville Distribution (WVD) can provide a significantly more enhanced time-frequency representation for non-stationary signals [50]. Unlike the linear STFT, WVD is a bilinear convolution integral allowing both time and frequency to be linked together in one function. In Equation 2-13 [23], WVD uses an instantaneous autocorrelation function to construct the power spectrum of the signal. By avoiding the use of a window function, WVD minimizes the smearing effect seen in STFT and thus can provide higher resolution analysis of

non-stationary signals. However, the use of autocorrelation function can lead to interference terms when a multi-component signal is analyzed.

$$W(t,f) = \int_{-\infty}^{\infty} s\left(t+\frac{\tau}{2}\right) s^*(t+\frac{\tau}{2}) e^{-j2\pi\nu\tau} d\tau \qquad \text{Eq. (2-13)}$$

As shown in the following Equations, WVD can suffer from interference between different signal components $x_1(t)$ & $x_2(t)$. The W12 & W21 terms in Equation 2-15 are interference terms that complicate the interpretation of the energy distribution [18].

$$x(t) = x_1(t) + x_2(t) \qquad \text{Eq. (2-14)}$$

$$W(t,f) = W_{11}(t,f) + W_{22}(t,f) + W_{12}(t,f) + W_{21}(t,f) \qquad \text{Eq. (2-15)}$$

Wavelet Transform

Wavelet transform (WT) represents a more favorable alternative to STFT for the analysis of non-stationary signals [24] [25]. By allowing for multi-resolution analysis, WT overcomes the typical time-frequency resolution trade-offs encountered in STFT. In WT, a mother wavelet is used as the basis function from which a family of wavelets can be obtained through dilation and scaling. The use of scale is the reason why WT is usually referred to as Time-scale analysis.

From an analysis point of view, WT can be viewed as a bank of band-pass filters each with a constant relative bandwidth. The central frequency of these filter banks can be determined using Equation 2-16 [51] where $\Delta f, f$ and c are the frequency resolution, centre frequency and a constant, respectively. From the previous equation, it can be seen that the frequency resolution is

directly proportional to the frequency band analysed resulting in increased frequency resolution for high frequency components and increase temporal resolution for low frequency components according to the Heisenberg inequality previously mentioned. This multi-resolution analysis feature of WT can be readily seen in Figure 2-15.

$$\frac{\Delta f}{f} = c \qquad \text{Eq. (2-16)}$$

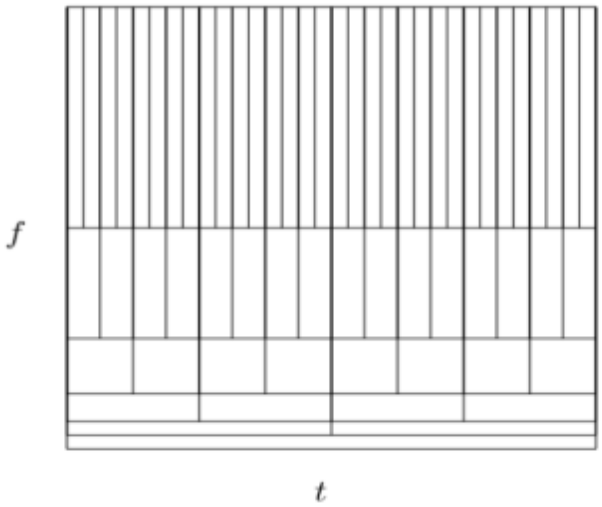

Figure 2-15: Multi-resolution Analysis Using Wavelets (taken from [63])

The advantages and disadvantages of the different Time-frequency analysis techniques discussed in this section are presented in Table 2-4.

Table 2-4: Comparison between Different Time-frequency Analysis Methods (adapted from [14])

Technique	Resolution	Interference Terms	Speed
CWT	Good frequency resolution and low time resolution for low frequency components Low Frequency resolution and good time resolution for high frequency components	No	Fast
STFT	Dependent on window function, good time and frequency resolution	No	Slower than CWT
WVD	Good time and frequency resolution	Severe interference terms	Slower than STFT

The results of all the DSP techniques in this section require specialized training on the part of the maintenance practitioner to interpret. As a result, the data collection and analysis of machinery parameters was restricted only to large scale critical machinery given the expenses associated

with collecting and interpreting the results by specialists. The recent advances in data processing and computing are paving the way for development of autonomous CM solution. Artificial intelligence allow for the CM system to independently analyse the collected data to determine the machinery health. Such automation minimized the need for specialists thus rendering the application of CM systems economical to smaller-scale machinery. The following section will present the major computing techniques used to automate the application of CM solutions.

2.3 State of The Art in Condition Monitoring for Machinery in Non-stationary Operation

In recent years, there has been a growing interest in the development of novel CBM techniques that are applicable to machinery operating in non-stationary manner. The bulk of this interest has been in an academic context given the complex nature of the problem at hand. Driven by the rapid advancements in computing power, the majority of state of the art research in non-stationary machinery diagnostics draws heavily on recent innovations in the Signal Processing and Artificial Intelligence (AI) domains.

So far, all methods discussed are essentially measuring the amplitude of certain features within the vibration signal in one way or another irrespective of signal enhancing processing or whether the analysis is in the time or frequency domain. Such amplitude measurement techniques have two major drawbacks limiting their use in the context of non-stationary duty machinery:

- Vibration levels are dependent on the operating duty of the machinery. Load or speed changes would eventually introduce amplitude or frequency signal modulation, respectively. As such, to be able to successfully assess machinery condition, amplitude

measurements must be compared with previous measurements collected under the same operating conditions

- Machinery vibrates even when they are operating in a fault free condition. For instance, the conjugate meshing of gear teeth excites vibration at the meshing frequency, which is the same frequency a tooth fault would excite. In effect, the frequency response of the forcing function due to this tooth fault is actually competing with the meshing frequency of all other gears. This in effect complicates tooth fault detection.

According to Worden, [26] recent advancement in AI has been adopted in the context of machinery condition monitoring such that the equipment fault detection challenge is reduced to a pattern recognition problem. Unlike level measurement techniques, pattern recognition characterizes the vibration signal into intrinsic features that the classifier uses to determine the membership of current vibration signal to predetermined classes. The details of different classification techniques will be presented in the following subsections. On the other hand, section 2.3.2 will present a different approach to solve the problem of non-stationary machinery CM, the system identification approach.

2.3.1Classification Approach

For the pattern recognition approach, a classifier is used to determine the membership of processed information into pre-determined groups. Those pre-determined groups correspond to different machinery health conditions. Generally, classification techniques fall into two major groups: supervised and unsupervised classification. Given the computing complexities associated with unsupervised classification, most classification approaches proposed in the CM context fall under the former group. In a supervised classification technique the classifier is trained to

recognise, by example, all the patterns it is required to detect using pre-labeled data. To further understand the implications of this learning style, a proper presentation of the pattern recognition approach is required.

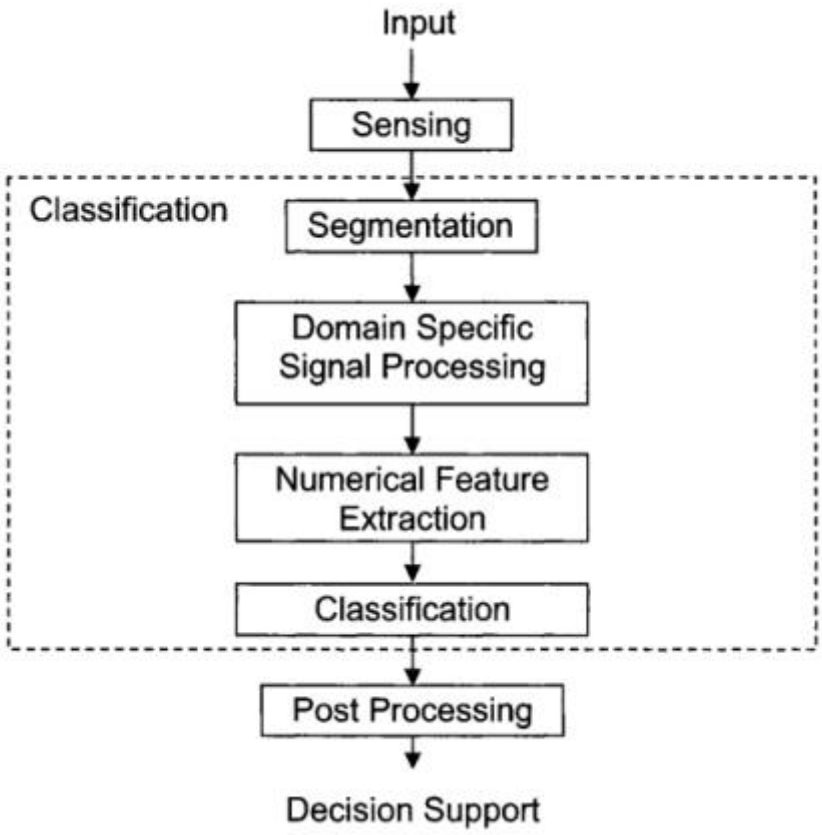

Figure 2-16: Typical Pattern Recognition Flowchart (taken from [27])

The goal of a typical pattern recognition system; such as the one presented in Figure 2-16, is to extract useful information from a data set and recognize the underlying patterns associated with different types of data sets. In the context of CM, the input is the vibration signal picked up by the mounted accelerometer. The classification process starts by segmenting the data into separate individual segments or events from the continuous signal. For instance, the vibration signal from

a gearbox is usually segmented into chunks representing one complete rotation; analogous to the TSA approach which is followed by the signal enhancing DSP techniques presented previously.

As previously mentioned, the main role of such signal processing is to enhance the details of the features representing the condition of the machinery. The Feature Extraction (FE) process represents an important step in the pattern recognition approach. In simple words, the successfulness of the classification step depends mainly on the proper selection of signal feature in the FE process. The role of FE is to present all the important features of the vibration signal in a compact form; the Feature Vector (FV), required to present all the signal attributes required for classifier training in the most concise way. If the FV is too limited, the classifier would not be able to determine the underlying patterns in the signal. On the other hand, if the FV is too broad, the classifier will face the "curse of dimensionality" where the classifier would be overwhelmed by information. As it will be shown in the subsequent paragraphs, the goal of the classifier is to provide mapping from the feature domain to the condition monitoring domain [28].

Artificial Neural Networks and Support Vector Machines

Artificial Neural Networks (ANN) represent one of the earliest applications of 'soft' computing techniques motivated by biological analogues. Compared to traditional serial algorithms, 'soft' computing techniques can generally accommodate vagueness and uncertainty by adopting 'learning from data' style that allows such computing techniques to be dependent on inductive reasoning and inference [26]

The power of ANN in terms of mechanical system research is their suitability for sensor data processing problems that require parallelism and optimisation due to high-dimensionality of the

problem space and complex interactions between the analyzed variables. The most important elements allowing ANN to complete this task are:

- Nonlinearity: ANN are usually designed to be nonlinear and thus can accommodate the underlying non-linearity associated with the system being modelled
- Parallelism: ANN are parallel by design allowing for significant reduction in required computing time
- Adaptively: an ANN will continuously self-adjust to produce consistent responses to given training data

The non-linear operation of ANN and the inaccessible nature of its hidden nodes render it as some sort of 'black box'. The designer has little knowledge of the way the neurons are self-adjusting the weights thus affecting this approaches' repeatability.

Unlike ANN, Support Vector Machines (SVM) are motivated by statistical learning theory. As such, the approach is fairly systematic and reproducible. As kernel-based learning algorithms, the inner working of this approach can be investigated and reproduced easily. SVM uses feature vectors to represent the different data points and then creates multi-dimensional boundary (hyper-plane) that separates different data classes.

As forms of supervised learning, both SVM and ANN classification techniques requires extensive training using pre-labelled data to successfully diagnose the fault type in a given machine. The need for pre-labelled data limits the use of supervised learning in the context of

condition monitoring to machinery with extensive maintenance history documenting the vibration response of the machine at different faults.

Practically, the existence of data describing fault conditions for expensive or high integrity machinery is very rare [29]. In his thesis, M. Timusk [27] summarized the complexities associated with obtaining such data sets in an industrial setting as follow:

- The comprehensive training data set should include all potential failure modes. If this requirement is not met, and the running machine exhibits a failure which the ANN has not encountered before, erroneous diagnostic results will occur.
- Even if all possible faults are determined, the resulting fault signature for all machinery faults must be collected. In practice, saving the vibration response collected for all plant machinery would be economically non feasible
- Fault concurrency represents a situation where two different faults occur at the same time. In this case, the resulting vibration response would be different from the one collected for just one fault and would thus be unrecognizable for a trained ANN

To overcome the aforementioned limitations of conventional pattern recognition approaches, an alternative strategy would be based on Novelty Detection presented in the following subsection

Novelty Detection

According to [30], novelty detection is the process where "a description of normality learnt by fitting a model to the set of normal examples and previously unseen patterns are then tested by comparing their novelty score against some threshold". In effect, this approach only requires a data set representing the normal operation of the machine.

The strategy is straight forward, train a classifier using only data collected from healthy machinery. After this training, the CM solution is then installed and is used to continuously analyze the machinery vibration. If the vibration signal belongs to the same class the classifier has been trained with, then the machine is assumed to be in its healthy condition. As soon as a fault occurs, it is expected that the machinery vibration signal would change accordingly and would no longer fit into the previously trained class. The further the model deviates from the one used to train the classifier, the higher the novelty score is. This approach is usually referred to as 'one-class' classification.

In [31], the author devised a novelty-detection approach by combining expert rules and ANN to implement a CM solution for the hydraulic pumps of a mine's conveyor system. The same author went on and utilized a one-class classifier approach to implement a CM for an open-pit mining excavator in [27]

2.3.2 Limitations of Pattern Recognition Approaches to CM of Variable-duty Machinery

As previously mentioned, all machinery vibrates even when they are brand new. As such, the CM approach is to constantly compare the machinery vibration to a baseline. Initially, this was achieved using a form of amplitude measurement. Latter on with the advances in computing and signal processing, the application of a fully automated CM solution became viable.

With the multi-dimensionality and nonlinearity of the mechanical vibration signals monitored, researchers utilized the recently developed 'soft' computing algorithms used in pattern classification. However, as it was shown, the need for an all-inclusive data set limited the

applicability of such techniques. To overcome this limitation the use of Novelty Detection strategy has eliminated the need for the all-inclusive data set, and thus improved the practicality of CM using pattern recognition.

Still, the wide-scale application of CM is hindered by its current limitations in the context of CM for variable-duty machinery. The problem originates in the need for a baseline against which the current measurements are to be compared. Even using the one-class classification approach, the healthy data used to train the classifier represent the machine's vibration response at certain operation conditions. Any changes in operation speed or load would ultimately change the vibration signal and would deviate from the data used to train the novelty detector. In this case, the novelty score would increase significantly suggesting a fault even though the machinery health has not changed. What is needed is a way to decouple mechanical response changes due to operation changes from response changes due to structural faults. A possible solution to this problem would be the use of system identification techniques.

2.3.3 System Identification Techniques

To make up for the lack of a pre-determined baseline for variable duty operating machinery, System Identification (SysID) techniques can be used to generate a model for the machine under consideration. Assuming that the model developed truly represents the machine's dynamics, the output of the model is compared to the machine's vibration signal with deviations indicating a possible fault.

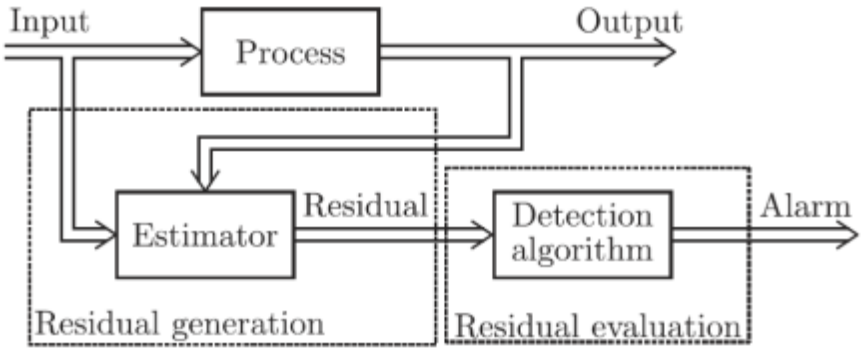

Figure 2-17: General Structure for a Residual-based Fault Detection System (taken from [32])

All SysID CM techniques share the basic flowchart shown in Figure 2-17 with the two main processes being residual generation and evaluation. The residual is the difference between the model's output and the machine's vibration signal and thus the modelling and comparison step is commonly referred to as 'residual generation'. With the model representing healthy machinery condition, the residual is expected to grow when the machine experiences a fault. However, sometimes the evaluation of the residual may not be as straight forward.

In the ideal case, the residuals for a fault-free system should be zero. However, this is never the case. All processes are physically nonlinear, of infinite order, and are time-varying. As such, any mathematical model is simply an approximation. In summary, disturbance, noise and modelling uncertainties all drive the residual to be non-zero even in fault free conditions. Therefore, residual evaluation is usually done using statistical methods rather than hard thresholds to accommodate the dynamic nature of the residual.

Depending on how the model is generated, the next subsections will discuss residual generation through analytic techniques and through data modelling.

Analytic Residual Generation

Classical alarm-based CM methods are only able to react after a relatively large sudden fault, and cannot provide fault diagnosis. By utilizing well established system theory techniques, different analytic residual generation schemes can be employed for fault detection and isolation in dynamic systems. According to [33], Rault, *et al.* [34] were the first to consider the application of identification methods to the detection of jet engines faults. Since then, that the application of FDI techniques is currently widespread in various fields including; aerospace, automotive, chemical and manufacturing. The foundations of analytic residual generation are based on the relationship among instantaneous outputs of sensors or among the time histories of sensors outputs and actuators inputs constituting direct or temporal redundancies, respectively.

In his classical survey of Fault Detection and Identification (FDI), A.S. Willsky [35] categorized model-based fault detection methods into three categories: Parameter estimation, Observer-based and Parity equations fault detection.

Parameter Estimation

For a process with a transfer function $G_p(s)$, the input-output model is as shown in Figure 2-18. In most practical cases, the process parameters are not known and thus recursive equation error minimization is required to determine the parameters. Fault detection in this parameter estimation method is achieved by monitoring the deviations of the process parameter $\Delta\Theta$. Given that Θ is actually a function of process parameters (like stiffness, damping or resistance), determination of changes in $\Delta\Theta$ provide a deeper insight on the inner working of the system.

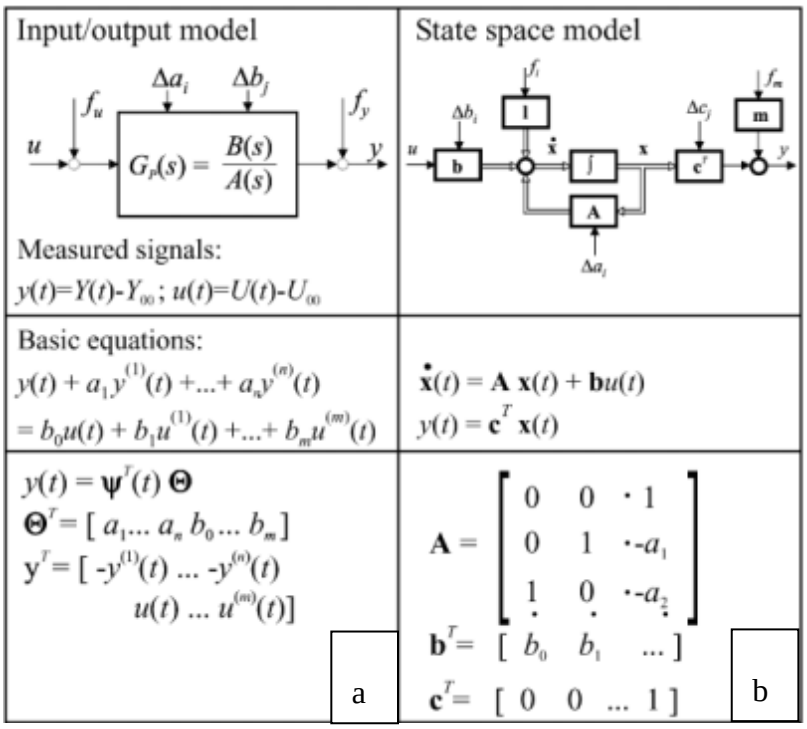

Figure 2-18: System Modelling; (a) input/output, (b) state space (adapted from [33])

Practically, the recursive nature of some estimation techniques can prevent its application in real-time situations and is limited by its inherent assumption of linearity. To account for non-linearly behaving parameters, Walker, *et al.* [36] utilized extended Kalman filters based on a non-linear model to detect faults in an industrial motion platform in real time.

In their paper [37], Lee *et al* used this model-based approach to develop a Fault Detection and Isolation (FDI) system for an automotive electric power steering system. First principles were used to derive a mathematical model for the power steering system which was then used to estimate the driver's wheel steering torque and compare it against the torque measured by the power steering column torque sensor. Using this direct comparison, the difference between the estimated and measured torque can be used to detect system faults. Moreover, the use of a mathematical model allows torque estimation for different loading conditions.

Fault Detection with Observers

In the state space model presented in Figure 2.18(b), if the effect of a given fault can be modeled as a change $\Delta \boldsymbol{x}$ then a state observer can be used for fault detection. Depending on the MIMO system arrangement, a bank of observers can be excited by all system outputs and then hypothesis testing can be done to determine which system output represents a fault. This technique was presented in [35] where Willsky and his coauthors investigated the problem of aircraft gyros self-testing.

Another observer layout is the use of a bank of observers where each one is excited by a single output such that the estimates of the $\boldsymbol{y_{est}}$ vector can be compared to the actual $\boldsymbol{y_{act}}$ thus allowing for the detection of multiple faults.

Fault detection with parity equations

According to [33], parity equations are suitable for the detection and isolation of additive noise while being simpler to design and implement compared to the observer-based approach. This method was firstly generalized by Chow & Willsky [38], where they presented the derivation of the parity vector $\boldsymbol{P}(\boldsymbol{k})$ which is equal to zero in the absence of noise and faults, has a non-zero mean random vector for noise but no fault and has a bias with noise and fault. The general representation of the parity vector with the presence of actuator inputs is presented in equation 2-17.

$$\boldsymbol{P}(\boldsymbol{k}) = \Omega\left\{\begin{bmatrix} Y_1(k,n_1) \\ \vdots \\ Y_M(k,n_M) \end{bmatrix} - \begin{bmatrix} B_1(n_1) \\ \vdots \\ B_M(n_M) \end{bmatrix} U(k,no)\right\} \qquad \text{Eq. (2-17)}$$

Note that equation 2-17 involves only the inputs and outputs of the system. In this form, $\boldsymbol{P}(\boldsymbol{k})$ represents the generalized parity vector and the dimensional space represents the generalized parity space. In this space, equation 2-17 characterizes all the analytic redundancies for the system since it specifies all possible relationships among the actuator inputs with each linear row combination representing a parity equation [32]. Depending on the fault occurring, different biases in the parity vectors will be obtained. This means that through residual evaluation, not only the presence of faults can be confirmed, but also the source of the fault can be determined by analysing the 'direction' of the bias in the parity vectors.

In aerospace and related control literature, parity equations are commonly used in generating input-output residuals. Those residuals are used in FDI systems for inertial navigation sensors [35], and aircraft control surfaces [39].

The practical application of the analytic residual generators discussed in this subsection is non-trivial. The main concern in the development of any FDI system is its detection performance; minimization of missed and false alarms, and the minimization of the reaction time of the FDI system to a fault in critical applications. In this analytic approach, moderate information about the system's model is needed, e.g. transfer function, state space representation or system matrices. However, as it was mentioned at the start of this subsection, the underlying nonlinearities and disturbances in the system's model affect the model's robustness to uncertainties.

An alternative model-free approach for residual generation is the use of data-driven techniques where the historical data of the monitored machine can be used to create a virtual image of the machine without the need for *a priori* knowledge.

Data Driven Residual Generation

In this approach, soft computing techniques are used to convert the measured machine signals into a model space by identifying the multi-dimensional relationships within the system. The main improvement here is that model identification is accomplished solely based on the on-line recorded measurements thus requiring no *a priori* knowledge of the system. This is especially advantageous for applications where generating a mathematical model is unpractical.

Serdio *et al.* developed a data-driven residual generation technique for the FDI of steel rolling mills [40]. The main challenge for implementing a CM solution for such a complex application is the fact that neither an analytic description of the faults and the process models nor the collection of typical fault patterns exists. With the absence of pre-determined fault patterns, pattern classification techniques discussed previously cannot be used; except for a one-class classifier used in an anomaly detection scheme. Serdio and his coauthors utilized genetic Box-Cox models and Takagi-Sugeno fuzzy models to infer the underlying relationships between the different process parameters using only on-line measured parameters. The data-driven models were then used for residual generation.

The advantage of this data-driven modelling technique is that the model can accommodate system changes, whereas analytic models would have to be reworked in the case of any system modifications. However, as with the pattern recognition approaches presented earlier, data driven

generation techniques require a large amount of historical data and is fairly complex requiring the knowledge of specialists.

2.4 The Need for a Silver Bullet

This chapter presented the different techniques encountered in the literature for the application of CM solutions. Classical signal processing algorithms presented in subsection 2.2.2 till 2.2.4 represent well established CM techniques widely utilized in the industry. The biggest advantage of such level monitoring algorithms is their simplicity and reliability. However, their use is limited to stationary operating plant machinery such as generators and turbines.

To ensure the plant-wide application of CM solutions, significantly more complex AI techniques are utilized to monitor the condition of non-stationary operating machinery. Employing the recent advancements in AI and computing, the techniques presented in section 2.3.1 applied pattern recognition algorithms for the classification of machinery operation. Even though the literature presents numerous applications for this type of monitoring strategy, their field use is still limited due to their complexity. Pattern recognition approaches typically require pre-labelled data sets representing different faults for the training phase, which are not typically available in practical settings as discussed in 2.3.2.

A different approach was presented in section 2.3.3 where modelling techniques are used to generate a model that runs in parallel to the machine. By comparing the output of the model to the actual machine's output, a residual is generated which is subsequently evaluated for fault detection. Depending on how the model is generated, residual generation techniques were

classified into analytic and data driven models. The use of Analytic models was prevalent in the context of FDI for aerospace and chemical process application. The main reason for this is that the aforementioned applications typically required detailed modelling as part of their design phase. However, for industrial applications, the existence of such detailed models is rare thus limiting the use of analytic techniques in practice.

To avoid the need for *a priori* models, data-driven residual techniques were developed. Utilizing historical data and on-line measurements, this technique uses soft computing algorithms to infer the underlying multi-dimensional relationships between the different measurements. Even though, this technique avoids the need for pre-labelled data sets, it is definitely complex and computationally expensive to apply in a real-time monitoring solution.

In summary, we can see that even though the literature is full of innovative ways to tackle the CM of non-stationary operating machinery, the majority of the algorithms proposed are highly specific to certain case studies and generally require extensive computing. The added complexity of the proposed methods affects their reliability and their field applicability. A testament for this is the fact that up until today, plant maintenance personnel are still using vibration analyzers, comparable to the ones that rolled out in the 1980s, to detect machinery faults using the classical signal processing techniques presented in subsection 2.2 such as RMS trending and so forth.

The aim of this research is to extend the applicability of the classical signal processing-based CM techniques to a specific class of non-stationary operation machinery; parallel machinery. By utilizing the mechanical redundancy between the subsystems of parallel machinery, the problem of CM can be reformulated into an exercise of signal comparison. Given that both parallel

subsystems are experiencing the same loading conditions, vibration signal variations due to duty changes are now common between both subsystems. Hence, significant changes observed when comparing the vibration response of both subsystems would indicate a change in the structural condition of the subsystem, a mechanical fault. As such, continuous comparison of the two parallel subsystems can serve as a means for fault detection.

In instances where machinery is configured with parallel subsystems, the problem of fault detection can be reduced to a simple exercise of signal comparison; for this particular class of machinery. If identical subsystems experience the same loading conditions, it is postulated that their vibratory response should be similar. As such, fault detection can be achieved by monitoring a similarity index computed for the vibration signals of identical subsystems. The proposed approach of monitoring identical subsystems eliminates the need for duty cycle identification given that that loading variations are common to both subsystems. Additionally, the process of determining signal similarity is much less complex than the advanced pattern recognition and system identification techniques commonly used for fault detection for non-stationary operating machinery. Requiring no prior knowledge of the system, complex AI algorithms or extensive data collection, it is expected that the proposed monitoring technique can represent the silver bullet for CM of the aforementioned class of non-stationary operating machinery.

The following chapter will present the proposed utilization of mechanical redundancy for the parallel drive stations of a local mining material haulage system including *in-situ* data collection, fault detection algorithm development and experimental testing using a table-top simulator.

Chapter 3

3 Simultaneously Loaded Non-Stationary Machinery: Parallel Machines

A quick walk through most process plants would reveal the abundance of simultaneously loaded, parallel-operating machinery. For instance, parallel pumping stations are commonplace in various applications. Deep mine dewatering stations utilize an array of parallel pumps to ensure a flow rate high enough to prevent mine flooding [41]. Municipal watering systems also utilize this parallel arrangement to generate the required head for demanding applications. A different application of parallel pumps can be seen in the use of cold-standby redundant pumps in critical chemical plant delivery systems [42].

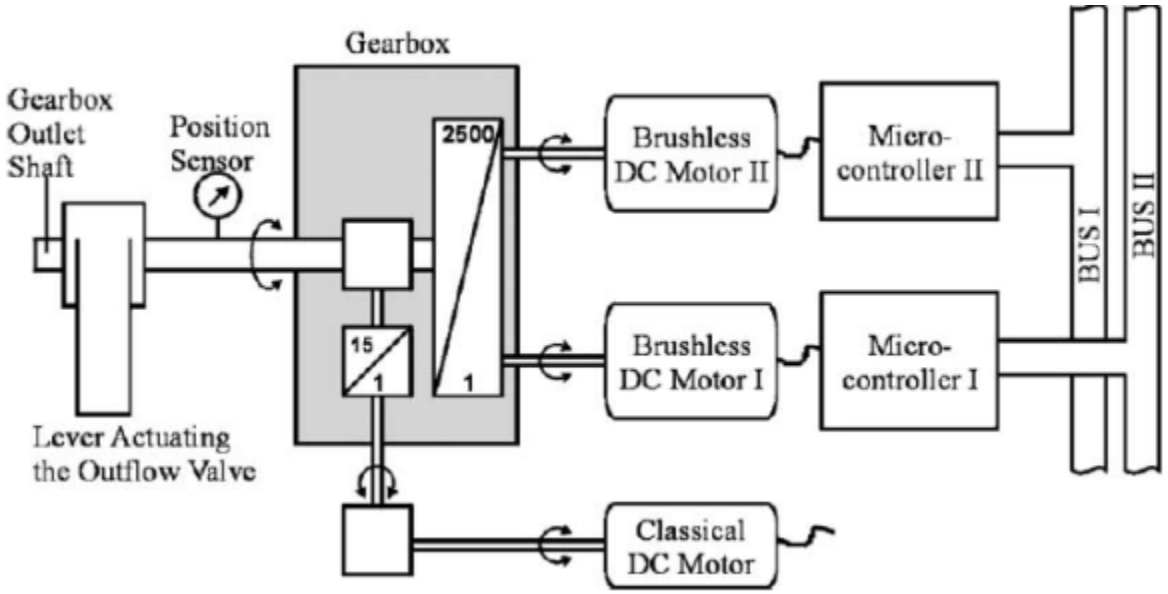

Figure 3-1: Redundant Actuator Servo-drive for Cabin Pressure Control (taken from [33])

The utilization of hardware-based redundancy is also commonly used in aerospace applications where triple redundancy is required for instrumentation systems while duplex redundancy is commonly used for aircraft hydraulic subsystems. For instance, a duplex system is used for air pressure control in passenger aircrafts as shown in Figure 3-1 [33]. In this application, two DC motors are used in parallel to control the lever actuating the outflow valve for cabin pressure control. At all times, the two motors are running concurrently in an active hot-standby arrangement, and thus are operating at the same duty cycle. Another aerospace application representing simultaneously loaded machinery can be seen in the accessory drive system of military helicopters. As shown in Figure 3-2, the UH-60 powertrain system has two identical accessory system each driven by identical turbines.

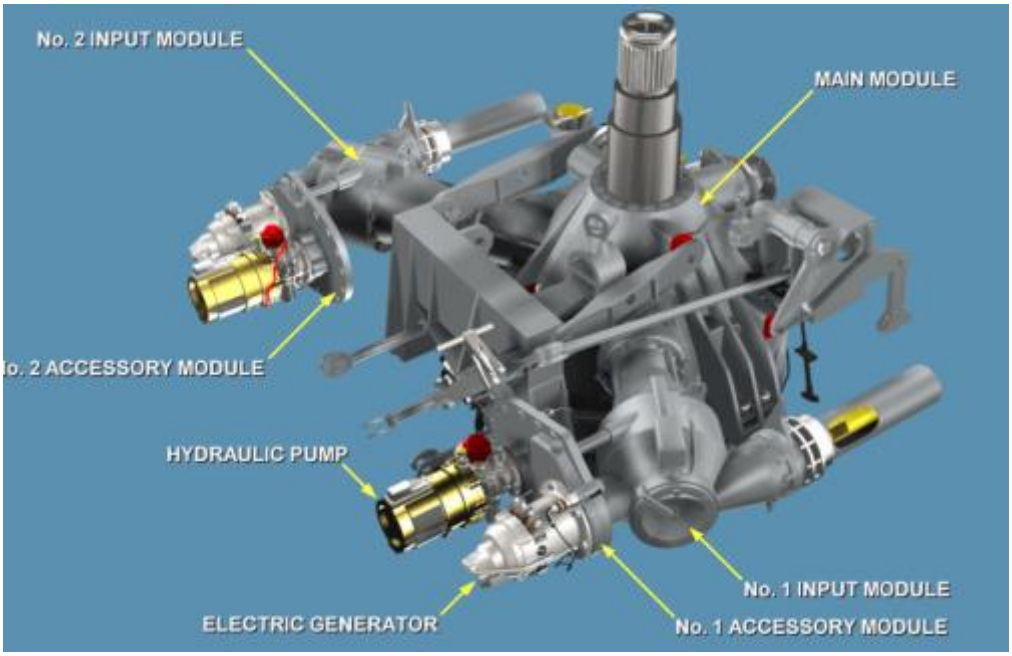

Figure 3-2: Parallel Accessory Modules in a UH-60 Powertrain (taken from [43])

Yet another example for a parallel system can be seen in the hydraulic rudder control system for transport ships. In the Electro-hydraulic piston type steering system shown in Figure 3-3, two identical hydraulic power packs are used to operate two opposing hydraulic cylinders attached to the rudder's yoke. The direction of the rudder steering is dictated by the extension and retraction of the opposing pistons. Given that the two pistons are attached to the same yoke, both hydraulic power packs are essentially sharing the same load and are operating at the same speed thus constituting a simultaneously loaded machine.

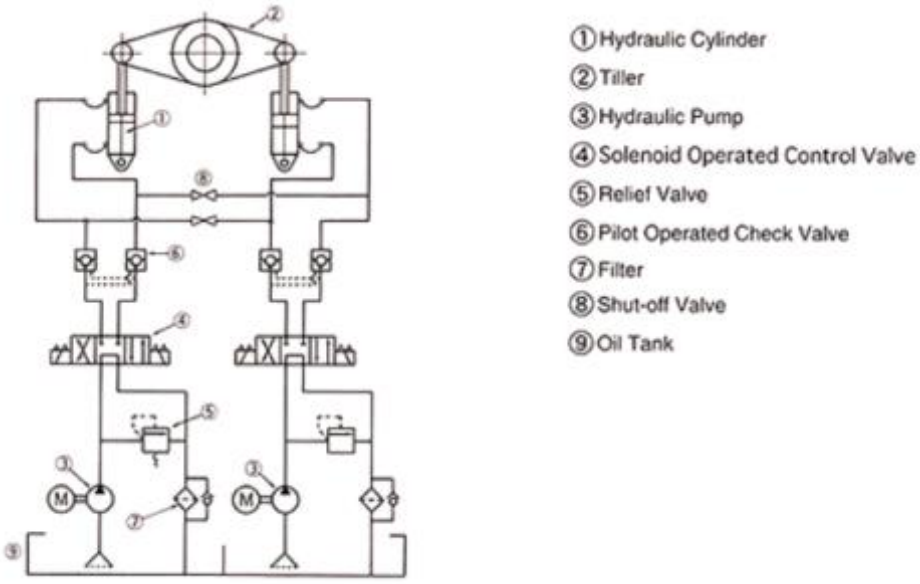

Figure 3-3: Electro-hydraulic Piston Pump Gear Steering System (taken from [44])

The utilization of hardware redundancy in fault detection was investigated, albeit in a very general sense, in fault detection of epicyclical gears for a helicopter gearbox. In their paper [45], Girondin *et al.* utilized the mechanical redundancy of the planets in an epicyclical gearbox, as shown in Figure 3-4, for fault detection. Their detection scheme depends on the observation that in the meshing of healthy equidistant planet gears, the suppression and amplification of certain

frequency peaks were observed. As such, the authors used a signal separation algorithm to separate the vibration contribution of each planet for fault detection.

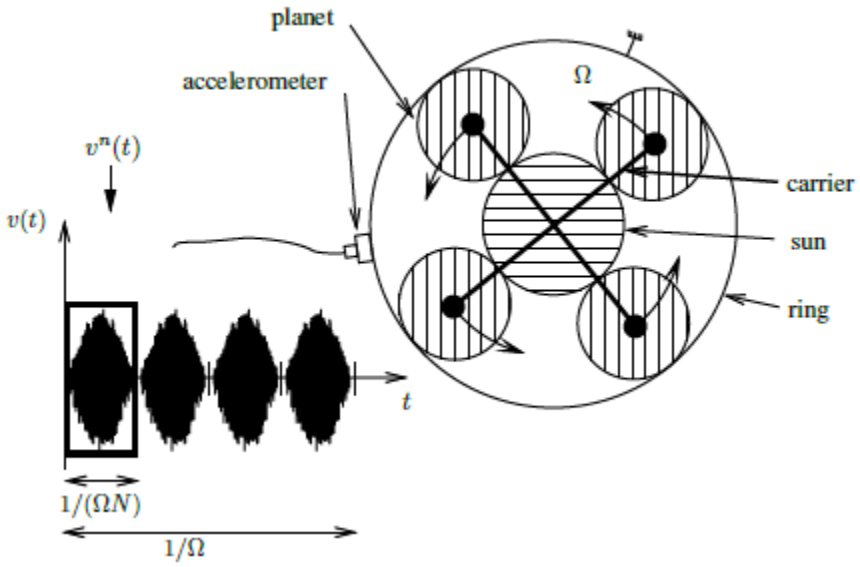

Figure 3-4: Epicyclical gears from (taken from [45])

3.1 Rail-Veyor™

As presented in chapter 1, Rail-Veyor™ is a novel material haulage system currently installed at Vale's 114 Ore Body in Sudbury Ontario. Utilizing electrical drive stations to propel the rail-trough, the system is tele-operated, requires minimal drift sizes and produces minimal emissions. The fact that the propelled train has no driving front locomotive means that the continuous operation of all electrical drive stations is critical for the uninterrupted operation of the system. As such, this material haulage system would greatly benefit from the application of a CM solution such that incipient faults are detected in their infancy and remain monitored till the upcoming maintenance shutdown. The main challenge in providing such solution is the fact that

the subsystems of the electrical drive stations are operating in a variable-speed, variable-load duty cycle. As such, the conventional alarm and trending techniques are not applicable.

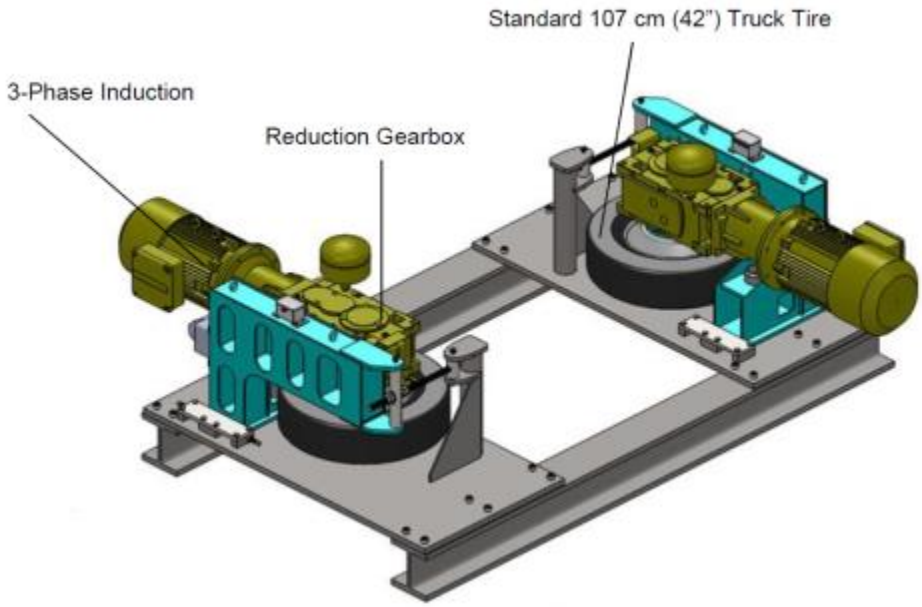

Figure 3-5: Rail-Veyor Parallel Drive Station (taken from [8])

Representing a perfect candidate for parallel operating machinery, the Rail-Veyor™ drive station shown in Figure 3-5 is made up of two identical drive systems. Each drive system consists of a 100 HP AC motor, a 39:1 reduction gearbox and a rubber tire used to transfer the driver's torque to the trough. This particular arrangement ensures that for any given load or speed, the two drive systems in a drive station will be experiencing the same duty cycle. As such, if a relationship can be established between the machinery measurements done on each of the parallel system's sister components, then the existence of any fault would affect this relationship and thus indicate failure.

3.1.1. In-situ Data Collection

To investigate the existence of a similarity relationship between the parallel components of each drive station, *in-situ* vibration measurements were completed at Rail-Veyor's demo site. As shown in Figure 3-6, the parallel drive systems for a single station were instrumented. A set of two 500 mV/g (g = 9.81 m/s^2) accelerometers were installed on the output bearing of each motor and the input bearing of each gearbox for the drive systems. Additionally, an encoder was used to determine the rotational speed of the drive system. Ideally, the rotational speed signal should be acquired at the output of the motor, before the speed is reduced by the gearbox. However, for practical purposes, installing the encoder at the motor shaft proved cumbersome and speed measurements were done on the output side of the gearbox. Additionally, in a previous site visit, a fellow researcher used Rogowki coils to instrument the phase current drawn by the parallel motors in the drive station. All data collection was completed using a LABVIEW™ PXI system at a sample rate of 15 kHz.

Initially, a test matrix was constructed such that data is collected at different operating speeds and loads. However, the data collection process was interrupted when the hydraulic brake system of one of the stations failed to disengage thus stopping the trough from moving. In the end, data was only collected for a heavily loaded trough at three different speeds; 1, 2 and 3 meters per second.

Figure 3-6: Parallel Drive Station Instrumentation at Rail-Veyor™ Demo Site; (a) Accelerometers mounted to motor and gearbox casing of each subsystem, (b) Cables being routed for instrumenting both subsystems in a drive station, (c) Optical speed sensor setup, (d) NI® PXI data acquisition system

3.1.2 Validating the Loading Similarity

The loading similarity between the two gearboxes of the Rail-Veyor™ drive station can be confirmed visually by comparing their vibration response presented in Figure 3-7. As it can be seen, the loading cycle can be divided into three parts. The First part is a ramp experienced when the trough engages the drive station; this is followed by a quasi-stationary loading condition as the drive station propels the whole length of the trough. Finally, a ramp down in loading is experienced as the trough disengages from the drive station. Furthermore, Figure 3-8 presents the current draw similarity between the two motors of both drive stations for two loading cycles.

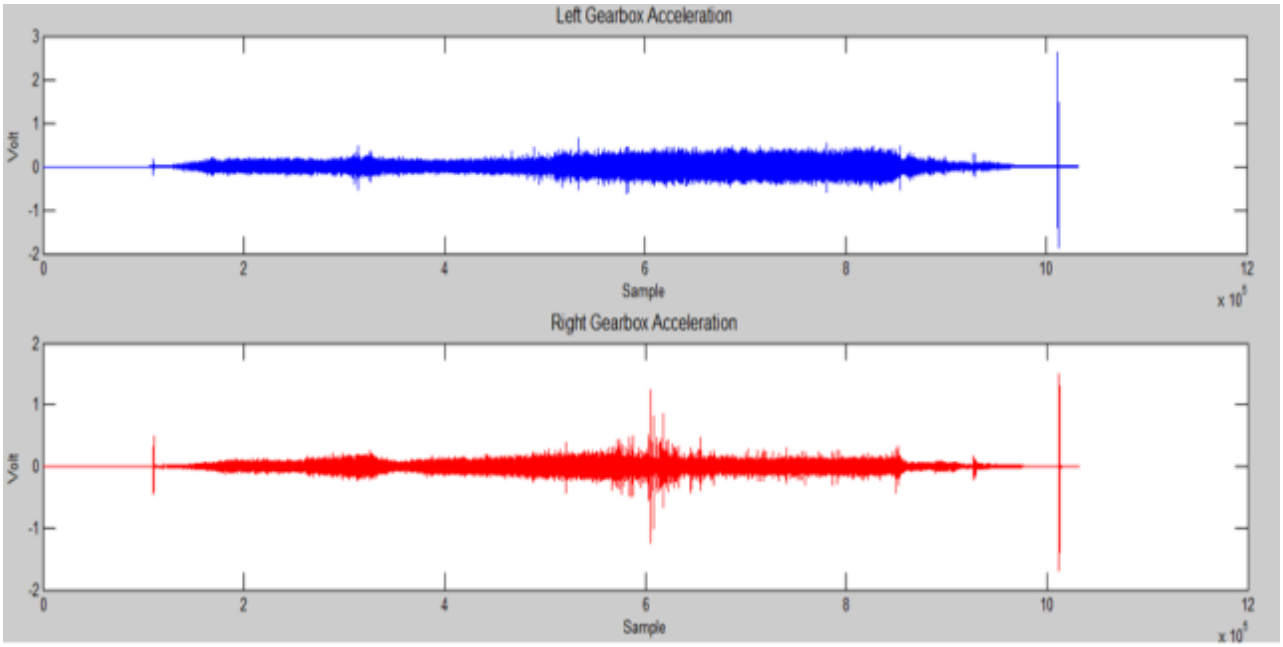

Figure 3-7: Vibration Signal at Both the Left and Right Gearboxes of Rail-Veyor® Drive Station

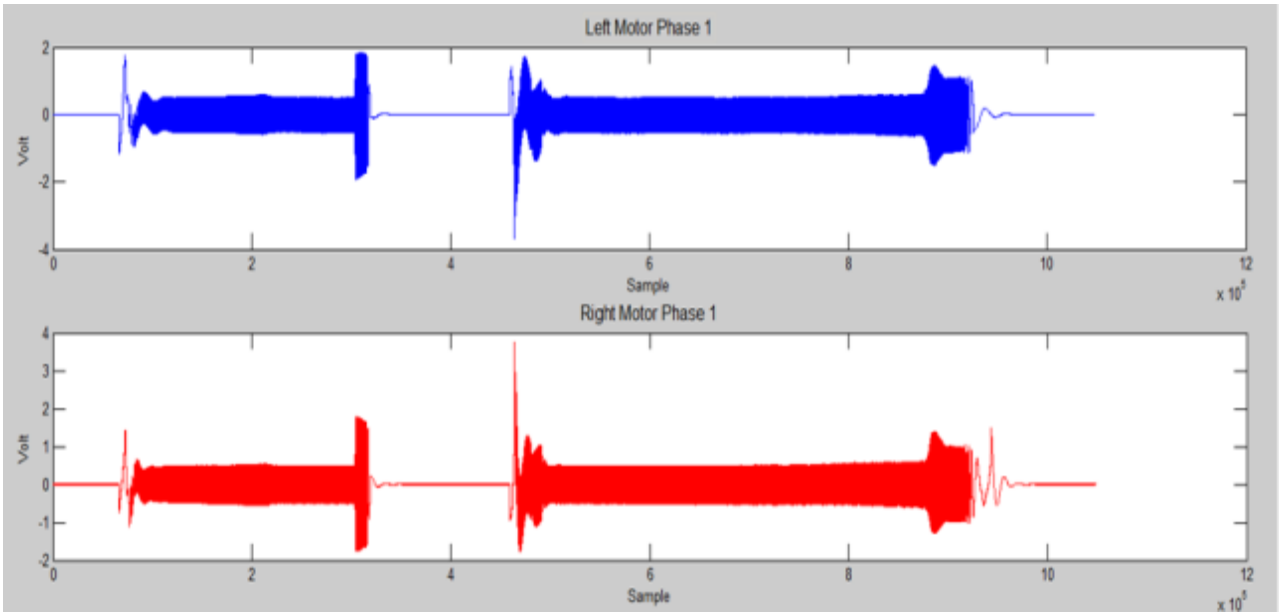

Figure 3-8: Current Draw for Both the Left and Right Motors of Rail-Veyor® Drive Station

After confirming the mechanical and electrical response similarity between the parallel subsystems of the Rail-Veyor™ drive station, a fault detection algorithm is developed to utilize the mechanical redundancy of simultaneously loaded machinery components to simplify the problems associated with implementing CM solutions to equipment operating in non-stationary manner. In order to accomplish this, the parallel systems needs to tested under different health conditions which involves the processes of intentionally seeding machinery components for testing purposes. However, given the size of the Rail-Veyor™ drive station components, the process of disassembling a drive station, hoisting an industrial gearbox into a workshop to fault is not practical. As such, an experimental setup is first used as a proof of concept to investigate the validity of the proposed approach. Both the experimental setup and the fault detection algorithm are discussed in the following section.

3.2 Development of a Preliminary Solution

The variable operation nature of the Rail-Veyor™ drive would affect the monitoring reliability of conventional alarm based CM solutions. A standard alarm based monitoring system might monitor a single parameter such as the Root Mean Square (RMS) of the signal, and issue an alarm when the RMS surpasses a certain threshold that is usually selected based on experience. As mentioned in chapter 1, such alarm based monitoring systems assume that changes in the monitored parameter are solely caused by structural health deterioration assuming stationary duty cycle. However, Rail-Veyor's drive stations, like many other mining equipment, are not subjected to a constant duty cycle. The load cycle experienced by the drive stations depend on how full the rail cars. It can be expected that the increased load will cause an amplitude modulation of the gearbox mechanical response. Such modulation would cause the RMS of the

signal to surpass the predetermined threshold and would fire a false alarm even though the structural health of the gearbox has not changed. A monitoring solution is required that would be insensitive to duty cycle variations.

However as discussed in Chapter 2, such load-speed insensitive CM solutions suggested in the literature are computationally expensive, require knowledge of the system model, or huge amount of pre-labelled training data.

The novelty of the proposed approach is that monitoring both motors and gearboxes of each Rail-Veyor drive station means that duty cycle variations are no longer extraneous variables; the variations are common between the two simultaneously loaded machinery. In effect, the complexities associated with the study of non-stationary operation are eliminated from the engineering problem allowing is to present a reliable easy to use solution that can be implemented using well-established signal processing techniques.

3.2.1 Proposed Algorithm

The main theme behind the proposed algorithm is that the vibration level of a monitored component is continuously compared to the vibration level of its parallel counterpart. Given that both components experience the same duty cycle, vibration level changes associated with duty cycle variations will be common to both components, and thus distinguishable from vibration level changes due to structural damaged. As a result, the proposed algorithm is capable of discriminating mechanical response changes that are due to duty cycle variation from the changes cause by structural damage. For example, consider the mechanical setup shown in Figure 3-9 where a vibration simulator was setup such that there is a pair of similarly loaded

rolling element bearings *A* and *B* at both ends of a common shaft loaded radially with a centre-hung weight.

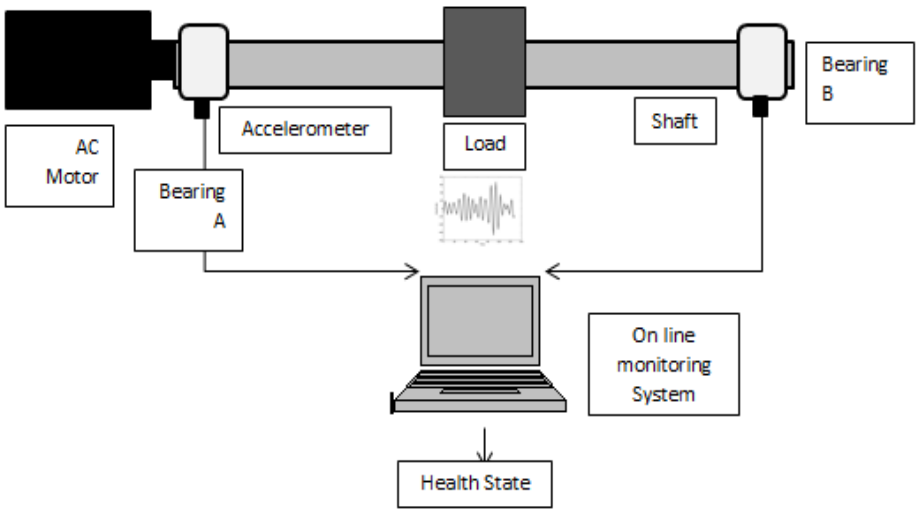

Figure 3-9: Parallel Machinery Model

To compare the collected vibration signals for each bearing housing, this algorithm proposed focused on a technique that utilizes statistical distribution analysis of correlation scores to measure the similarity between the two recorded signals. The details of this algorithm are shown in Figure 3-10. Vibration waveforms for both components *A* and *B* were collected and segmented into equal windows. A proper choice of window size is one where each window represents a certain number of complete cycles; just as done in Time Synchronous Averaging. For each window, a Feature Vector (FV) was assembled to include a specific set of 10 statistical parameters computed for the segmented waveform including as presented equations 3.1 till 3.11 adapted from [8] and [27] where *E* is the expectation operator, p_i is the probability function, and $\bar{x}_{ABS}$ is the absolute value of the signal average.

RMS	$x_{RMS} = \sqrt{\frac{1}{N}\sum_{i=1}^{N} x_i^2}$	Eq. (3-1)
Standard Deviation	$s = \sqrt{\frac{1}{N}\sum_{i=1}^{N} (x_i - \bar{x})^2}$	Eq. (3-2)
Maximum	$Max = \max(x)$	Eq. (3-3)
Minimum	$Min = \min(x)$	Eq. (3-4)
Skewness	$Sk = E\left[\left(\frac{x - \bar{x}}{s}\right)^3\right]$	Eq. (3-5)
Kurtosis	$\sum_{i=1}^{N} \frac{(x_i - \bar{x})^4}{Ns^4}$	Eq. (3-6)
Shape	$SF = \frac{x_{RMS}}{\bar{x}_{ABS}}$	Eq. (3-7)
Impulse Factor	$CF = \frac{x_{max}}{x_{RMS}}$	Eq. (3-8)

Energy, $$En = \sum_{-\infty}^{\infty} |x[n]|^2$$ Eq. (3-9)

Entropy $$H(x) = -\sum_{i=0}^{N-1} p_i \, log_2 p_i$$ Eq. (3-10)

The corresponding feature vectors for vibration signal *A* and *B* are further reduced into a single correlation vector. The correlation vectore is an array of the same size of the feature vectors such that each element in the correlation vector -the correlation factor- is a value from 0 to 1 that represents how a given feature in signal *A* correlates to the same feature of signal *B*. If the two features are very close in value, the correlation factor would be close to one, or close to zero for significantly different feature vectors. From the previous step a correlation vector was assembled as an array of correlation factors for all features in a feature vector.

Finally, the correlation factors within each correlation vector were summed together such that each correlation vector was represented by a correlation score. This score is a positive number with a maximum value of 10 representing the similarity between the vibration response of bearing *A* and *B*. The rationale behind this is that when signals *A* and *B* are similar, the correlation factor for each feature within the correlation vector would be close to 1. Subsequently, when the correlation factors are summed, the correlation score for this window would be close to 10.

The final step in this online classification algorithm was the construction of a histogram representing the distribution of the correlation scores calculated over the last five seconds. From this sample distribution a discrepancy metric was calculated by summing the total occurrences of correlation scores less than five with higher discrepancy metrics indicating highly dissimilar signals, and thus a possible fault.

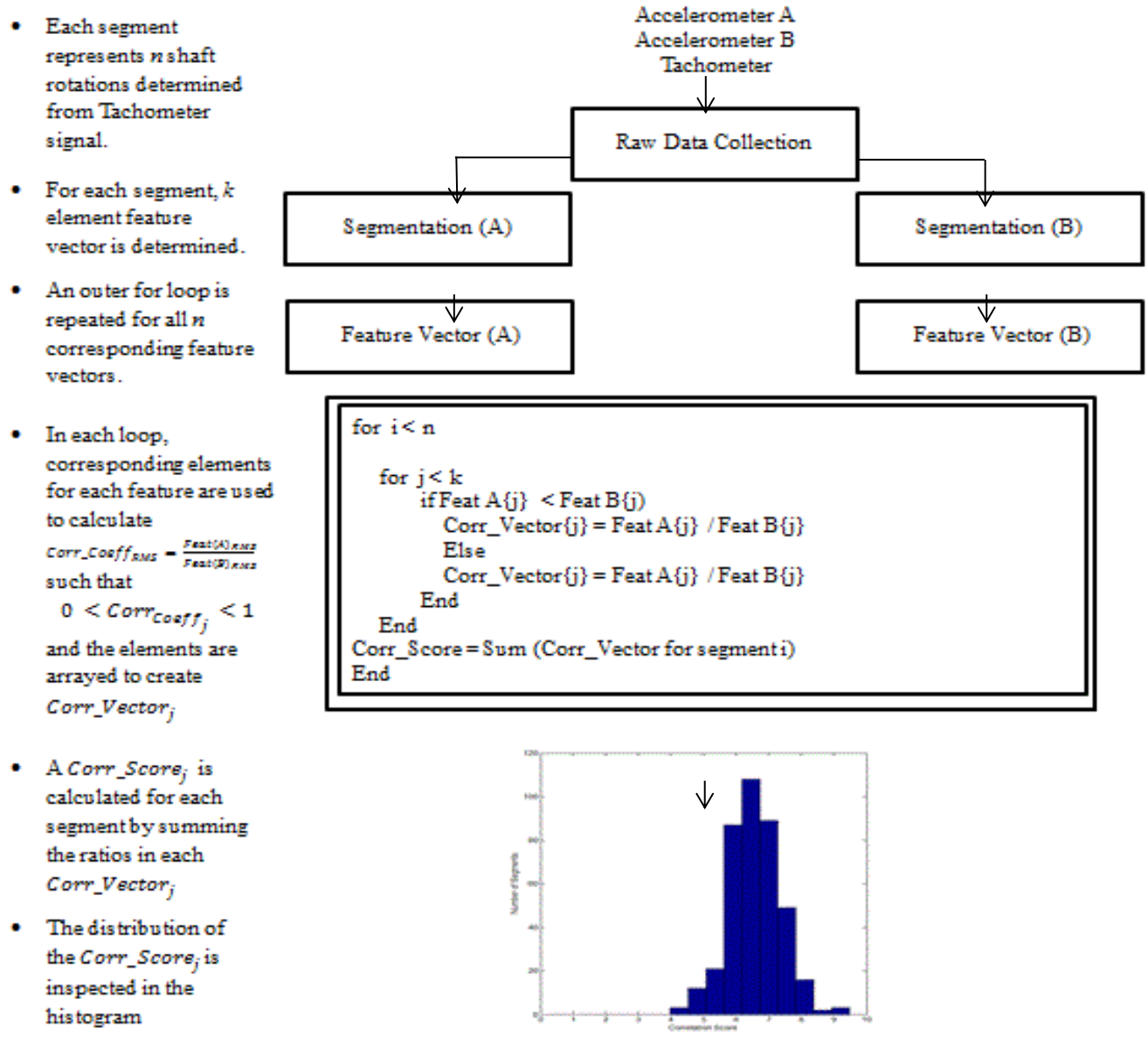

Figure 3-10: Proposed Algorithm

3.2.2 Experimental Setup

The data employed in this analysis were generated on the SpectraQuest® machinery fault simulator shown in Figure 3-11. The simulator was configured such that it had the same layout presented in Figure 3-9 to analyze bearing faults. Data was collected at 15 kHz using a National Instruments PXI data acquisition system with a total of four analog signals recorded for the experiment: a pair of vertical and horizontal acceleration signals for both Roller Element Bearing (REB) housings *A* and *B*.

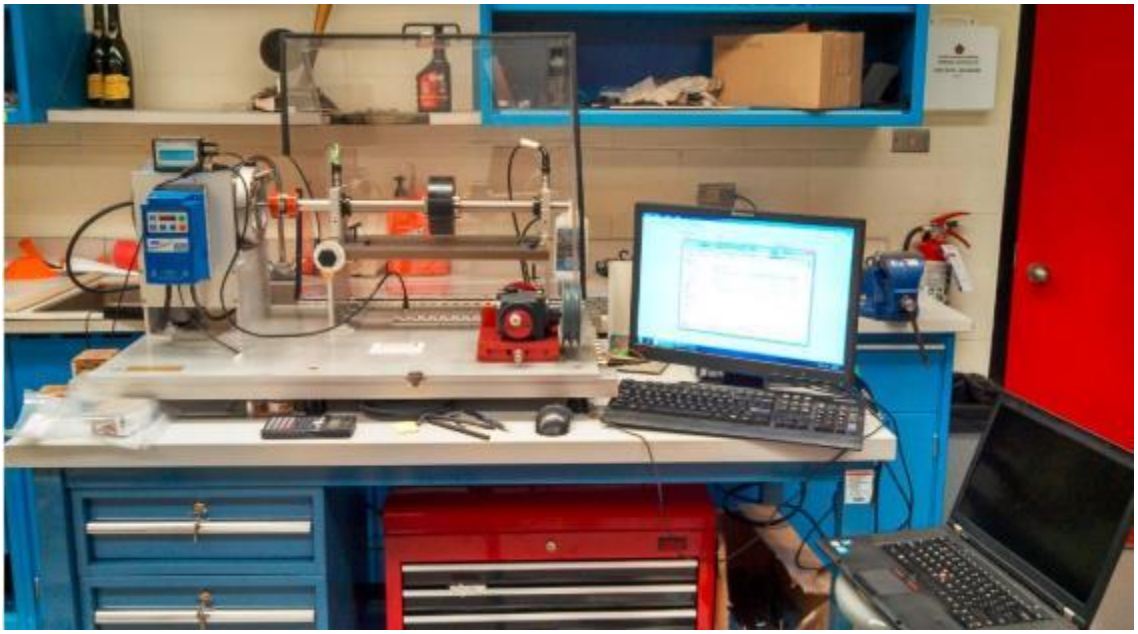

Figure 3-11: Experimental Setup Using SpectraQuest Bearing Fault Simulator

To investigate the performance of the proposed algorithm in non-stationary operation, a test matrix was constructed such that vibration measurements were taken at different combinations of loads and speeds for different rolling element bearings as shown in Table 3-1. This table presents a total of 36 tests conducted in which faulty rolling element bearings were replaced in the right

hand bearing housing and tested against an unchanged healthy rolling element bearings at the left bearing housing. Three laboratory-faulted ERLK16 rolling element bearings were used representing a ball fault, an outer race fault, and an inner race fault in addition to a healthy rolling element bearing.

Table 3-1: Test Matrix for SpectraQuest Tests

Load (Lb)	0			10			20		
Frequency (Hz) / Condition	5	15	20	5	15	20	5	15	20
Healthy	X	X	X	X	X	X	X	X	X
Ball Fault	X	X	X	X	X	X	X	X	X
Outer Race	X	X	X	X	X	X	X	X	X
Inner Race	X	X	X	X	X	X	X	X	X

3.2.3 Experimental Results

Mathworks MATLAB® was used for offline post processing of the collected data. Figure 3-12 presents how the proposed algorithm is insensitive to speed or load variations with the top three histograms presenting how the discrepancy metric remains almost zero regardless of the shaft speed increase from 5 Hz to 25 Hz. The bottom three histograms in the same figure shows how the discrepancy metric also doesn`t change with changes in loading condition. In essence, the proposed algorithm managed to ignore vibration level changes associated with variations in the duty.

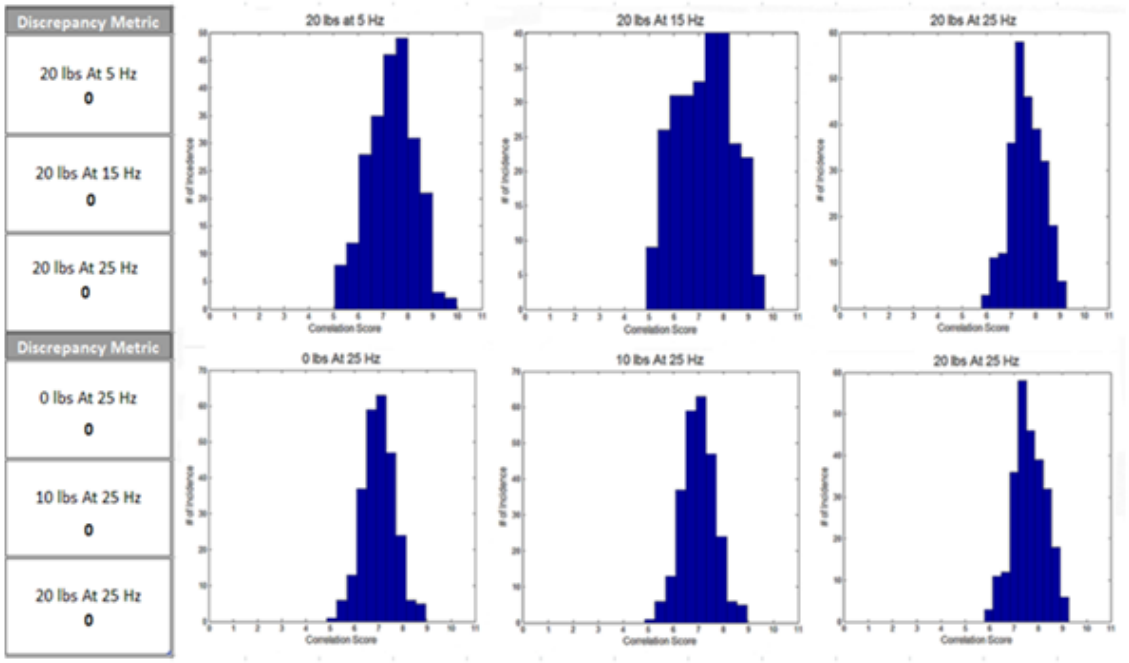

Figure 3-12: Histograms Discrepancy Distribution for SpectraQuest® Test Data

In the proposed algorithm, a discrepancy metric measures the dissimilarity between the mechanical responses of the two rolling element bearings, with higher scores indicating faults. Discrepancy scores for all 36 experiments are presented in Table 3-2. One should note how the

discrepancy changes with the increase in load and speed and become significant in the presence of bearing faults. This can be explained by natural frequency shifts due load and speed variations which move the mechanical system through regions of damping or resonance. Generally, theses deviations are minor for healthy bearings but can become quite substantial for faulted bearings [46]. A close look at Table 3-2 shows that healthy bearings have discrepancy scores of zero irrespective of the duty cycle. Building on this observation, the proposed algorithm monitors the system's discrepancy score and detects a fault when the discrepancy score is more than zero.

Table 3-2: Discrepancy Scores for SpectraQuest Tests

	Load(lbs.)_Frequency(Hz)								
	0_05	0_15	0_25	10_05	10_15	10_25	20_05	20_15	20_25
Healthy	0	0	0	0	0	0	0	0	0
Ball Fault	7	9	13	18	24	26	13	29	30
Outer Fault	7	9	12	7	13	36	6	15	50
Inner Fault	4	6	14	9	24	22	14	30	29

4.2.4 Experimental Results: Limitations of Alarm Based Approach

In order to appreciate the performance of the proposed algorithm, we will demonstrate how the previously mentioned changes in duty cycle would disturb an alarm based monitoring system.

Consider Figure 3-13 showing the RMS trend for the same experimental apparatus running at 5 Hz at no radial load with average RMS of 0.0015. Assuming stationary duty cycle, a monitoring system was implemented such that an alarm would be issued if the average RMS of the monitored waveform was three times the average RMS calculated previously. Thus the system assumes that a change in the vibration waveform of the monitored bearings indicates structural damage of the bearings.

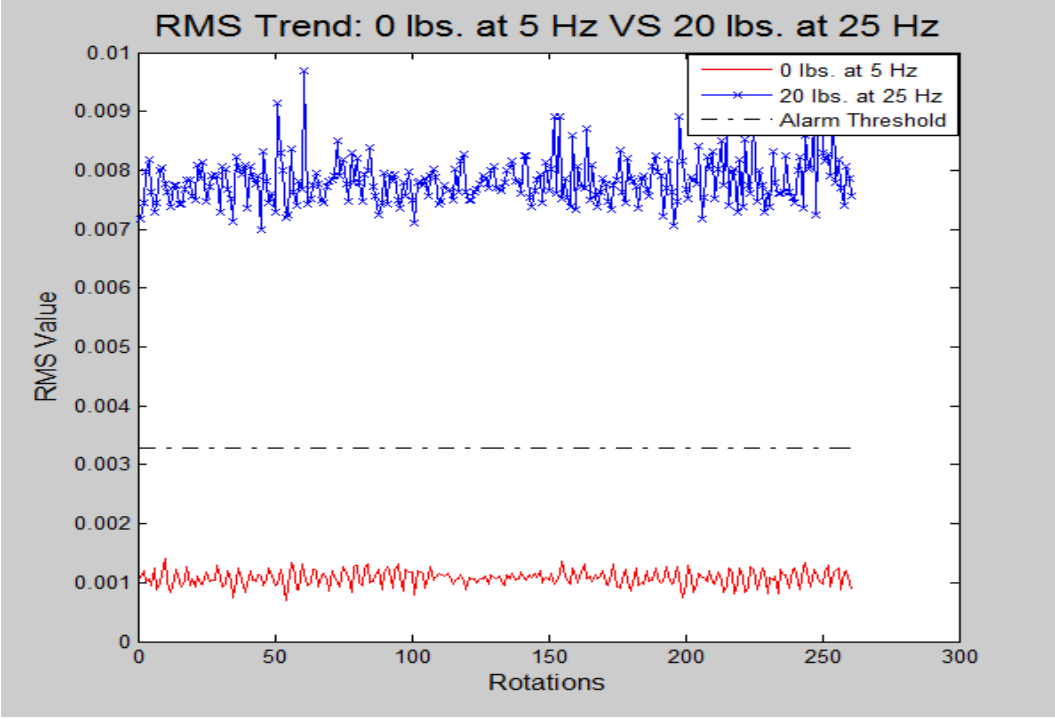

Figure 3-13: Limitation of Alarm-based Approach

Now when the duty cycle is changed such that the experimental apparatus is running at 25 Hz with 20 lbs. radial load, the resulting vibration waveform is amplified as shown in Figure 3-13 with average RMS of 0.0075. Clearly, this change in duty cycle increased the average RMS of the vibration waveform causing the implemented monitoring system to issue a false alarm. This demonstrates how alarm based monitoring systems have difficulties discriminating vibration signal changes that are due to duty cycle variation from those caused by structural damage.

3.2.5 Application of Proposed Algorithm Using Rail-Veyor™ Data

In order to test the performance of the proposed algorithms for CM of the Rail-Veyor™ drive stations, we need data sets representing different drive station faults; chipped gears in the gearbox, race fault for the motor outboard bearing, etc. Given the size of the drive station components; 500Lb industrial gearbox and 100 HP AC motor, physically inducing faults *in-situ* is not practical.

Even though, the experimental setup shown in Figure 3-11 sufficiently replicates the simultaneous loading of two identical bearings, the setup is fairly limited in the amount of loading that can be applied on the bearings; especially compared to the loading capacity of 1'' bore ball bearings. Additionally, the setup didn't allow for simulating the continuous load and speed variation typically experienced in the duty cycle of non-stationary machinery. Finally, the setup only allowed for the investigation of bearing faults in the absence of other deterministic vibration signals commonly encountered in a gearbox; vibration due to gear meshing.

From the previous discussion, it should be obvious that the vibration signal obtained from the inboard bearing of the drive station's gearbox would be significantly different from the signal obtained using the aforementioned simplified experimental setup. This could be attributed to numerous reasons including the lower signal to noise ratio encountered during field data collection and the inherent construction difference of the drive stations. As such, even though the statistical correlation algorithm presented in section 3.2.1 was successful in detecting bearing faults for the experimental setup, its performance in detecting drive-stations faults is still questionable.

Consequently, a new experimental setup was needed to reflect the complexities associated with the operation of the Rail-Veyor™ drive station. The new setup was required to incorporate two separate drive stations including a variable speed electric prime mover, a gearbox, and a variable load. By continuously controlling the speed and loading for both drive stations, the non-stationary duty cycle of the Rail-Veyor™ drive stations can be simulated. Additionally, the smaller scale of the experimental drive stations should make the process of fault seeding more practical.

The details of the new machinery fault simulator are presented in the next chapter including the design, component selection and manufacturing of the station's different sub-systems.

Chapter 4

4.0 Design and Fabrication of Experimental Apparatus

In the ideal case, the performance of a newly developed condition monitoring system for a certain machine should be determined by implementing the solution to the said machine. In this process, a test matrix is constructed such that the monitoring solution is applied for different machinery conditions with the aim of confirming that the solution can successfully detect faults. This testing process is even more involved in the case of monitoring variable duty machinery such as the ones addressed in this thesis. For such class of machinery, the test matrix should be expanded to include the ranges of possible different load and speed operating conditions.

Substantial practical considerations can sometimes limit the use of the actual machine to be monitored for the solution testing phase. Most importantly, intentionally seeding a fault in the actual machine can be unattractive from both an economical and practical considerations. Consider the development of a monitoring system to detect gearbox failures for the Rail-Veyor® drive stations. Fault seeding the station's gearbox involves total disassembly of the drive station, transporting the gearbox to the workshop and disassembling the gearbox. For every different fault tested, this whole process has to be repeated thus affecting the system's operation and the mine's production cycle. As such, scaled-down experimental setups are commonly used in the development of fault detection systems.

This chapter presents the development of a flexible machinery simulator that has been designed and fabricated to replicate, as closely as physically possible, the operation of the Rail-Veyor®

drive stations. The most important objective of the design was to replicate the parallel system arrangement used for the systems such as the Rail-Veyor® stations and the observed duty cycle.

4.1 Overview of Fault Simulators Used in the Literature

The need to replicate different machinery faults over a range of operating conditions necessitated the development and use of machinery fault simulators for the development of condition monitoring techniques. Different fault simulators can be seen in the literature with a range of features and capabilities corresponding to different design requirements. The simulators overviewed in this section can be classified into two main groups: highly specialized simulators developed to simulate specific machinery and flexible tabletop simulators used in a laboratory setting.

4.1.1 Specialized Test Stands for Fault detection

This class of fault simulators generally share the following features in common: they are specially designed to simulate a certain machine, they are fairly large in size thus capable of simulating realistic machinery loads and they are mostly significantly expensive. Such simulators are commonly found in fault detection research in the energy and aerospace domains.

Shown in Figure 4-1, a gearbox test stand is used by the United States National Renewable Energy Laboratory for developing fault detection algorithms to monitor the operation of wind turbines gearboxes. This setup was used to generate the 'Wind Turbine Gearbox Condition Monitoring Round Robin Study – Vibration Analysis' technical report funded by the United States Department of Energy [52]. This specific Round Robin project involved the collaboration

of sixteen partners including seven universities and nine private sector companies such as General Electric. The results of the aforementioned technical reports were formulated into recommended maintenance practices for the wind turbine industry.

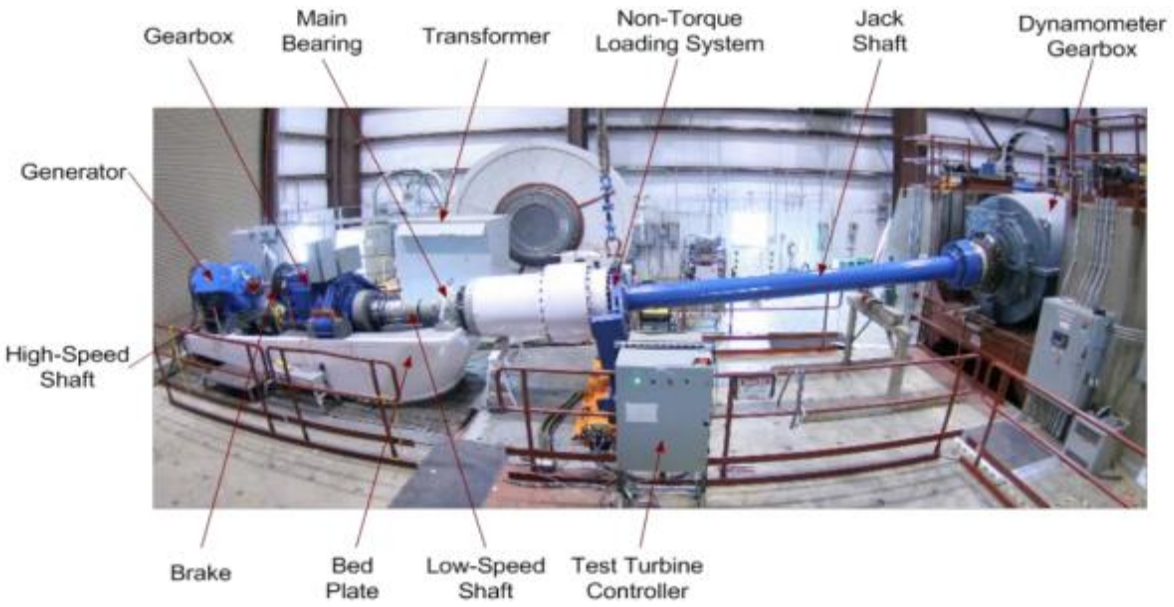

Figure 4-1 Wind Turbine Gearbox Simulator Used by the National Renewable Energy Laboratory (taken from [64])

Another example for specialized test stands used in condition monitoring research can be found in aerospace applications such as the Tail Rotor Drive Train (TRDT) test stand used at the University of South Carolina to develop fault detection techniques for the AH-64 “Apache” tail rotor drive train [53]. As shown in Figure 4-2 the TRDT test stand truly replicates the rotor drive system used in the Apaches featuring all six tail rotor drive shafts, both the intermediate and tail rotor gearboxes and the swashplate assembly. Using a motor-generator setup, the aforementioned system is powered and loaded by 800 HP AC motors generating 1200 ft.lb of torque. By allowing multiple drivetrain components to be evaluated simultaneously under realistic loading,

the TRDT setup has been used for generating research data sets used to develop different TRDT monitoring techniques such as the ones presented in [53], [54], [55], and [56].

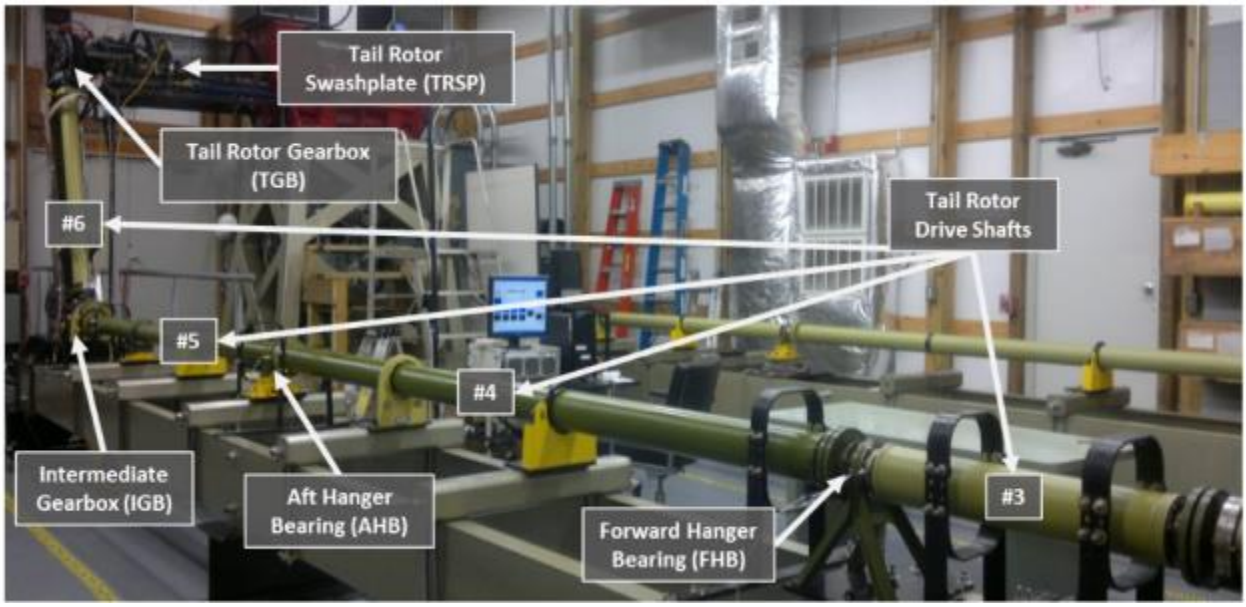

Figure 4-2: Tail Rotor Drive Train Test Stand at the University of South Carolina (taken from [65])

4.1.2 Flexible Table-top Simulators

In contrast to specialized test stands, this class of simulators feature simpler modular design providing a less expensive option for academic fault detection research on bearings and gearboxes. The simpler setup allows the simulator to be small enough to fit on a table and modular enough that component replacement can be done in minutes. Even though this type of fault simulators lacks the ability to simulate real-life loads and duty cycles, their simple construction allows them to generate smooth baselines with high signal to noise ratio by avoiding the use of complex mechanical components.

As an example, the SpectraQuest MFS shown in Figure 4-3 is typically used as an educational vibration trainer. Similar to the fault simulator used in Chapter 3, the MFS can be used to simulate bearing faults, shaft faults, belt drive faults and gearbox faults. As an educational kit, the MFS is sold with a set of faulted components that can be easily used to simulate different faults thus making the MFS a valuable educational tool in vibration monitoring.

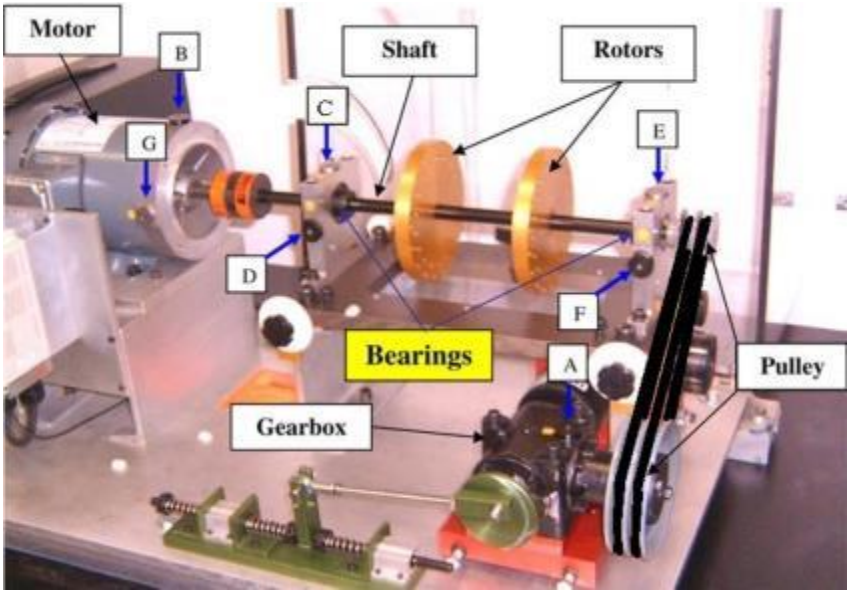

Figure 4-3: SpectraQuest MFS Machinery Fault Simulator (taken from [57])

The simple construction and modular design of the MFS allows it to be used as a research tool for fault detection research. For instance, the same simulator was configured to simulate bearing faults for Chapter 3 in the thesis at hand. S. Zhang [58] and I. Bozchalooi [59] among others also used the SpectraQuest MFS for research on bearing fault detection. Using a different configuration, the MFS was also used by A. Purvee and G. Banerjee [60] to investigate squirrel-cage motor faults.

As presented in subsection 3.2.5, the SpectraQuest simulator was limited in its capabilities to simulate parallel simultaneously-loaded machinery studied in this thesis. The setup didn't allow for simulating the continuous load and speed variation typically experienced in the duty cycle of non-stationary machinery and only allowed for the investigation of bearing faults in the absence of other deterministic vibration signals commonly encountered in a gearbox; vibration due to gear meshing. As such, the following subsection presents the need for a new custom fault simulator and presents the required design specifications.

4.1.3 The Need for a Custom Test Stand

Lacking a gearbox and the ability to simulate parallel drive stations, the experimental setup presented in the previous chapter had to be replaced with a new experimental apparatus. The main design objective for the new simulator is to have parallel drive stations with identical subsystems sharing the same duty cycle in terms of loading and speed. To replicate the operation of most industrial gearboxes, each subsystem should encompass a prime mover, a transmission unit and a load. Additionally, provisions must be made to ensure that the loading and speed of each station can be continuously variable to simulate the operation of continuously variable machinery.

Given that the simulator is mainly used to represent machinery operating over different health conditions, ease of access is crucial to allow for component replacements. Furthermore, the mechanical design must be rigid enough to allow for safe continuous running of faulted systems. Finally, the design must be easy to manufacture, install and should fit the given grant budget.

The development of this new simulator involved the design, validation, fabrication and setup of a fully instrumented mechanical test stand loaded by a mechatronically controlled custom hydraulic loading circuit in order to meet the following design objectives:

- True replication of the parallel system arrangement used in the Rail-Veyor™ drive station design
- Capable of simulating repeatable different loading and speed profiles in a continuous manner
- Capable of simulating realistic speed and loading scenarios for target machinery
- High precision setup providing smooth repeatable baseline operation
- Modular design allowing for continuous modifications and upgrades
- A mechanical design that is highly accessible such that component replacement does not require disassembly
- Full instrumentation with data logging capabilities
- Highly flexible allowing for simulation of different faults whether individually or concurrently including bearing, gear, motor, hydraulic and belt drive faults

The following sections will cover the design, fabrication, validation and setup of the different subsystems making up the newly developed flexible fault simulator.

4.2 Design Overview

The gearbox fault simulator shown in Figure 4-4 represented the first starting point for the new apparatus design. In the previous arrangement, the simulator featured a motor-generator setup in

which a 20HP AC motor was coupled to a 50HP loading generator through a 3:1 reduction gearbox. With a prime mover, a transmission unit and a load, the previous setup featured all of the fundamental components Rail-Veyor® drive station. Still, the previous configuration could not replicate the parallel system arrangement used for the Rail-Veyor® stations. As such, the previous gearbox simulator had to be fully redesigned.

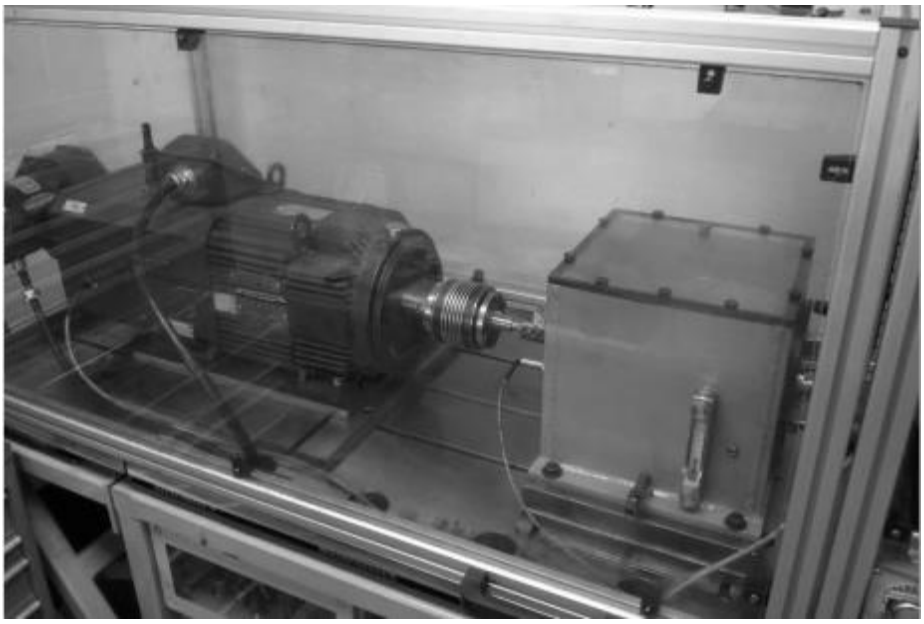

Figure 4-4: Motor-Generator Setup for Gearbox Fault Simulator

The final design shown in Figure 4-5 incorporated two identical substations each powered by an AC motor and loaded by a hydraulic gear pump. The power from the motors is transmitted through a custom-made single stage reduction gearbox and a multiple-pulley automotive accessory drive system. The end result is a flexible machinery simulator that truly represents the parallel operation of the simultaneously loaded machinery with a flexible configuration that can be used to replicate different component faults including gears, bearings, shafts, belts, hydraulics

and electrical components. The design is modular allowing for future upgrades and provides easy access for component replacement to facilitate the process of fault seeding.

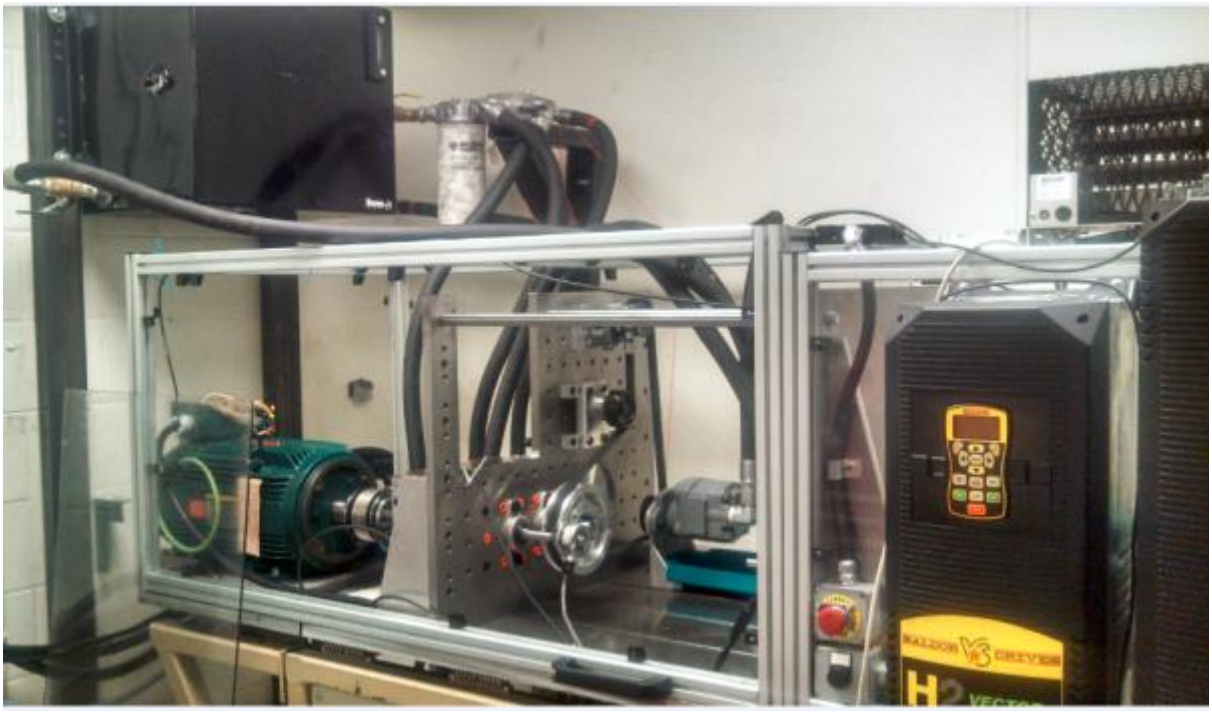

Figure 4-5: The Flexible Machinery Fault Simulator with Two Parallel Drive Stations

Finally, the machine was built under a research grant by a research student with minimal machining experience. Thus, the machine was designed such that it was relatively easy to fabricate, install. Moreover, expenses were controlled by utilizing existing components whenever possible such that costs fall within the given grant budget.

4.2.1 Overall Mechanical Design

One of the design challenges was to minimize the foot print of the mechanical system given the limited bench space. Therefore, the custom-made gearbox and the new serpentine belt drive

system were combined into a single transmission system by bolting the gearbox to the front plate.

A complete parametric CAD model was created for the mechanical system using SolidWorks. As shown in Figure 4-6, both drive stations are identical in configuration and thus faithfully represent the arrangement of parallel machinery such as the Rail-Veyor's drive stations. The simulator was designed such that the left drive station is designated for fault seeding. Therefore, the left front plate was configured to have 10''×12'' (253×304.8mm) rectangular cut placed at the gearbox side to facilitate access for component replacement. The negative of effect of such rectangular cut is that it would reduce the stiffness of the plate which could potentially induce unwanted structural resonance. This however was corrected by bracing both front plates together using tire rods for the physical setup.

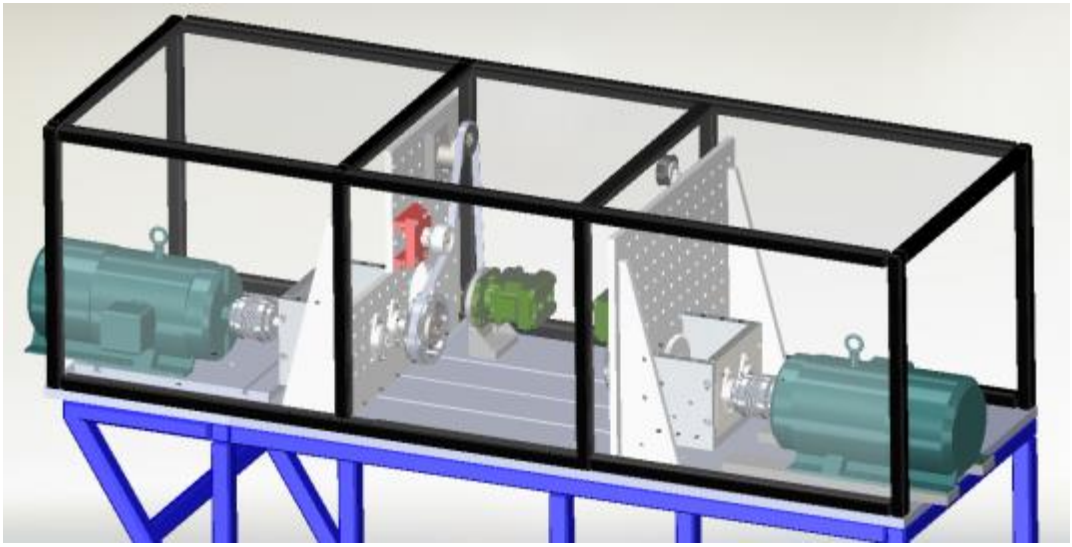

Figure 4-6: Final Mechanical Design for the Flexible Machinery Simulator in SolidWorks™

The following sections will cover a detailed presentation of the mechanical, hydraulic, instrumentation and control design of the new simulator

4.3 Mechanical Sub-systems: Prime Mover and Transmission

4.3.1 Prime Movers

Due to the high reliability of Alternate Current (AC) motors, the new simulator was designed to use induction motors as prime movers. Additionally, the Variable Frequency Drivers used in the previous gearbox setup could be easily modified to allow for continuous speed control of both drive stations in the new flexible machinery simulator.

As previously mentioned, one of the design objectives was to control expenses by utilizing existing machines and components. This objective was met by using an existing set of Baldor Reliance® 10 HP AC motors as the prime movers for the new machinery simulator. The specifications of the motors used are listed [61]:

- Power: 10 HP (7.46 kW)
- Number of Poles: 4 Poles
- Speed at 60 Hz: 1800 RPM
- Rated Torque: 30 lb.ft (41 N.m) at 1800 RPM

In a previous study, a set of five identical Baldor motors were obtained for Motor Current Signature Analysis (MCSA) research. During that past research, three of the 10 HP Baldor motors were intentionally faulted and the remaining two were untouched.

Utilizing the fault free 10 HP motors as the prime movers for the new simulator met the design objective of using identical components for each drive station. Additionally, the remaining three faulted motors can be used to test the performance of the similarity-based fault detection algorithm in detecting motor faults. This could be done by simply replacing one of the healthy motors with a faulted motor of the same model. This increases the flexibility of the new fault simulator by allowing it to be used for future motor fault detection research.

As presented in Figure 4-7, induction motor faults are generally classified as either mechanical or electrical faults [62]. Significant research efforts have been put into the online detection of motor faults such as presented in [63], [64] Generally, state of the art fault detection strategies encompass mechanical fault detection through vibration signal analysis and electrical fault detection through MCSA. Lately, new research is aiming to utilize the MCSA techniques for the detection of motor mechanical faults based on the fact that mechanical faults would cause fluctuations in the air gap between the stator and the rotor assembly. Such air gap fluctuation induces changes in the magnetic flux that can be detected through MCSA as done in [65].

By utilizing the set of 10 HP motors previously mentioned, the new flexible fault simulator can be used for the analysis of existing induction motor fault detection algorithms. Additionally, by incorporating two simultaneously loaded identical induction motors, the new simulator opens the door for new algorithm developments that can utilize the loading similarity between the motors for fault detection in non-stationary operation.

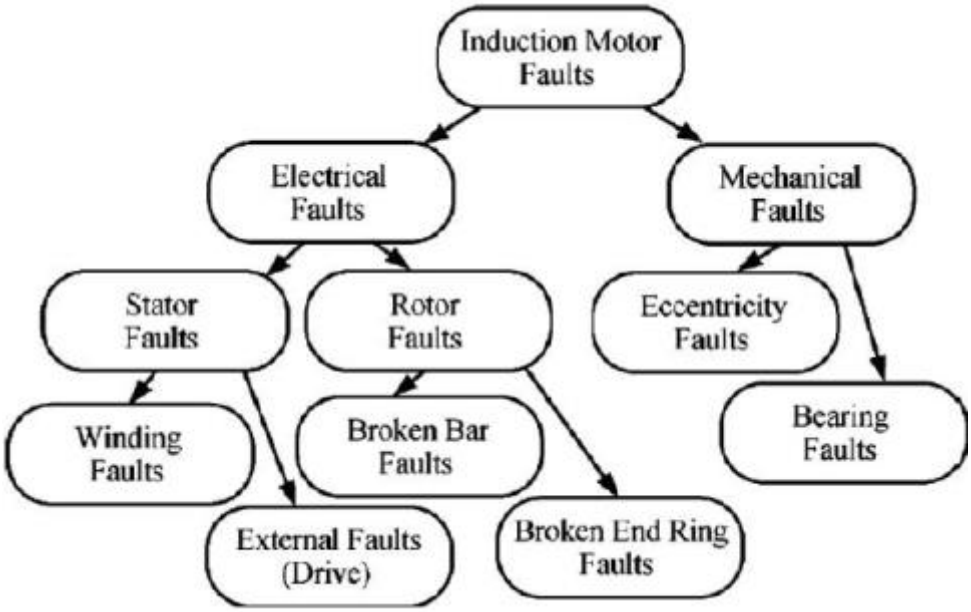

Figure 4-7: Electrical and Mechanical Faults in Induction Motors (taken from [62)])

4.3.2 Fault Simulator Gearbox

Most industrial mechanical setups will eventually include a transmission system for load or speed manipulations between the prime mover and the load. As such, research in gearbox fault detection represents an integral part of the CM literature. The majority of gearbox fault detection algorithms presented in the literature have been developed using experimental test benches.

The simplicity of spur gears makes them an excellent choice for the validation and development of gearbox fault detection algorithms. For instance, in the previous fault simulator configuration the single stage reduction spur gearbox shown in Figure 4-8 was successfully used in developing several fault detection techniques such as [65], [66] and [67]

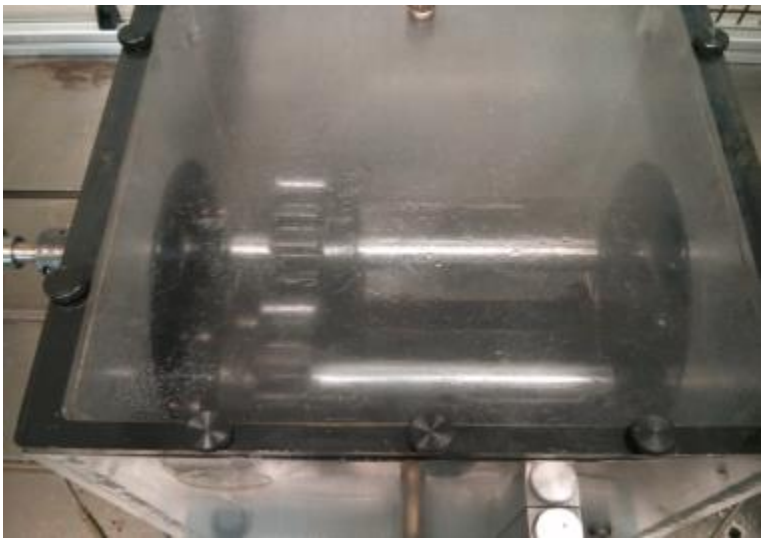

Figure 4-8: Gearbox from Previous Simulator Setup

Even though the experimental gearbox used in the previous setup was specifically designed to be easily accessible for the gear replacement process, the gearbox was oversized compared to the bench eliminating the possibility of adding another identical gearbox for the second drive station. As such, it was decided that a different gearing system is needed. An initial candidate was the HUB CITY bevel gearbox shown in Figure 4-9. This gearbox was included in the table-top SpectraQuest fault simulator presented in Chapter 3 and came with different sets of faulted gears making it a good choice for a fault detection oriented gearbox.

Figure 4-9: Hub City Model 44 Gearbox (taken from [68])

With a cost of $640 CAD each, a total cost in excess of $1285 CAD was required for the simulator's transmission system. Another point to notice is that fault detection experiments with gearboxes involves the experiments with faulted bearings and faulted gears. As such, the aforementioned $1285 CAD cost did not include the costs of acquiring faulted gear and bearing sets for experimentation.

Given that one of the design objectives was to minimize expenses by utilizing existing machinery and components, it was decided to design and fabricate two identical gearboxes that would utilize the same gears used in the previous simulator setup and the same set of ERK-16 bearings from the experimental setup presented in Chapter 3. This way, the existing set of faulted gears and bearings can be used with the new simulator for future fault detection research.

Custom-made Gearbox

The main design objectives for the new gearboxes were ease of component replacement and utilization of existing gear and bearing sets. In contrast to a safety factor of 3.0 typically required for drive system design, a low safety factor is needed for the gear arrangement in the simulator such that induced faults can actually affect gear meshing to levels detectable through vibration analysis. Given that both gear geometry and material were already fixed, the same as the gear set from previous setup, changing the gear face width represented the only way to minimize the safety factor of the gears. As such the gears used for the simulator's gearbox were specified to have a face width of face width of 0.5'' (12.69 mm) which yielded a lower safety factor of 1.1 needed for fault detection experiments.

The designed gearbox used a set of aluminum bearing flanges such that the vibration measurement could be done directly on the flange for each bearing. For the design shown in Figure 4-10, the use of bearing flanges increased the accessibility of the gearbox significantly where bearings could be easily changed by unbolting the flange without having to disassemble the gearbox.

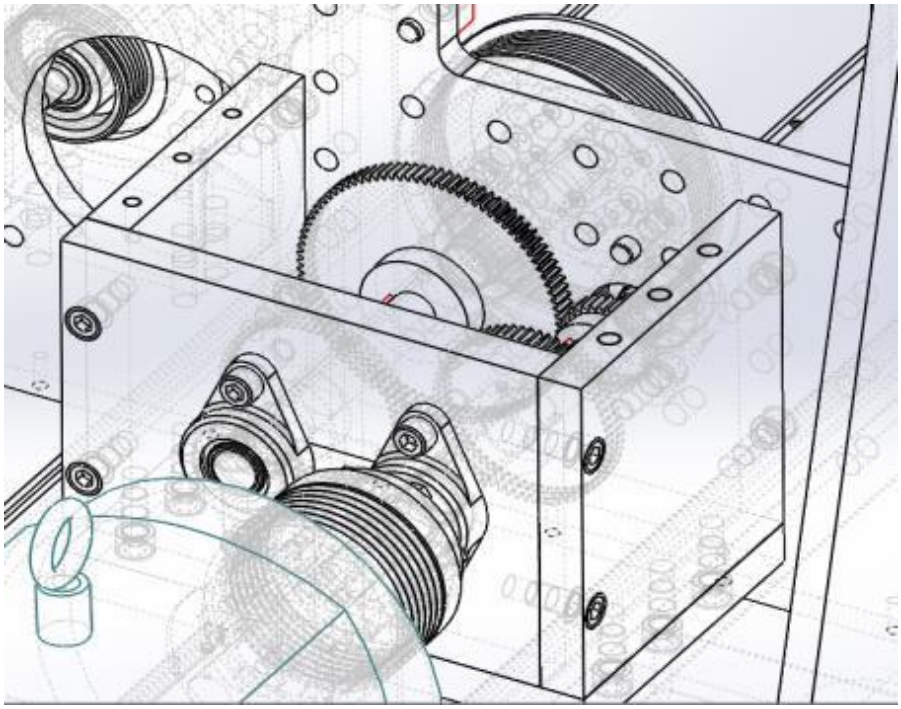

Figure 4-10: CAD Model of Custom Made Gearbox

4.3.3 Serpentine Belt Drive

With a gearbox to transmit torque from the prime mover to the load, the transmission system design should have been complete. However, it was decided to extend the transmission system to include a serpentine belt drive. Firstly, the addition of a belt system would increase the flexibility of the new experimental rig allowing the flexible fault simulator to be used in the development and validation of fault detection techniques for automotive accessory drive system. Secondly, the research group was able to obtain a set of factory-faulted serpentine idlers from Litens Automotive. This set of idlers is of significant use for future automotive accessory drive fault detection research.

As it will be presented later in this chapter, truck gear pumps were used as loading systems for each drive station. Therefore, it was decided that the serpentine belt system arrangement should reflect the arrangement used to drive automotive hydraulic power steering pumps.

Several constraints dictated the geometrical design of the simulator's serpentine system. The space available on the simulator's table limited the centre distance between the driver and driven pulleys to be less than 16 inch (406.40 mm) minus the driven sheave diameter. An existing pair of Aluminum K-section pulleys was used with modified bushing to fit the new simulator and the driven pulleys were salvaged from a Ford Dually belt tensioner.

Given the previous design constraints, the challenge was to configure each drive's serpentine system such that a 6.4'' (162.56 mm) eight groove K section pulley was used to drive a 2.8'' (71.12 mm) pulley with a maximum centre distance of 13.2'' (335.28 mm) for each drive station. Inspired by the serpentine configuration of automotive accessory drives, the serpentine drive system shown in Figure 4-11 was designed for the new machinery simulator.

With a total of four pulleys, the setup used a 6K belt with an outer circumference of 62 inches (1574.80 mm). According to [69], the current wrap angles are in the standard range with angles of 148.5° and 90° at the gearbox and pump pulleys, respectively.

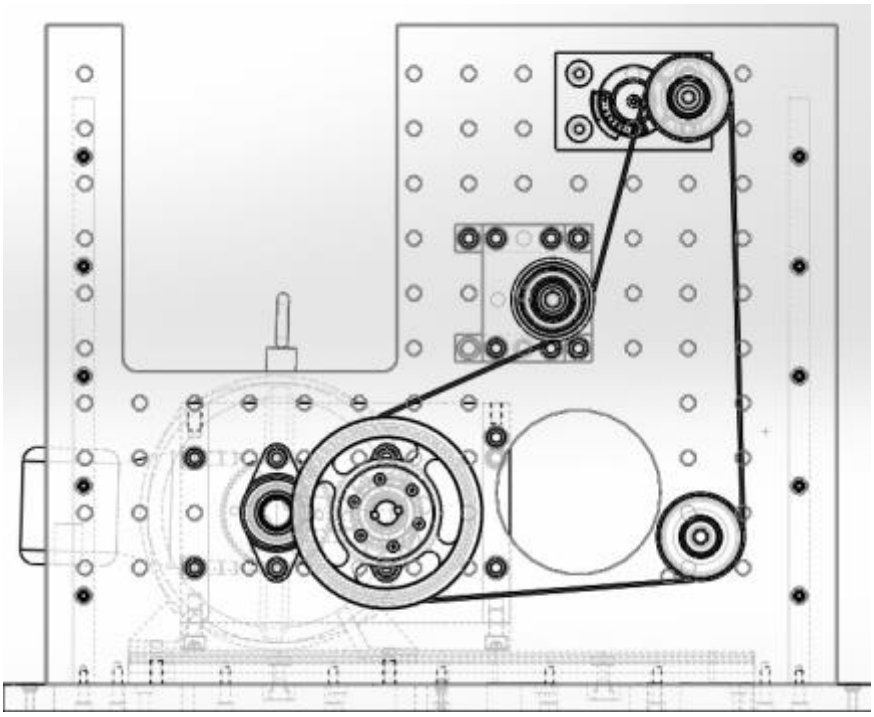

Figure 4-11: Serpentine Belt Configuration for the Flexible Machinery Simulator

4.4 Mechanical Sub-systems: Fabrication and Setup

The process of fabricating the custom made gearboxes, the front plates, the motor mounts and accessory drive fixtures was completed by the author in the university's workshop shown in Figure 4-12. This section covers the fabrication and installation processes required to develop the flexible simulator shown in Figure 4-5.

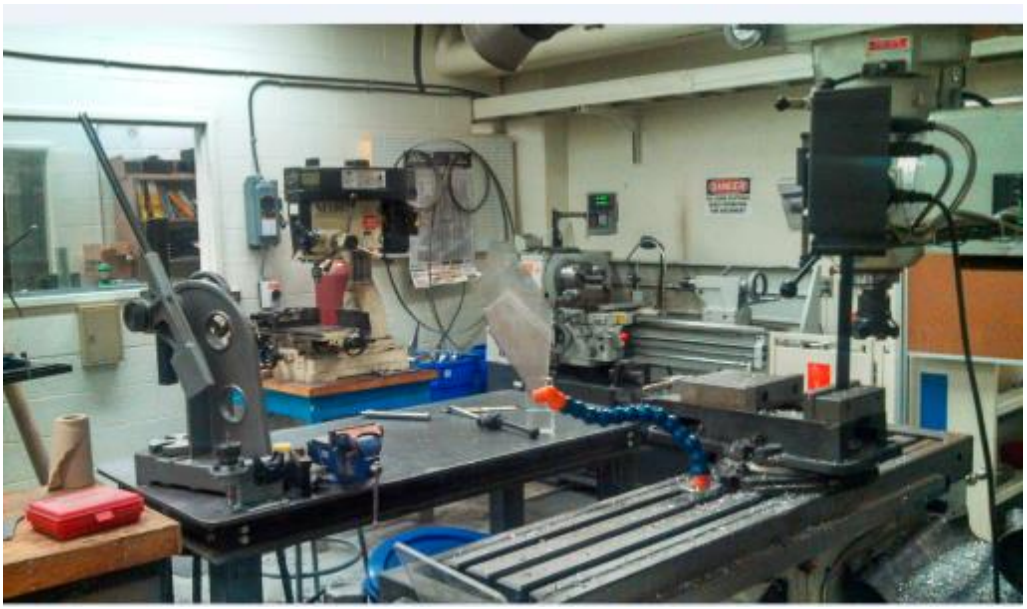

Figure 4-12: Laurentian University Workshop

4.4.1 Front Plate Fabrication

The front plate shown in Figure 5-13 has been fabricated out of a 29”×29” (736.3×736.6 mm), 0.75” (19.05 mm) thick Aluminum plate. As with the majority of fabricated components, Aluminum T60 was chosen for ease of fabrication. Making the plate involved drilling a hole pattern of 88 holes 27/64” (10.71 mm) in diameter. The holes were then tapped for 1/2’’ (12.70 mm) bolts. The purpose of this hole pattern is to provide an opportunity to experiment with serpentine fixture location. Additionally, the hole pattern increases the flexibility of the simulator by allowing additional components to be attached to and repositioned to the front plate easily.

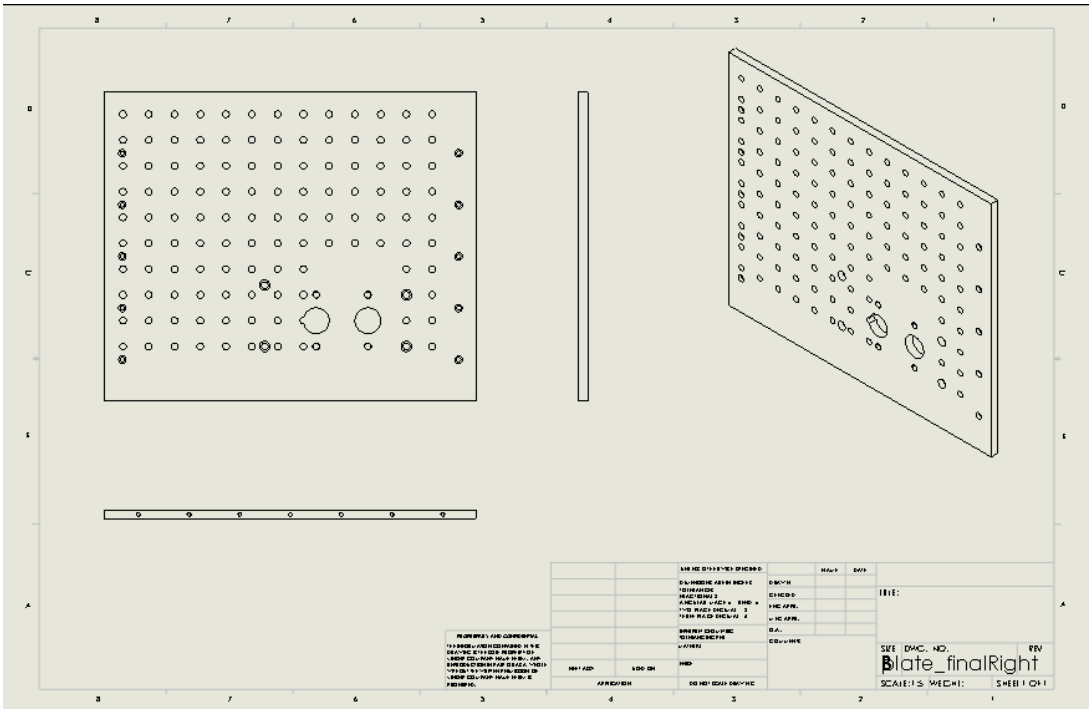

Figure 4-13: Front Plate Work Drawing

The front plate was secured to the bench table using seven M8 bolts at the base of the front plate. Additional support was accomplished by using the aluminum ribs shown in Figure 4-14 to support the front plate at the sides. Both ribs were also made out of an aluminum stock plate and were bolted to the table using two M8 bolts each. A total of 10 countersunk holes were drilled in the front plate to support it to the ribs at the sides.

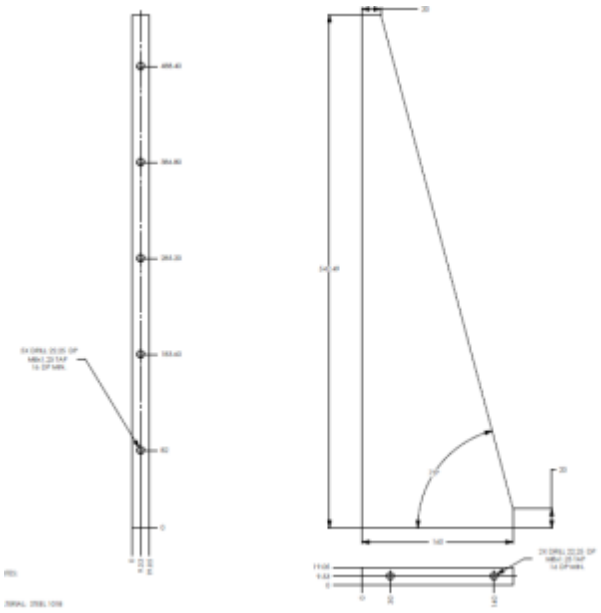

Figure 4-14: Front Plate Ribs

In order to rigidly attach the custom made gearbox, a total of four countersunk holes were drilled such that 1/2'' (12.70 mm) bolts can be used to fix the gearbox. Additionally, two 2" (50.80 mm) holes were drilled through the front plate to make clearance for the gearbox shafts and four 13/16" (20.64 mm) holes were drilled and tapped to attach the gearbox bearing flanges.

4.4.2 Gearbox Fabrication

Each of the custom made gearboxes shown in Figure 4-10 was made up of four rectangular 1" (25.40 mm) thick aluminum plates. The plates were bolted together using a total of ten 1/2'' (12.70 mm) bolts. All holes were countersunk such that socket cap head bolts were used. At the backside of the gearbox, a bolt pattern was used to fix the bearing flanges. The total length of the gearbox from front plate to backside is 8" (203.20 mm) . Even though the gears used were only 2 inch's thick (50.80 mm) (face width is 0.5''(12.70 mm) and collar is 1.5" (38.10 mm)) the

extra space in the gearbox allows several gears to be attached to each shaft such that the process of switching from healthy to faulted gear is simplified to just moving a different gear into mesh without the need to open up the gearbox for gear replacement.

Given the criticality of shaft alignment within the gearbox, all eight gearbox aluminum plates were machined in a vertical CNC mill using the Mastercam NC program. Both gears used 1'' (12.70 mm) shafts that were turned and keyed in order to couple the input shafts to the motor couplers and to the serpentine drive pulleys.

Figure 4-15: Cast Aluminum Bearing Flanges

To support the shafts, cast aluminum bearing flanges (Figure 4-15) were used to hold the rolling element bearings. Each of the eight flanges for the gearboxes was bored on a lathe to fit the bearing. The boring process had to be precise given that the bearings were designed to be press fit into the flange. As such, the flanges had to be turned such that the flange bore was exactly 3 thousands of an inch less than the bearing diameter. After bolting the flanges to the gearboxes

and the front plates, dowel pins were used to locate the bearing flanges to ensure that subsequent disassembly does not change the flange positions which would affect the shaft alignment in the gearbox.

To prevent oil leak, the gear plates were lined with Room Temperature Vulcanization (RTV) silicone. Additionally, Plexiglass ™ and cork were used to cover both gearboxes (Figure 4-16).

Figure 4-16: Gearbox with Plexiglass™ Cover

4.4.3 Serpentine Belt Posts and Bushings

As a design requirement, the driver pulley attached to the gearbox output shaft shown in Figure 4-10 had to be positioned such that the drive pulleys were at least two inches from the front plates. This space is needed for attaching the accelerometers used to instrument the vibration at the bearing flanges. As such, both the idler pulley and the active tensioners are fixed to spacers attached to the front plate. The spacers were fabricated out of the same T6 aluminum stock used for front plate and gearbox fabrication.

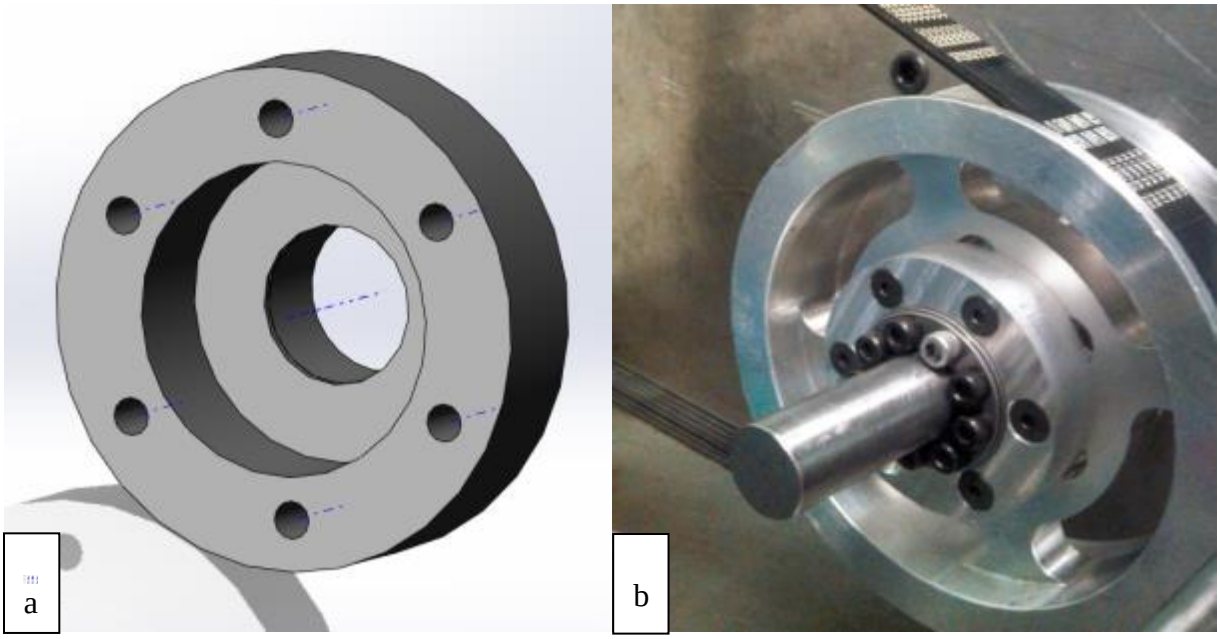

Figure 4-17: One of the Custom-made Bushings for the Belt Drive; (a) CAD model, (b) final bushing

As previously mentioned, the belt drive pulleys had to be modified to fit the new setup. Figure 4-17(a) shows the design for a bushing fabricated to fit the drive pulley to the right-hand drive station shown in 4-17(b). Similar bushings and spacers were fabricated to fit the driven pulleys on the pump shafts and space it out from the pump face.

4.4.4 Setup and Installation

In order to install the completed mechanical system on the test bench, a total of 28 holes had to be drilled and tapped into the existing bench plate using a magnetic drill press. Twelve M8 holes for the front plate, a set of eight 7/16'' (11.11 mm) holes for the AC motor mounts and eight 5/8" (16.12 mm) holes for the pump brackets needed for the hydraulic system presented later in this chapter.

Figure 4-18: Measuring Drive Pulley Run out

Before connecting the electrical motors, the alignment of all components was checked using dial indicators and height gauges as shown in Figure 4-18 to confirm that the actual setup was within tolerances.

As a summary for the machining operations completed during the fabrication stage, Table 4-1 lists the components fabricated and modified by the author of this thesis to fabricate the new simulator.

Table 4-1: Summarized List of Components Fabricated and Modified

Component	Machining Operations	Notes
Front Plate and Ribs	• 3× band saw to cut stock • 110× hole drill, tap and countersink • 4× circular saw cut	Design and fabrication
Gearboxes	• 8× band saw to cut stock • 34× hole drill, tap and countersink • 4× circular hole cut	Design and fabrication
Base Plate	• 27× hole drill and tap	Modification
Motor Mounts	• 2× band saw to cut stock • 8x hole drill and tap	Design and fabrication
Serpentine Belt Fixtures	• 8× band saw to cut stock • 8× vertical mill • 8× hole drill, tap and countersink	Design and fabrication
Drive Shafts	• 4× shaft cut and face • 4× shaft turn • 4× shaft key	Design and fabrication
Pulleys	• 6× stock cut and face for bushings • 6× bushing turn • 6× bushing bore • 2x bushing key	Design and fabrication
Pump Brackets	• 4× hole drill and 2× mill	Modification

4.5 Power Absorption Unit: Hydraulic Dynamometer

In the previous setup shown in Figure 4-4, the 25 HP AC prime mover in the gearbox fault simulator was loaded by a 50 HP AC motor acting as a generator. This motor generator setup is very common and can be found in most research-based fault simulators such as the ones in section 4.1.1. Given that two identical loading subsystems are required for each station, it was determined that the typical motor generator setup would be a challenge considering that all those units have to fit in the 21 ft^2 (6.4 m^2) area of the simulator bench.

As an alternative to the motor-generator setup, a hydraulic system was developed to load the drive stations of the new fault simulator. Referring to Figure 4-19, the hydraulic loading circuit was designed to include two identical pumps sharing a common reservoir and pumping it into a common loading circuit. A proportional pressure relief valve was used to control the circuit pressure and thus load the drive stations. By increasing the circuit pressure, the drive stations connected to the pumps will require more torque to pump the oil into the pressurized circuit at any given flow rate. As such, the hydraulic torque of the pumps acts as a reaction load against the prime movers. The relief pressure was controlled by modulating the current powering the solenoid of the relief valve. This allowed for the continuous load profiling required to simulate non-stationary operation. The components of the circuit are discussed in the following subsections.

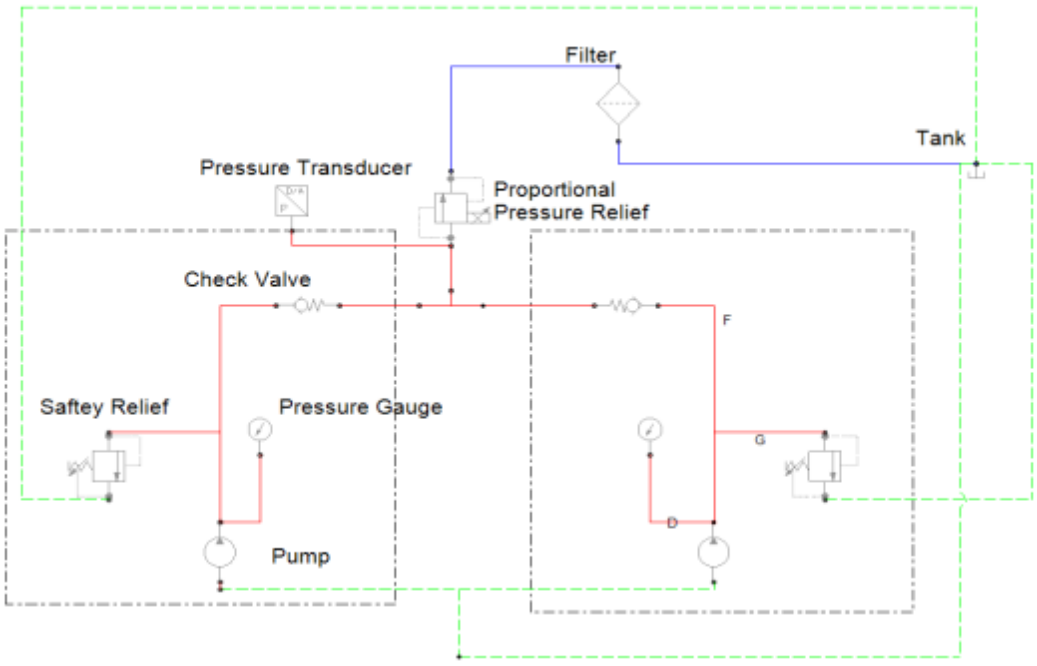

Figure 4-19: Proposed Loading Circuit for the Simulator's Hydraulic Dyno

4.5.1 Hydraulic Pumps

For both pumps, a model MPH20 Metaris ™ gear pump was selected. Typically close coupled to the Power Take Off system in mining trucks, the pumps purchased had to be configured to be belt driven. To this end, the pump was ordered to have a continental shaft supported by an outboard roller element bearing to withstand the hub load in a belt configuration. Table 4-2 lists the specific pump configuration used for the simulator.

Table 4-2 MPH20 Pump Configuration (adapted from [70])

Attribute	**Specification**
Displacement	1.9 in^3 (31.1 cm^3)
Direction	Bi-rotational
Ports	1″ NPT (25.4 mm)
Rated Pressure	3500 psi (241 Bar)
Maximum Speed	2100 RPM

Unlike OEM power steering pumps, the pumps purchased are fully serviceable. With a reliable supply of replacement components, the pumps selected increase the flexibility of the new simulator to include simulation of pump faults. Additionally, with four journal bearings and an outboard rolling element bearing, the selected gear pumps can be used in bearing fault detection research for hydraulic pumps. Figure 4-20 shown the pump rebuild kit obtained including the roller element and journal bearings together with seals and O-rings.

Figure 4-20: Spare Parts Acquired for MPH20 Metaris™ Gear Pumps

As shown in Figure 5-19, the flow from both pumps is delivered into a common loading circuit. In this circuit, a proportional pressure relief valve is used to control the circuit pressure and thus the loading achieved on both pumps. The following section presents the aforementioned pressure relief valve.

4.5.2 Proportional Pressure Relief Valve

Proportional valves are used to control pressure, flow direction, acceleration and deceleration from a remote position [71]. Unlike conventional on/off DC solenoid valves, proportional valves can operate at an infinite number of points within their working range. The operation of proportional valves is controlled by the proportional driver circuit which regulates the current into the solenoid. Through current manipulation, the magnetic field in the solenoid can be used to control the valve's spool position.

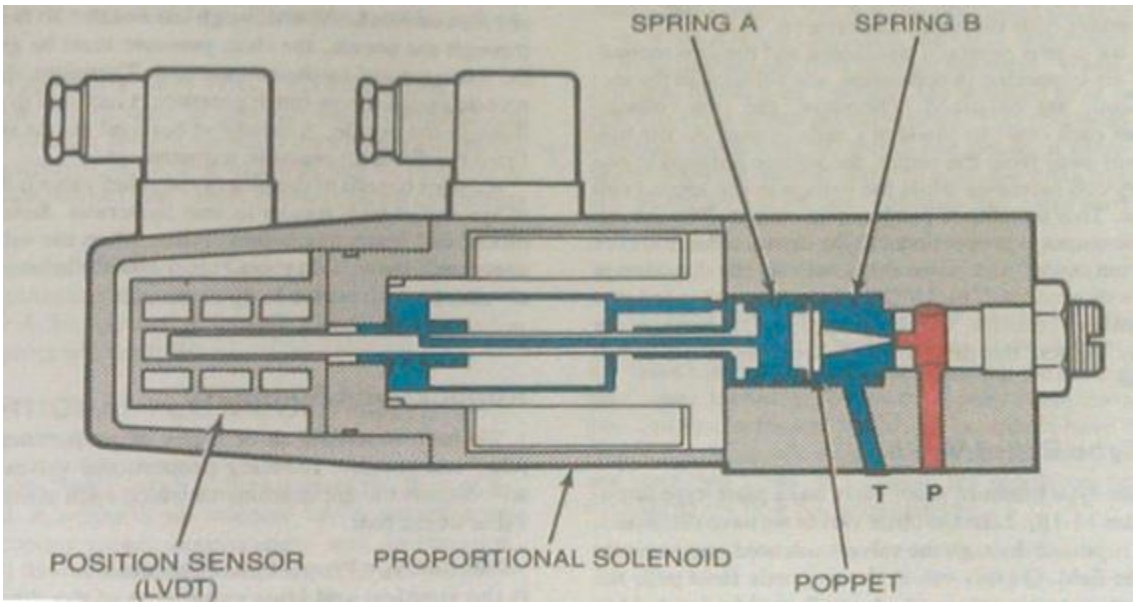

Figure 4-21: Proportional Pressure Relive Valve (taken from [83])

For a poppet-type proportional pressure relief valve such as the one shown in Figure 4-21, the control signal to the valve controls the stroke of the solenoid's push pin. At crack pressure, flow for the high pressure port is diverted into the low pressure one; port T in the figure. When the solenoid is activated, the push-pin compresses spring A and exerts a force proportional to the

excitation. Depending on the current supplied, the valve can relief at infinite number of pressure thus allowing for smooth continuous load profiling.

Shown in Figure 4-22, a TS12-26 Hydraforce® proportional pressure relieve valve was used for the simulator's hydraulic circuit. The valve was configured such that it was normally open. This means that the valve will provide pressure relief at a crack pressure of 72 psi (4.96 Bar) and will only pressurize the circuit when supplied with current. This represents a safety feature that prevents the circuit from over pressurization if power is lost. The specifications of this valve are listed in Table 4-3.

Table 4-3: Hydraforce™ TS12-26 Proportional Pressure Relief Valve (adapted from [72])

Attribute	**Specification**
Rated Flow	50 gallon per minute (189.27 litre per minute)
Maximum Operating Pressure	3500 psi (241.31 Bar)
Maximum Control Current	1.2 A
Coil	12 VDC

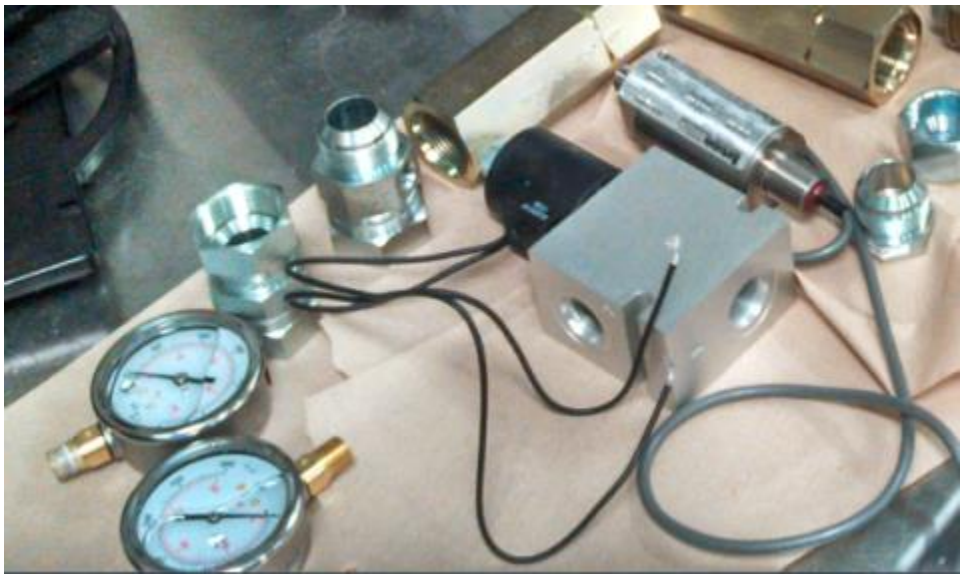

Figure 4-22: TS12-26 Hydraforce® Pressure Relief Valve with Attached Cartridge

4.5.3 Circuit Simulation and Proof of Concept

FluidSIM™ was used in the simulation phase to investigate the performance of several preliminary designs. By simulating and monitoring the pressures and flows for the final circuit shown in Figure 4-23, the following three important design considerations were confirmed. First, the pressure developed by the circuit is transmitted to both pumps equally. Second, the simulation confirmed that when the circuit pressure increased beyond safe operation, the flow is diverted through the safety relief valves. Finally, the check valves used for each pump succeeded in preventing reverse flow into the pumps.

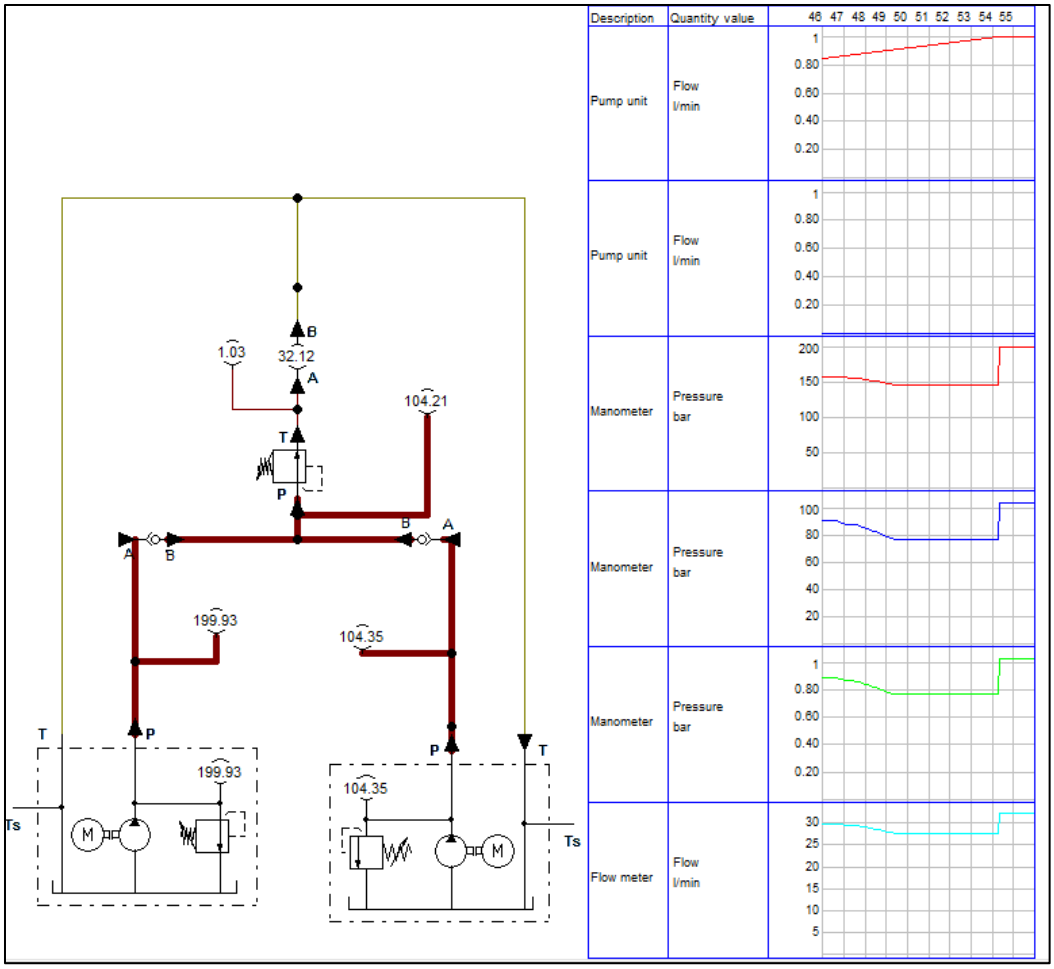

Figure 4-23: FluidSIM™ Simulation for the Hydraulic Loading Circuit

With promising simulation results, a physical prototype was used to test the circuit. A model TP-80 Festo™ hydraulic trainer was configured to replicate the loading circuit shown in Figure 5-19 as shown in Figure 5-24. The configuration featured all the components used in the proposed loading circuit such as the safety pressure relief valves, check valves, tee connection and current-driven proportional pressure relief valve. The physical setup presented an ideal chance to confirm the function of each component in the circuit. For instance, when a check valve for a pump was removed from the circuit, reverse flow was immediately noticed in one of the pumps. The most important conclusion from the circuit was the fact that proportional valves present the

highest pressure drop when compared to other circuit components. This pressure drop is also compounded by losses due to improper hose sizing. For instance, the trainer used 5/8" (16.21 mm) hoses which bottlenecked the combined flow of the two circuits as it emerges from the output port of the proportional valve. This opportunity to get a physical feel of the circuit was important for the design of the physical setup presented in the following subsection.

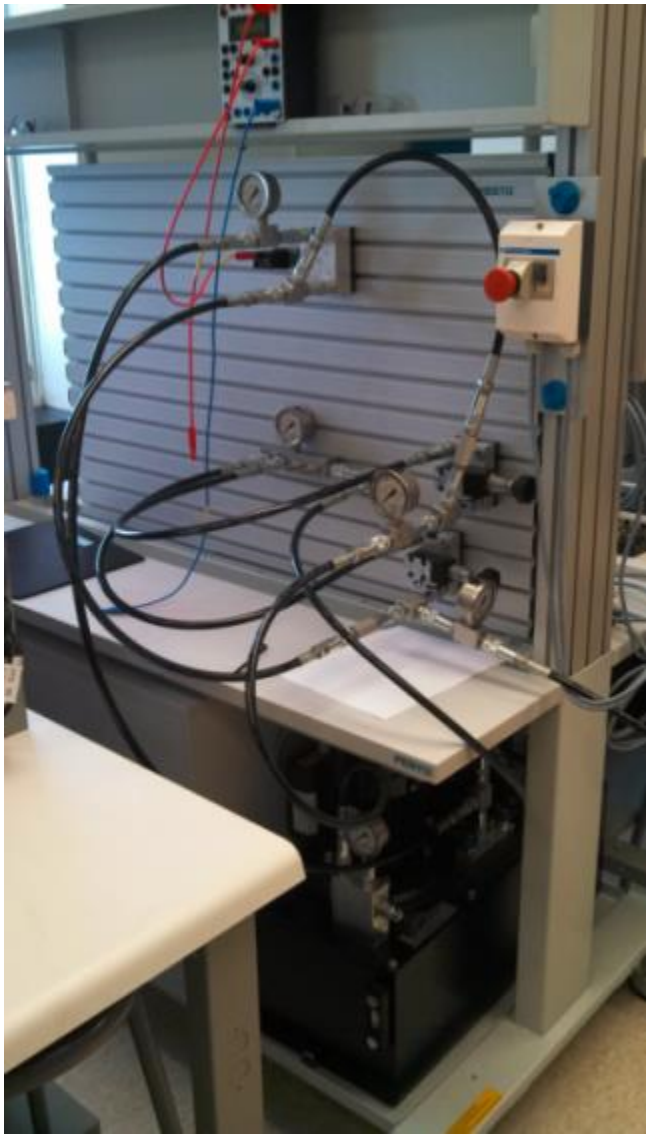

Figure 4-24: Proof of Concept for the Proposed Hydraulic Loading Circuit

4.5.4 Physical Circuit: Implementation and Testing

The parameters of the physical circuit components are determined by the pressure and flow expected in the normal operation range of the loading circuit. The theoretical flow rate Q_T of the positive displacement gear pumps used can be determined using the pump's displacement per revolution V_d in cubic inches and the operating speed N in RPM as shown in Equation 4-1 [73] The hydraulic torque T_T on the other hand is related to volumetric displacement and the operating pressure P as shown in Equation 4-2 [73]

$$Q_T(gpm) = \frac{V_d\,(in^3/rev)\times N\left(\frac{rev}{min}\right)}{231} \qquad \text{Eq. (4-1)}$$

$$Q_T(in.lb) = \frac{V_d\,(in^3/rev)\times P(psi)}{6.28} \qquad \text{Eq. (4-2)}$$

Given that the speed range of the simulator's AC drive, the operating speed and thus flow rates of both pumps were determined using Equation 4-1. For each flow rate calculated, Equation 4-2 was used to calculate the pressures used to generate the variable reaction torque required to load the motors. Using Equations 4-1 and 4-2, a maximum operating pressure of 3000 psi (206.85 Bars) needed to fully load the 10 HP AC motors at 1800 RPM

Using the simulator's drive ratio of 1:0.76 (between the AC motor and the pump) the pump's maximum operating speed was determined to be 1350 RPM for the AC motor's maximum speed of 1800 RPM. At this speed, the flow rate was determined using Equation 4-1 to be 11 gallons

per minute (41.63 litres per min). The physical circuit components selected for the loading circuit are listed in Table 4-4.

Table 4-4: Physical Circuit Components

Component	Model	Specifications
Safety Pressure Relief	Parker RDFA-LAN-CEM	500-3000 psi, 25 gpm
Check Valve	Parker C-1000-S5-SAE	Crack at 50 psi, 25 gpm
Pressure Transducer	Barksdale 420 Series	3500 psi, 12-24 volts
Proportional Relief Valve	Hydraforce™ TS12-26	3500 psi, 50 gpm

Given that the hydraulic circuit had to be placed within the safety cage of the simulator, the physical design of the circuit was geared for space optimization. As shown in Figure 4-25, 90° swivel fittings were used to connect the flow from each pump into the T-section to be diverted to the proportional relief valve. For increased safety, all fittings were chosen to be JIC fittings commonly seen in fluid power applications. The main advantage of JIC type fittings is that they use flared threads that prevent sudden explosion by providing a leak path in case of over pressurization.

The previously mentioned use of 90° fittings increased the sources of pressure drop within the circuit. Combining this with the significant pressure losses encountered with the undersized Festo™ trainer, it was decided that the hoses used for the physical setup should be sized such that hydraulic loses are minimized.

Figure 4-25: Physical Realization of the Circuit

In order to test the physical hydraulic circuit separately, the setup shown in Figure 4-26 was used in a local hydraulic shop. Using an industrial power pack, the circuit was tested and loaded for the first time. A National Instruments PXI portable data acquisition system system was used for instrumentation and control and the data collected confirmed the circuit could be used to subject two separate pumps to equal loading.

Figure 4-26: First Test for the Physical Circuit

4.5.5 Installing the Hydraulic Dyno on the Flexible Simulator

After confirming that the circuit designed met the requirements, the full dyno system was installed for the simulator as shown in Figure 4-27. The setup uses 1'' (25.4 mm) hoses all around to connect the pumps to the circuit and to the tank through a manifold as shown in Figure 4-27. Given a maximum flow rate of 22 GPM (83.28 LPM) for both pumps combined, a 30 Gallon (113.56 Litre) tank was used as a reservoir. The oversized tank minimizes the possibility of cavitation and cooling requirements for a circuit by providing more surface area for convective heat transfer. In order to further minimize the possibility of cavitation, the tank was raised above the simulator bench to gain static head at the suction ports.

Figure 4-27: Circuit Installed on the Simulator's Bench

For safety, the high pressure components of the circuit are restricted into the footprint of the simulator's enclosed cage. Additionally, drip pans are used to contain hydraulic leaks from the pumps or the circuit as shown in Figure 4-28

Figure 4-28: Physical Circuit with Drip Pan

4.6 Instrumentation and Control

In order to replicate the operation of non-stationary machinery, a real-time control system was designed for the new fault simulator such the both the load and speed of the machine can be profiled in a repeatable way. Additionally, an instrumentation system was implemented to monitor the speed, vibration, current and pressure signals of the new simulator. Figure 4-29 presents the data acquisition and control framework implement for the new simulator. The details of this framework are presented in the following subsections.

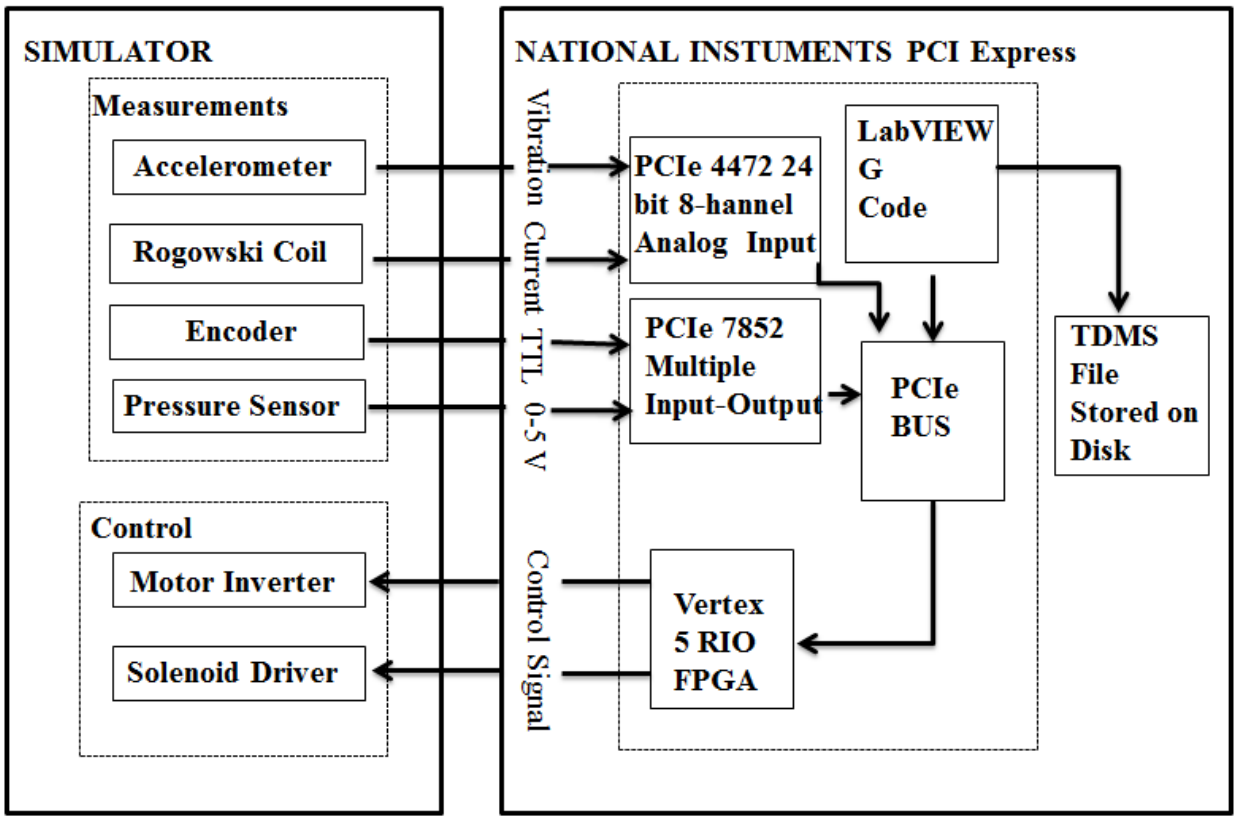

Figure 4-29: Data Acquisition and Control Framework

4.6.1 Control

In order to control both the speed and load profiles experienced by the new machinery simulator, a closed loop PID control system has been implemented in LabVIEW. In the control loop, both the motor speed and the circuit pressure are monitored using an optical encoder and a pressure sensor, respectively. The TTL signal from the encoder is decoded in the control loop to determine the shaft speed and the PID loops is then used to control the motor speed such that it tracks the required profile. On the other hand, the pressure measured in the loading circuit is represented by a 0-10 volts signal from the pressure sensor. Both signals are acquired by the PCIe™ system through a NI7852 MIO card.

The PID loop is hard coded into the PCIe™ RIO FPGA card. The RIO card sends the control signal for the AC motor inverters and the solenoid valve driver shown in Figure 4-30.

Figure 4-30: Simulator Speed and Pressure Drivers; (a) the AC Motor Inverter, (b) Lynch™ Solenoid Driver

4.6.2 Instrumentation

For fault detection purposes, a range of different machinery parameters are constantly monitored in the new machinery fault simulator. The gearbox bearing flanges, serpentine idler posts, motor main bearing and the outboard bearing of the pump are all instrumented with Integrated Circuit Piezoelectric (ICP) accelerometers. Figure 4-31 shows the accelerometer attachment points for the different components of the new simulator. All accelerometers are connected to the high speed analog input card (PXI 4472) using shielded BNC cables and vibration is sampled at a rate of 20 kHz. The high sampling rate is required to ensure that frequencies of interest are not aliased.

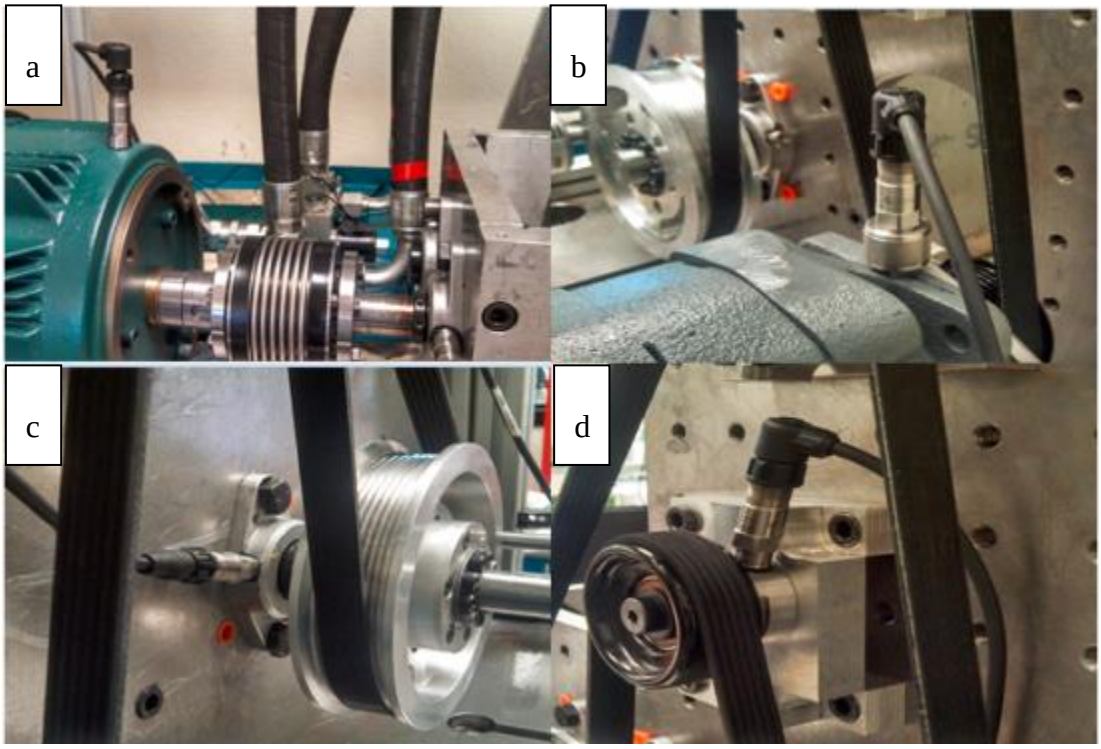

Figure 4-31: Different Accelerometer Attachment Points; (a) Outboard motor bearings, (b) Pump flange, (c) Output gearbox flange, (d) Idler bearing post

In addition to vibration monitoring, the current drawn into the AC prime movers is monitored using Rogowski-coils as shown in Figure 4-32. Like the vibration signals, the current signals are also connected to the high speed analog card through BNC cables and sampling is done at 20 kHz.

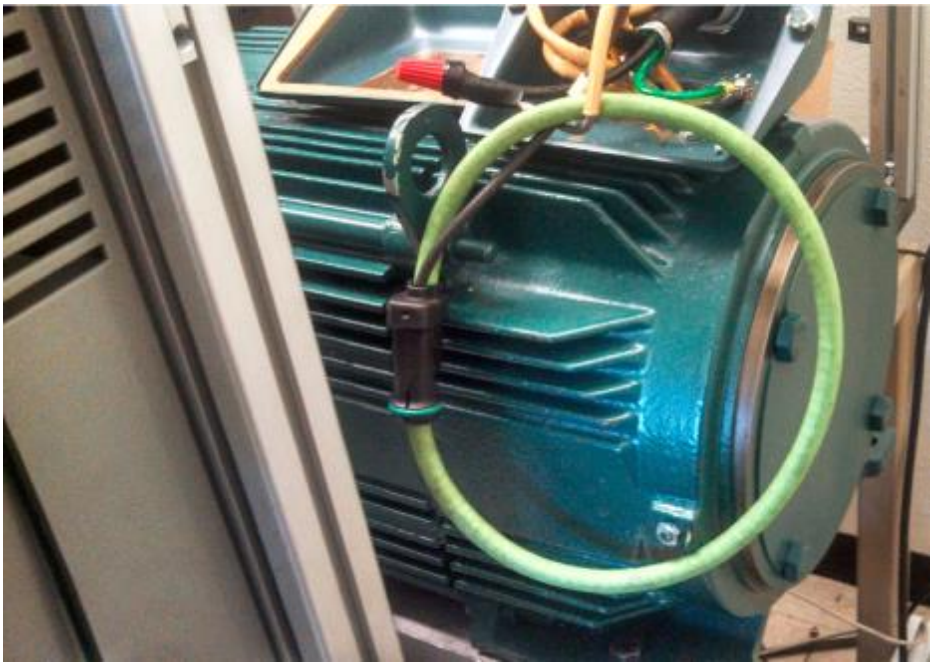

Figure 4-32: Rogowski Coil Installed for the Prime Mover

A BEI high speed Express Encoder™ is used to monitor the motor shaft speed. The TTL signal is acquired through the PCIe™ NI7852 RIO card and decoded in the LabVIEW program. Similarly, the 0-10V pressure sensor signal is acquired by the same card and is used in the control program for load profiling. The rest of the sensors used for the simulator are listed in Table 4-5.

Table 4-5: Sensors Used in New Simulator

Sensor	Excitation	DAQ
Rogawski-coil	External 9V battery	PXI 4472
Accelerometer	External 5V (DAQ card)	PXI 4472
Pressure Sensor	External 12V (power supply)	PXI 6351
Encoder	External 5V (DAQ card)	PXI 6351

4.6.3 Human Machine Interface

A LabVIEW virtual instrumentation panel was developed for the system's user interface. As shown in Figure 4-33, the panel developed presents the use with a set of graphs to monitor the signals acquired. A centre analog dial is used to show the determined speed for the simulator in addition to a numeric indicator showing the load value.

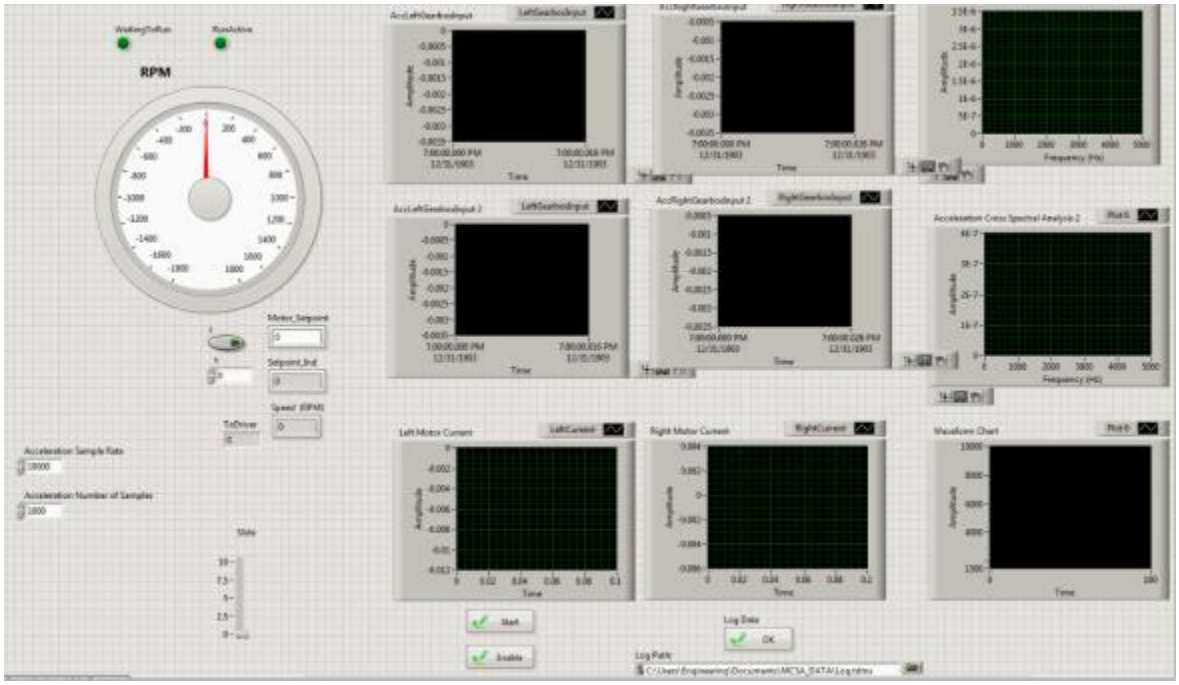

Figure 4-33: User Interface for New Simulator in LabVIEW

Initially, the user selects the filename for data logging, the sampling rate and loads the required speed and load profile. When ready, the user enables the control program such that data collection process is automated. Speed and load profiles can be changed by the user allowing the machine to replicate any desired profile.

The LabVIEW program is divided into two parts. A host program runs on a 3.2 GHz Windows™ machine while the real-time part runs on a Vertex 5 RIO Filed Programmable Gate Array (FPGA). Figure 4-34 shows the wiring diagram for the instrumentation part of the host program. This loop collects and logs data from eight different sensors instrumenting the simulator. Both the acceleration and current signals are collected directly from the high speed analog NI4472 DAQ card. The encoder and pressure sensor signals are collected from the NI7852 MIO card.

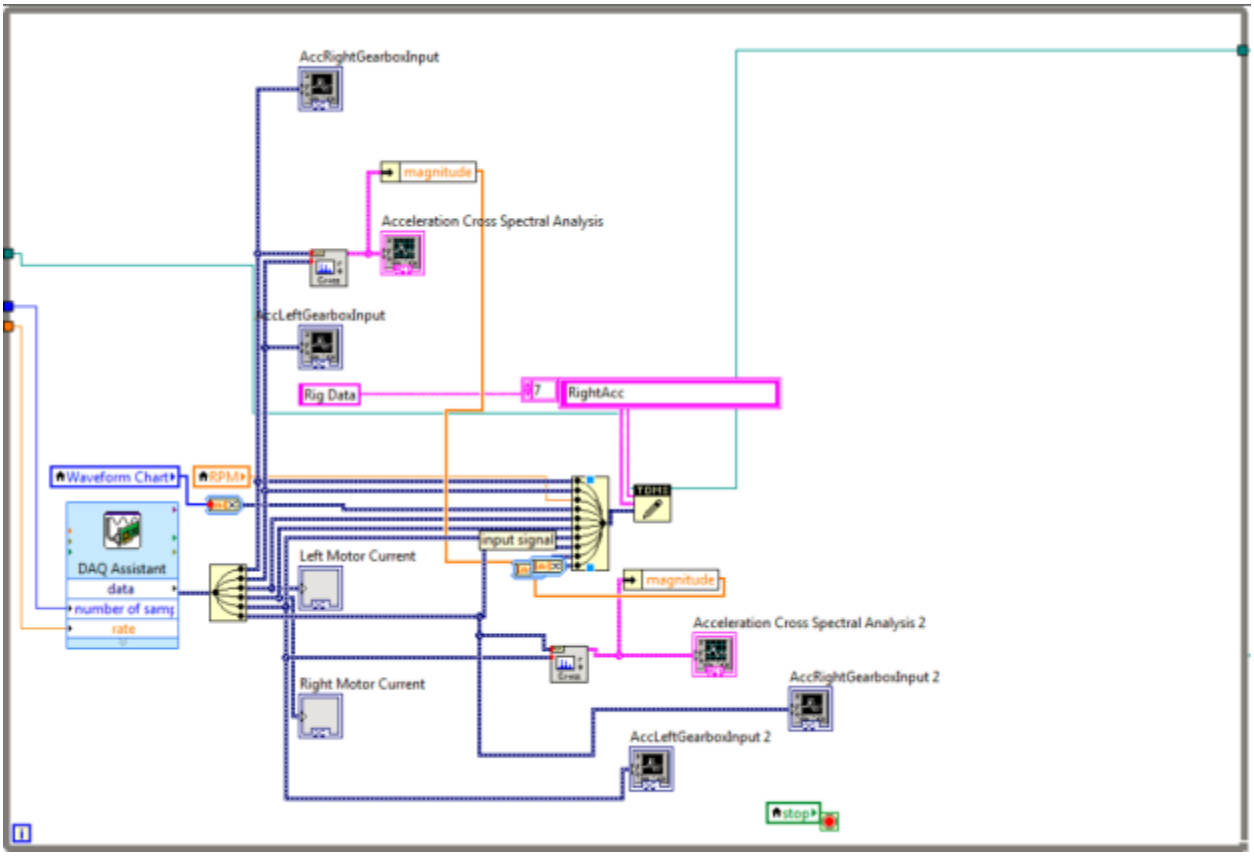

Figure 4-34: Data Collection Loop in the Host Program

The host program is also used to determine the required control signals needed to ensure that both the motor speed and the hydraulic circuit pressure are tracking the required speed and load profiles. This loop is shown in Figure 4-35.

The values determined in the aforementioned PID tracking loop are forwarded to the FPGA part of the program shown in Figure 4-36. The use of the FPGA ensures that the speed and load control are performed in real-time.

The following chapter presents the testing and data collection completed for the new simulator to establish healthy baselines needed to validate the loading similarity between the parallel drive stations.

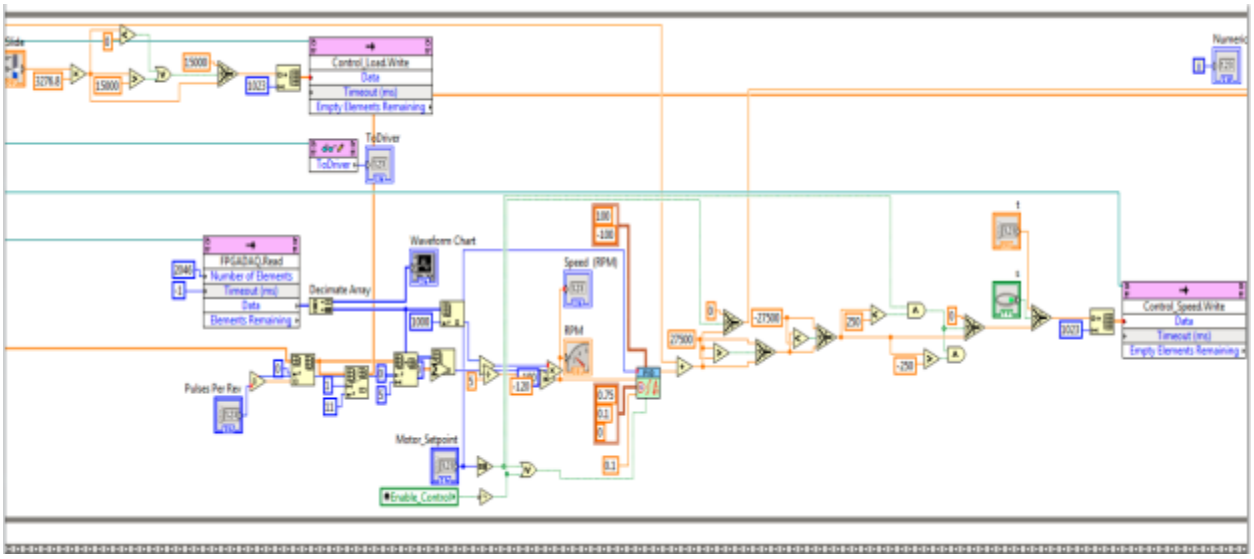

Figure 4-35: Tracking Loop in the Host Program

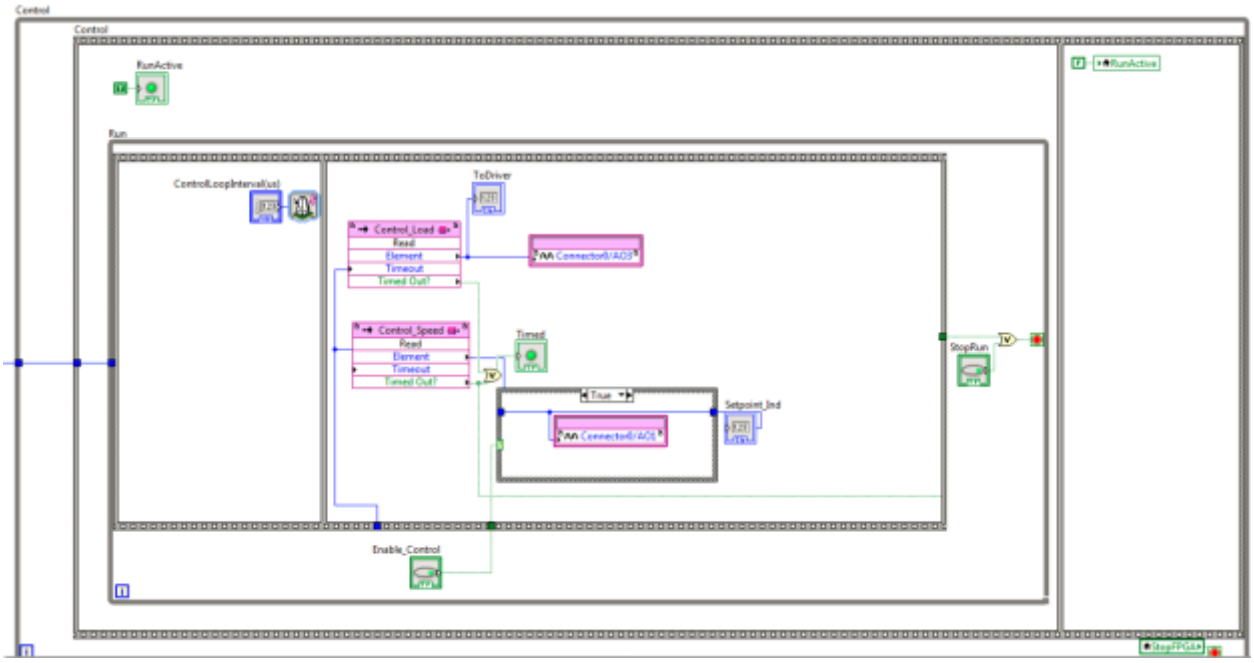

Figure 4-36: Part of the FPGA Control Loop

Chapter 5

5.0 Baseline Data Collection and Analysis Using the New Experimental Apparatus

This chapter presents the process undertaken to verify the operation of the new experimental apparatus presented in Chapter 4 and to confirm that the newly developed system met the design requirements.

To confirm the simultaneous loading features of the new machine, vibration signals were collected and verified for the different parallel components of both drive stations. Additionally, all tests were repeated for different speeds and loads to verify the variable duty capabilities of the new machine. Different ranges of speed and loading were used for the data collected in this chapter. Additionally, ramp-up and ramp-down speed and load variations were investigated for selected components.

As an initial step, the vibration signal analysis of parallel components in this chapter included visual inspection of the time waveform, FFT and Spectrograms of parallel identical components. The verification of smooth baselines represented an important step before the implementation of the previously proposed statistical correlation algorithm as presented in Chapter 3.

Instrumented system components for this chapter included AC motors, gear pumps, gearbox input and output bearings, and serpentine belt idler bearings.

5.1 Data Collection: Baselines

As mentioned in Chapter 4, an extensive measurement process was undertaken after setting up the new simulator. The main objectives for that process were to confirm that the final setup was within the required tolerances and to ensure that parallel components for both drive stations shared the same alignment. Even though the aforementioned step was critical to ensure the parallel setup of both drive stations, still extensive operational testing was required to validate the simultaneous loading of the drive stations.

Without establishing a smooth baseline, the process of fault detection can be daunting [8]. As such, the vibration baseline of different parallel components for the new simulator under different speed and loading conditions is investigated in this chapter. The duty cycles tested represented realistic loading and speed profiles experienced by industrial drive stations such as the Rail-Veyor™ stations presented earlier in this thesis. Speeds tested ranged from 500 to 1000 RPM at the motor side while loading ranged from 0 to 7 lb.ft (25 percent of the AC motor full torque). As presented in Chapter 4, a hydraulic loading circuit was designed and implemented to load the simulator's drive stations and the loading is achieved through circuit pressure variations. For the sake of simplicity, the loadings will be presented as a percentage of the full load capacity of the AC prime movers used (28lb.ft). The calculations of the theoretical reaction torques for the pressures used were based on Equation 4-2 from the previous chapter.

Using the simulator's instrumentation and control subsystem presented in Chapter 4, vibration signals were collected at a sample rate 20 kHz and saved using National Instruments TDMS file format for further analysis. The data collection was done for sister components of both drive

stations simultaneously using identical accelerometers each having an identical length of BNC cable to eliminate any voltage drop differences caused by using different cable lengths. The figures presented in following subsections were obtained using MATLAB®.

The following abbreviations listed in Table 5-1 are used throughout both this chapter and Chapter 6.

Table 5-1: List of Abbreviations Used

Item	**Abbreviation**
Left Gearbox Input Shaft Flange Bearing	RGFB_IN
Right Gearbox Input Shaft Flange Bearing	LGFB_IN
Left Gearbox Output Shaft Flange Bearing	RGFB_OUT
Right Gearbox Output Shaft Flange Bearing	LGFB_OUT
Right Drive Station Belt Idler	RD_ID
Left Drive Station Belt Idler	LD_ID

5.1.1 Gearbox Input Bearing

As shown in Figure 5-1, ICP accelerometers were mounted for both gearboxes input flange bearings. Ideally, the accelerometers should have been placed to line up with the bearings load zone at 45° to the horizontal which represents the gear pressure angle providing the radial load for the shaft supporting bearings. Still, given that condition monitoring approach proposed in the thesis involves vibration signal comparison of parallel sister components, the results of the comparison are not expected to change as long as the accelerometer positioning is identical for both sister components.

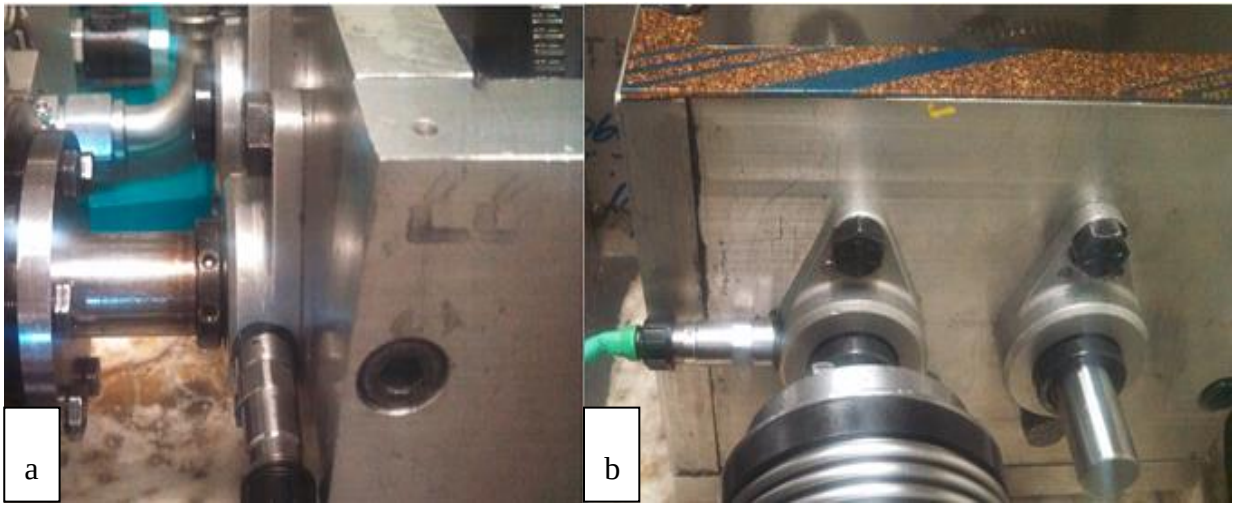

Figure 5-1: Instrumented Gearbox Input Bearing Flanges; (a) left gearbox, (b) right gearbox

For the aforementioned flanged bearings, Rexnord™ ERK-16 rolling element bearings were used with the specifications listed in Table 5-2. Using Equations 2-3 to 2-6 from Chapter 2, the bearing specific frequencies were calculated using the bearing specifications listed in Table 5-1 and the results are presented in Table 5-3 as a function of shaft speed f_r (Hz).

Table 5-2 ERK-16 Bearing Specifications [69]

Attribute	**Symbol**	**Value**
Number of Rolling Elements	n	9
Diameter of Rolling Element	d	0.3125 in
Pitch Diameter	D	1.516 in

Table 5-3 ERK-16 Bearing Calculated Specific Frequencies

Attribute	**Frequency (Hz)**
Ball Pass Frequency, Outer Race	$3.572 f_r$
Ball Pass Frequency, Inner Race	$5.430\ f_r$
Ball Spin	$2.322\ f_r$
Fundamental Train	$0.402\ f_r$

Figure 5-2 presents the FFT spectrum for the vibration signal of the LGFB_IN low-pass filtered at 60 Hz. The signal examined here was obtained for the gearbox operating at 500 RPM with at 25% motor load. The rationale behind filtering the signal is to prevent the gearbox meshing frequency from overshadowing the bearing specific frequencies shown in Figure 5-2.

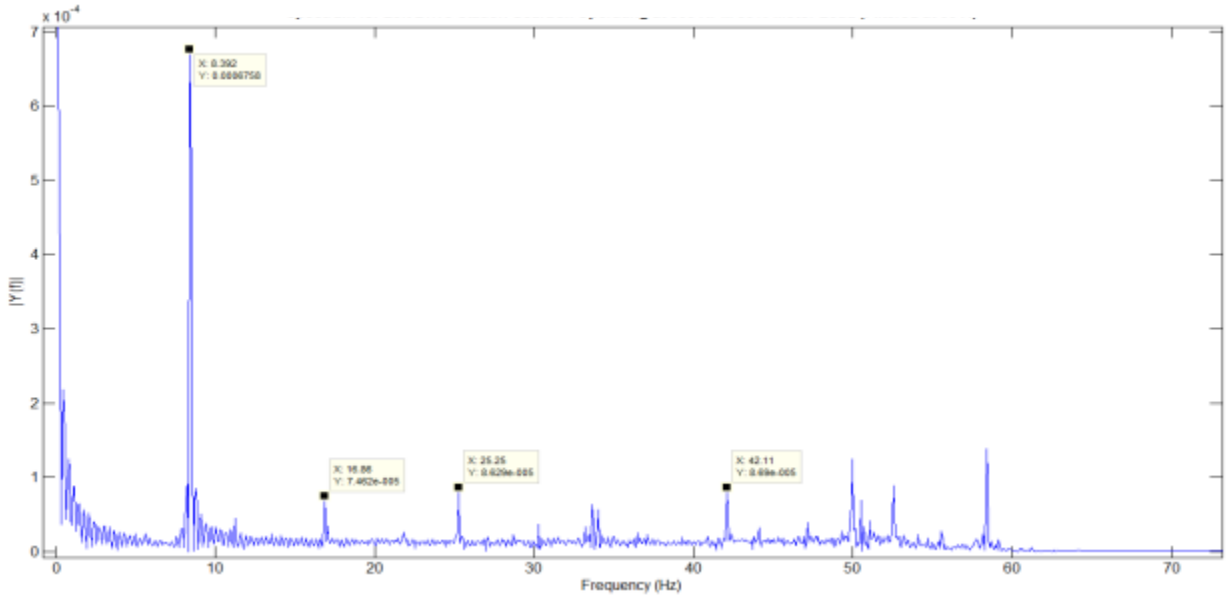

Figure 5-2: Input Bearing Vibration Signal with Bearing Specific Frequencies at 500 RPM Motor Speed and 25% Load

Time waveform, frequency spectrum and Spectrograms are used in Figures 5-3 to 5-5 to present a visual evaluation of the loading similarity between the two identical bearing flanges installed for each of the parallel drive station gearboxes. The vibration signals used to plot these figures were collected with both gearboxes driven at 600 RPM motor speed and 15% load. The spectrums were calculated for 4096 spectral lines while the Spectrograms were calculated using a Hamming window of 1024 data points.

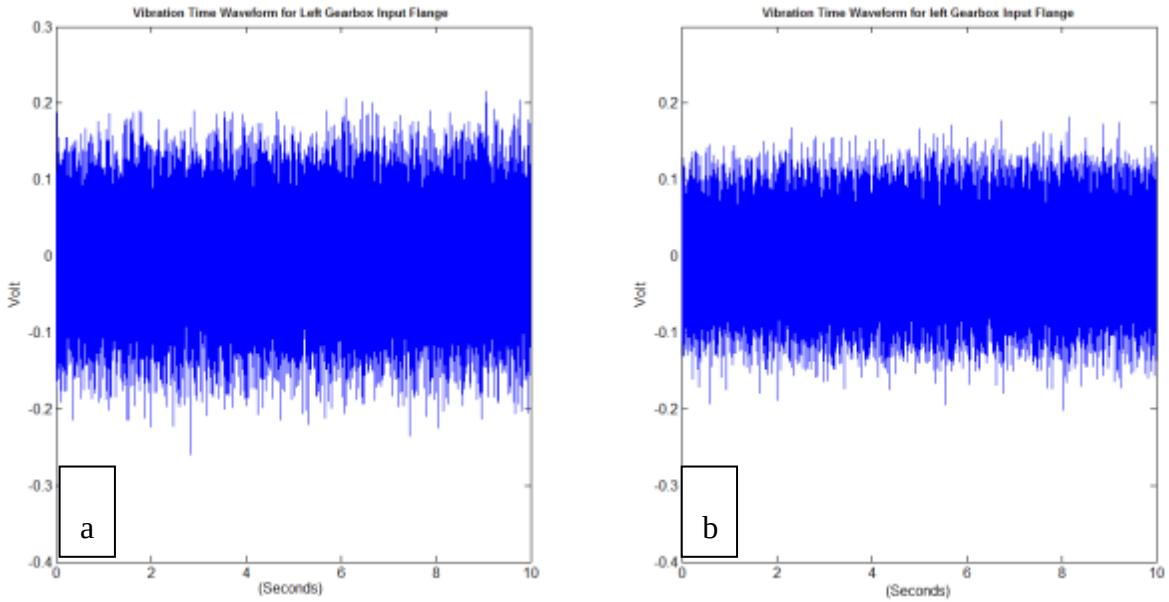

Figure 5-3: Time Waveform Comparison for Input Flange Bearing for Both Gearboxes at 600 RPM Motor Speed and 15% Load; (a) left gearbox input flange, (b) right gearbox input flange

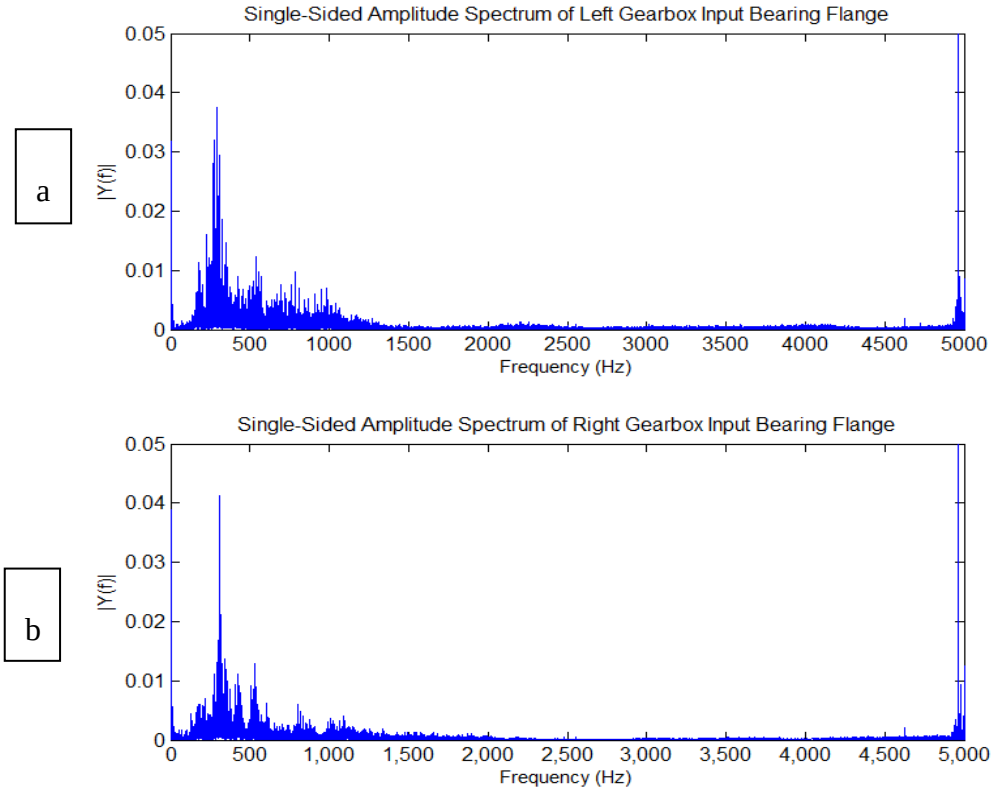

Figure 5-4: Input Bearing Flange Spectrum for Both Gearboxes at 500 RPM Motor Speed and 15% Load; (a) left gearbox, (b) right gearbox

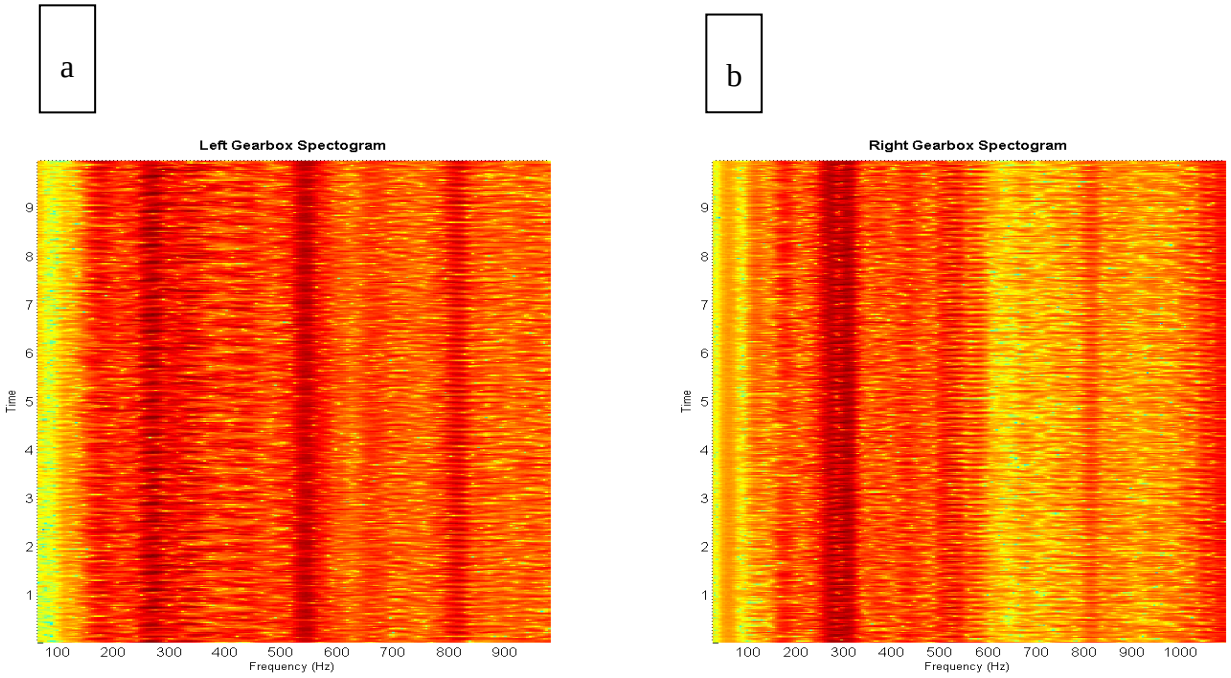

Figure 5-5: Input Bearing Flange Spectrogram for Both Gearboxes at 500 RPM Motor Speed and 25% Load; (a) left gearbox, (b) right gearbox

From initial examination, it can be seen that the input bearing flanges for both gearboxes are experiencing similar loading. As it can be seen in Figure 5-4 and Figure 5-5, the frequency spectrum and Spectrograms are dominated by the gear mesh frequency of 266 Hz calculated using Equation 5-1 [12] for the input gear with 32 teeth rotating at shaft frequency of 8.33 Hz.

$$F_{Gear\ Mesh} = Number\ of\ Teeth \times Shaft\ Frequency \qquad \text{Eq. (5-1)}$$

Further inspection shows some differences in the gear meshing frequency sidebands as shown in Figure 5-6. These differences were expected and can be accounted for by the fact the gears for both gearboxes are experiencing their first operation and are thus still in the process of wearing

in. It is expected that with further operation the two gear pairs will wear in uniformly further increasing their meshing similarity.

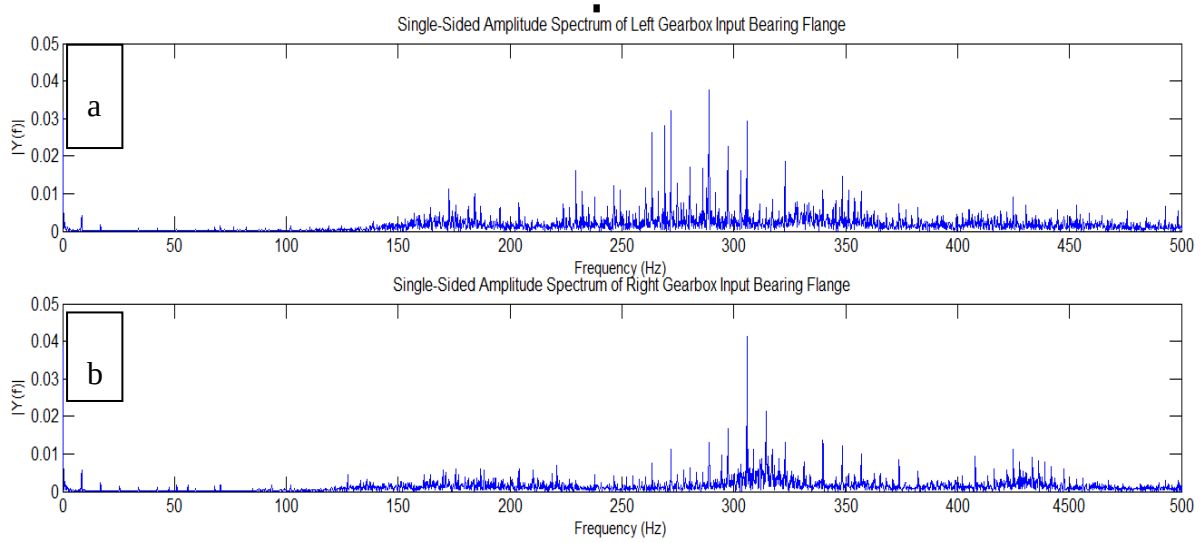

Figure 5-6 Zoom in at Gear Mesh Frequency for both Input Flange Bearings at 500 RPM Motor Speed and 15% Load; (a) left gearbox, (b) right gearbox

The effects of speed changes can be seen in the spectrums shown in Figure 5-7 for the output bearing flanges of the gearboxes driven at 700 RPM motor speed and 15% load. The speed increase resulted in frequency modulation of the bearing vibrations and thus shifted the bearing specific frequency and gear mesh frequency to the right when compared the gearbox spectrum at 500 RPM as shown in Figure 5-4. Figure 5-7 shows that the vibration spectrums for both gearboxes are not identical. This was expected given the underlying stochastic process involved in the mechanical signal generation. The difference in spectrums can also be attributed to non-identical alignment and fits for both gearboxes. Furthermore, given that the data collected here represents the initial operation of the new simulators, it was expected that the gearboxes would require a wear in period before the meshing similarity can be objectively compared

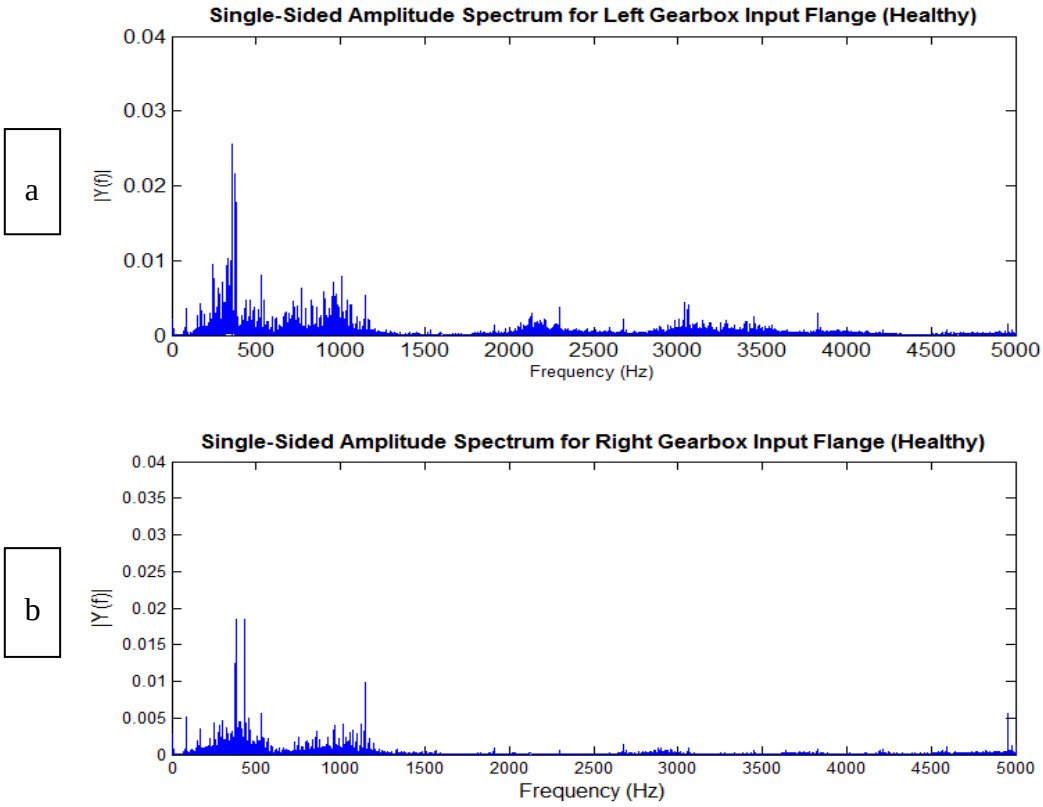

Figure 5-7: Input Bearing Flange Spectrum for Both Gearboxes at 700 RPM Motor Speed and 15% Load; (a) left gearbox, (b) right gearbox

5.1.2 Gearbox Output Bearing

As shown in Figure 5-8, ICP accelerometers were mounted for both gearboxes output flange bearings. These flanges support the gearboxes output shaft carrying the aluminum pulley driving the serpentine belt system presented in Chapter 4. The serpentine belt creates a radial hub load at 16° to the horizontal. In order to instrument the load zone of the gearbox output bearings, the accelerometers were attached such that they lined up at 16° to the horizontal.

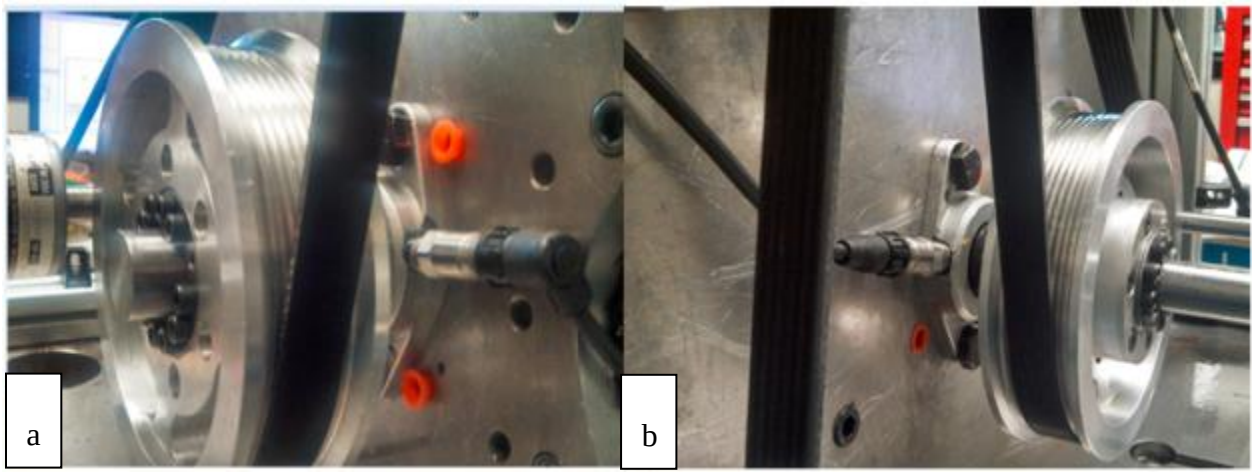

Figure 5-8: Instrumented Outboard Flange Bearings; (a) left gearbox, (b) right gearbox

As with the input flange bearings, the output flange bearings were also fitted with Rexnord ERK-16 rolling element bearings and thus had the same characteristic bearing frequencies calculated for the gearbox input flange bearings presented in Table 5-3. As shown in Figure 5-9, the characteristic bearing frequencies can be seen for the LGFB_OUT. The vibration data used to generate this spectrum was collected for the motors running at 500 RPM and 15% load and as such the shaft frequency at the output shaft was determined to be 2.78 Hz given the 3:1 gear ratio used. Both the Ball Spin and the Fundamental Cage frequencies are lost in the noise floor. However, the vibration signal is clearly dominated by the Inner Race frequency at 11.98. This can be explained by the significant radial load on the output flange bearing due the belt tension creating a hub load at the driver pulley attached to the gearbox output shaft as seen in Figure 5-9.

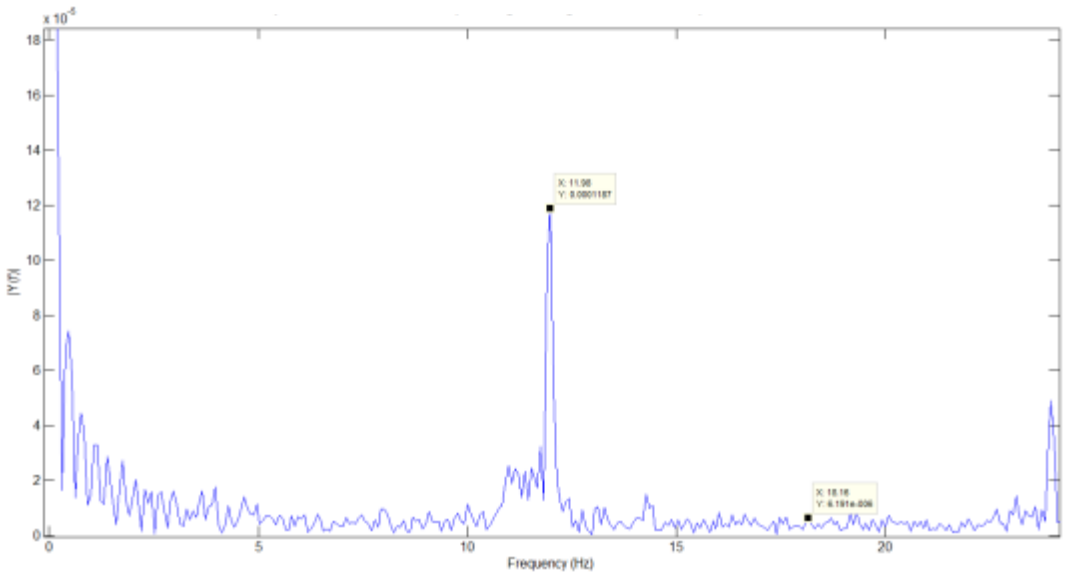

Figure 5-9: Left Gearbox Output Flange Bearing Vibration Signal with Bearing Specific Frequencies at 500 RPM Motor Speed and 15% Load

To confirm the response similarity of the output flange bearings of both gearboxes, Figure 5-10 presents the FFT of both bearings after low-pass filtering at 25 Hz. Given the identical construction of both parallel drive systems and the fact that both drive stations are sharing the same duty cycle, the frequency components presented for the output flange bearings are very similar. A closer look would indicate that the amplitude for the Inner Race frequency is almost 300% higher for the LGFB_OUT when compare to the RGFB_OUT. This discrepancy indicates that the radial loading is unequal for both output bearings or that the two belt systems are not sharing the exact alignments. The data used to generate the aforementioned FFT was obtained at a motor speed of 500 RPM at a load of 15%.

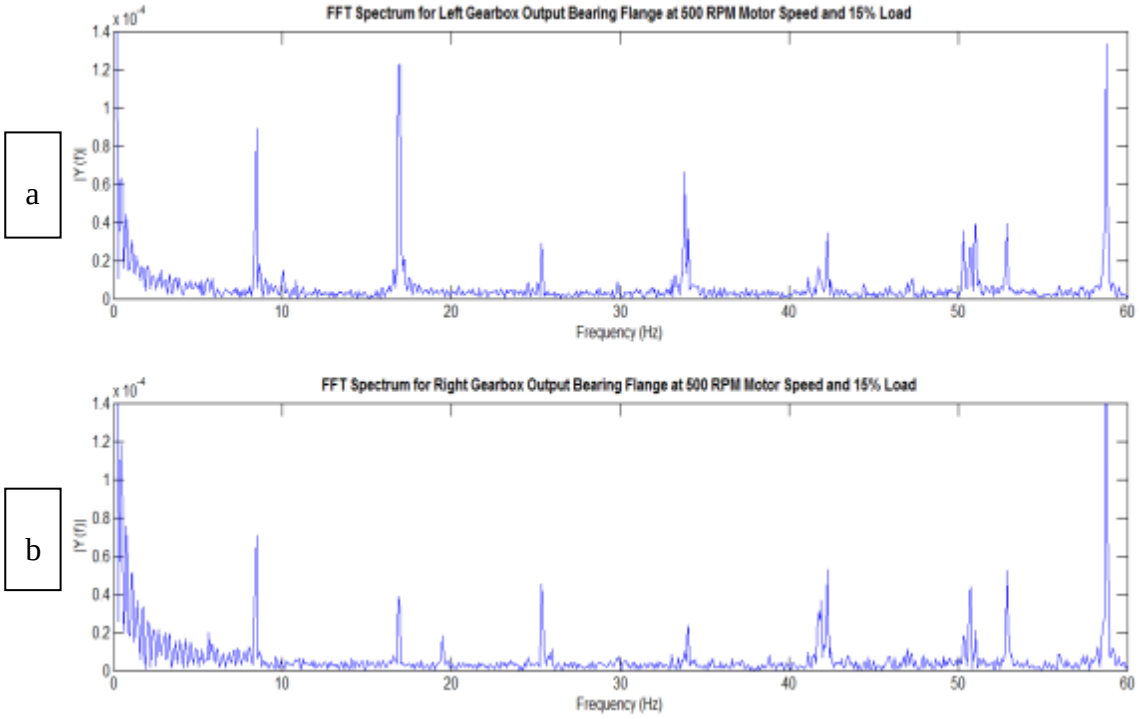

Figure 5-10: Input Flange Bearing Spectrum for Both Gearboxes at 500 RPM Motor Speed and 15% Load; (a) left gearbox, (b) right gearbox

Given that the radial loading on the output bearing flanges is mainly controlled by the belt tension in the serpentine accessory drive, changes in the reaction torque created by the hydraulic loading circuit would affect the belt tension and thus change the hub loading. As an example, Figure 5-11 presents the FFT spectrum for the output bearing flange for a motor speed of 500 RPM and a load of 25%. Compared to Figure 5-10(b), the load increase resulted in amplitude modulation of the frequency content of the bearing signal.

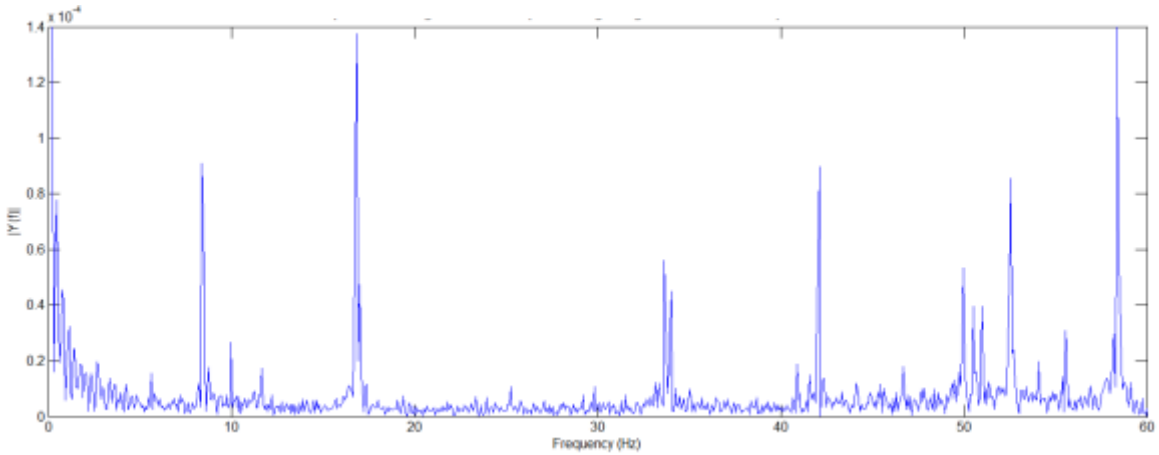

Figure 5-11: Input Bearing Flange Spectrum for Left Gearboxes at 500 RPM Motor Speed and 25% Load

5.1.3 Serpentine Belt Idler Bearing

In addition to supporting the gearbox shafts, rolling element bearings are also used to allow the serpentine belt idlers to rotate about their post. Figure 5-12(a) shows the support post used to fix the idlers used for the simulator's serpentine belt system. Figure 5-12(b) shows a closer look at the bearing fitted into the idlers used.

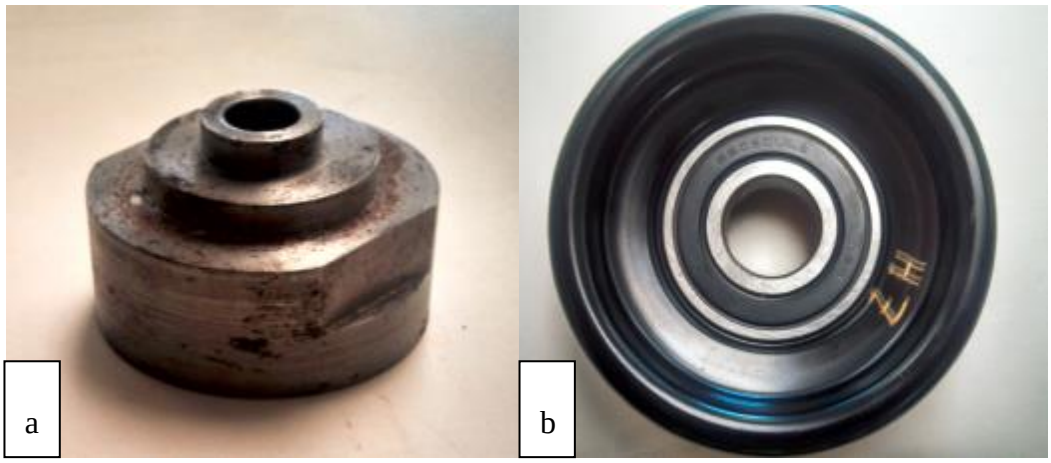

Figure 5-12: The Idler Post and Bearing Used for Simulator's Belt System; (a) post, (b) idler with bearing

The idler posts were instrumented for both drive stations as shown in Figure 5-13. Given a wrap angle of almost 170° at the belt idler, the accelerometer for both posts were aligned with the vertical such that they point to the bearing's load zone.

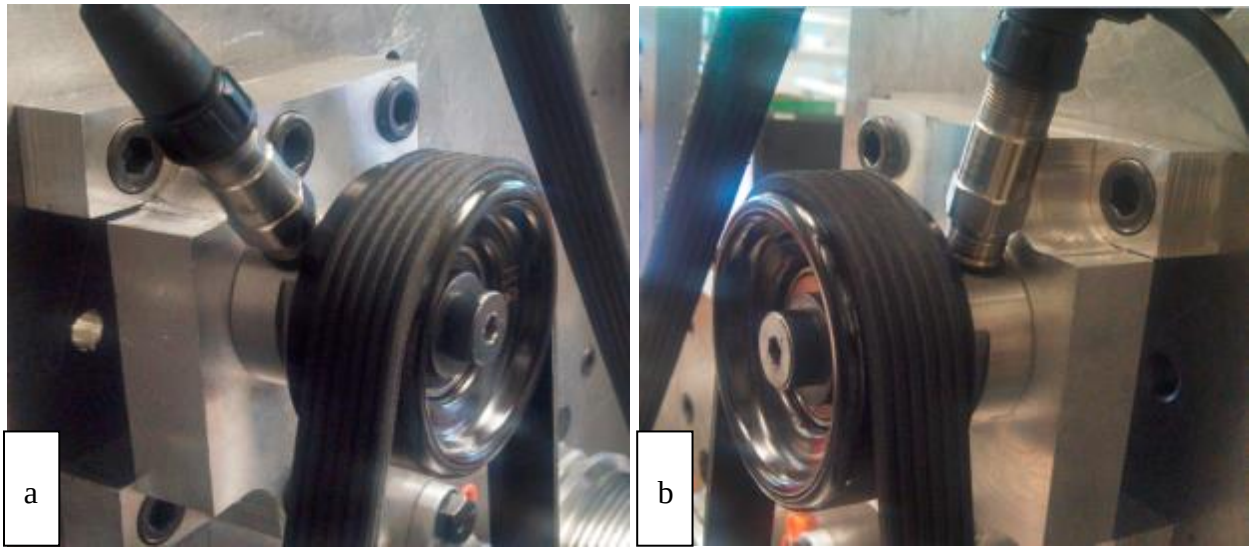

Figure 5-13: Instrumented Idler Post for Both Drive Stations; (a) left station, (b) right station

The loading similarity for the idlers is initially confirmed by comparing the time waveform of their vibration signals as shown in Figure 5-14. Further investigation confirms the similar spectral content of the signals as shown in Figure 5-15 for motor speed of 500 RPM and load of 25%. In order to determine the frequency range of the belt system idlers, the belt drive ratio for the serpentine drive system was used and the idler rotational speed was calculated at 355 RPM (5.97 Hz).

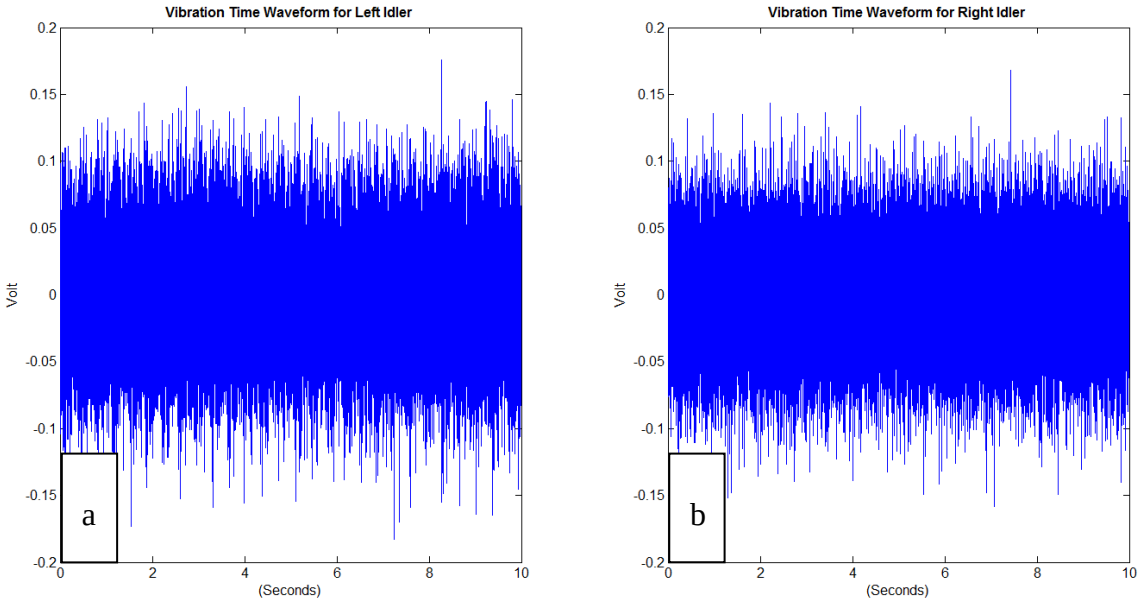

Figure 5-14: Time Wave Form for Idler Vibration; (a) left idler, (b) right idler

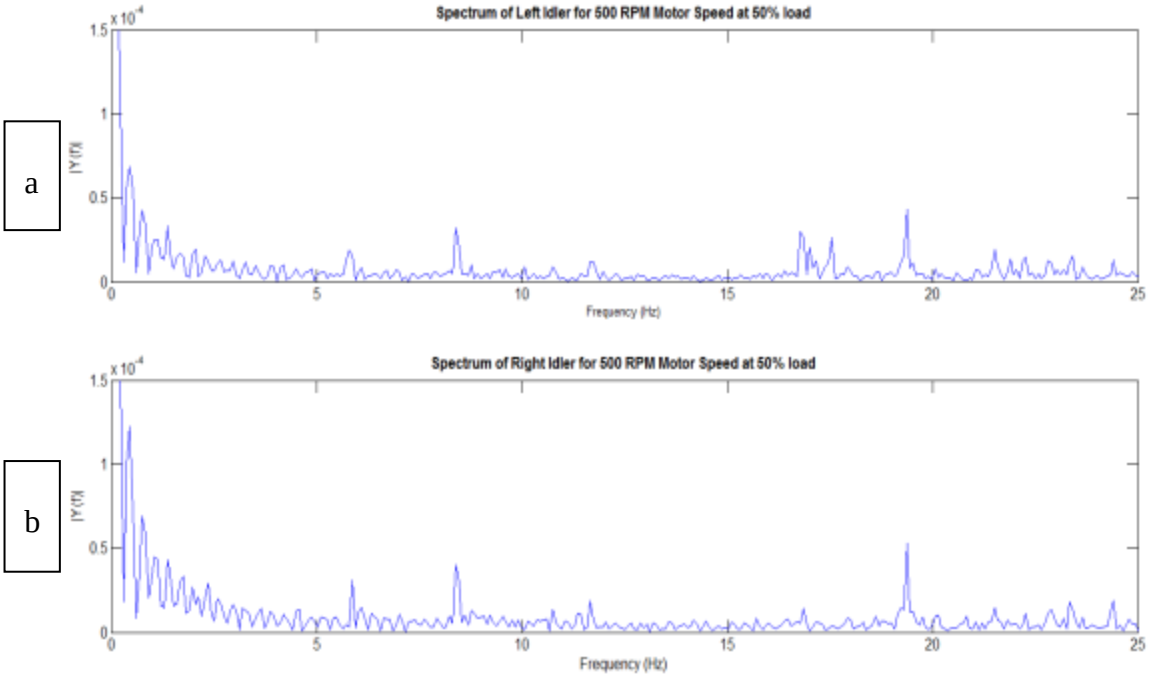

Figure 5-15: Idler Bearing Spectrum for Both Drive Stations at 500 RPM Motor Speed and 25% Load; (a) left idler, (b) right idler

5.1.4 Prime Mover: AC Motors

Vibration analysis can be used to detect different faults for electrical motors. As presented in Figure 4.3, for electric motors, vibration analysis can be used to detect eccentricity, bearing faults, motor installation problems such as soft-foot and misalignment. As shown in Figure 5-16, both AC motors for the simulator were instrumented using ICP accelerometers. The spectral content of the vibration signals acquired are shown in Figure 5-17 and Figure 5-18 for 700 RPM motor speed and 25% load. The similar spectral components for both motors represent an indication that both motors are actually sharing the same duty cycle and setup.

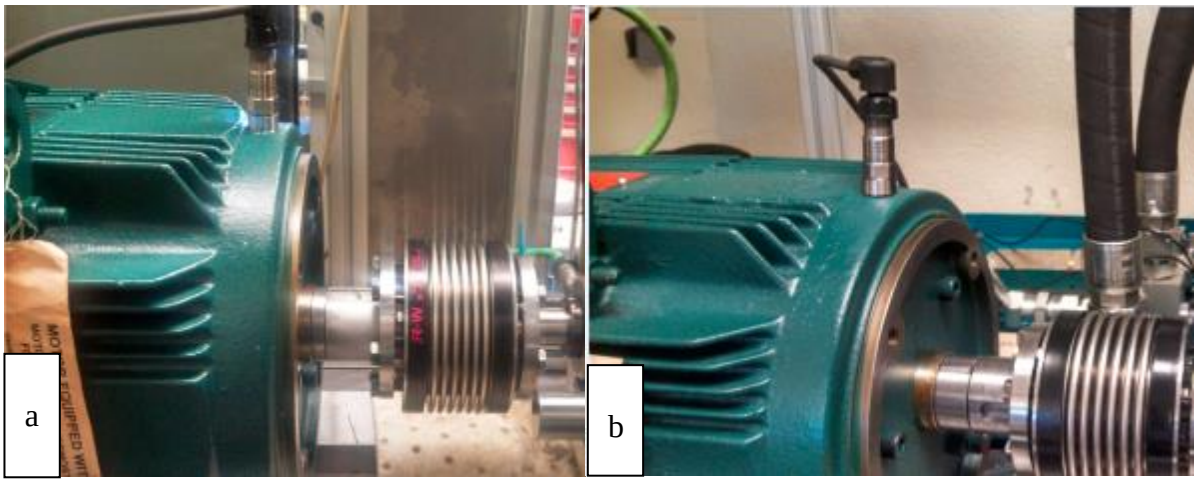

Figure 5-16: Instrumented Motors; (a) left station, (b) right station

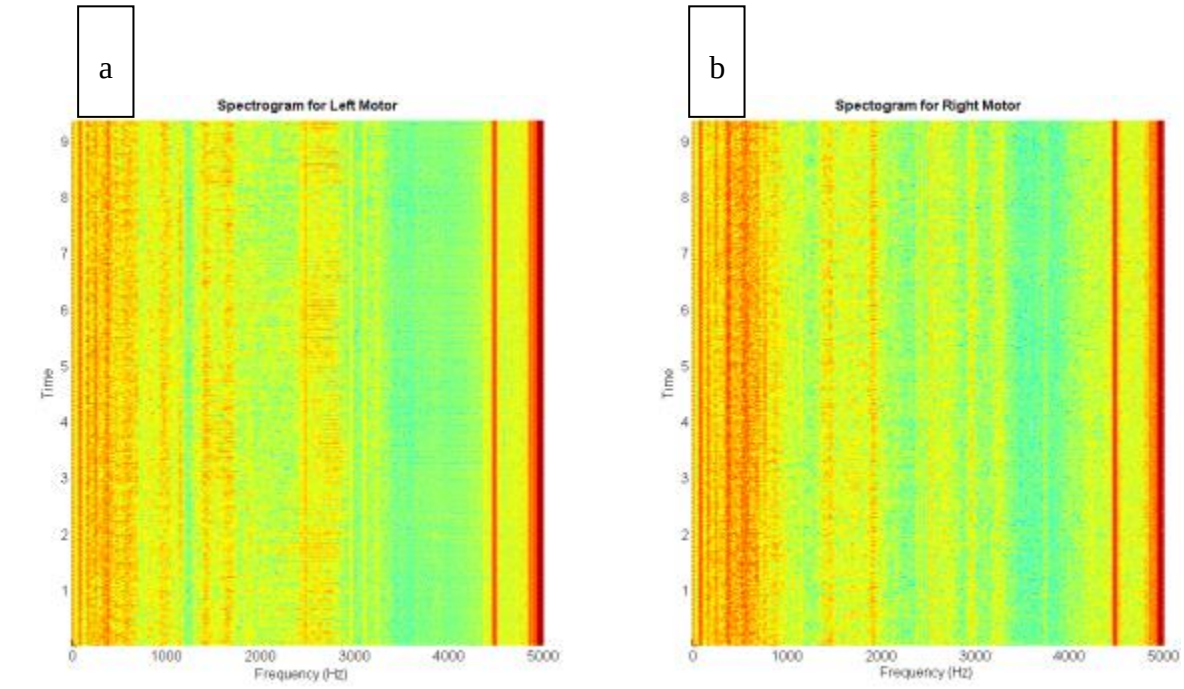

Figure 5-17: Vibration Signal Spectrogram for Both Motors at 700 RPM Motor Speed and 25% Load; (a) left station, (b) right station

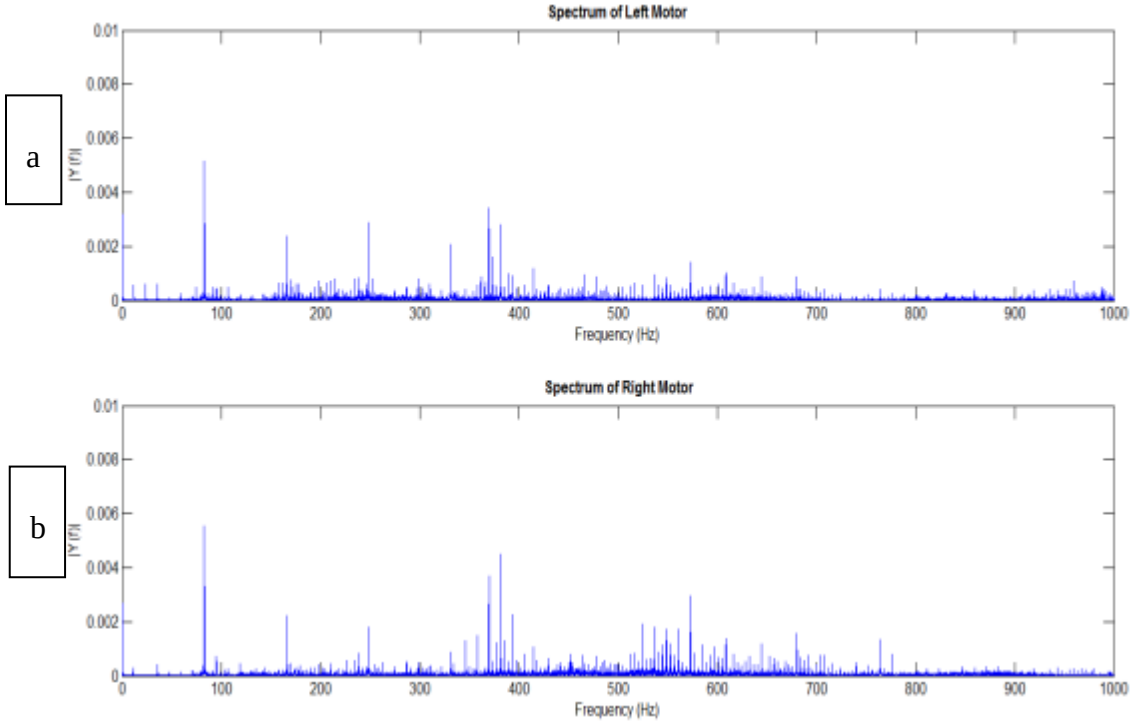

Figure 5-18: Vibration Signal Spectrum for Both Motors at 700 RPM Motor Speed and 25% Load; (a) left station, (b) right station

5.1.5 Loading System: Gear Pumps

As previously mentioned in Chapter 4, the pumps used in the loading hydraulic circuit are of the gear type and thus their mechanical construction encompasses gears and needle bearings as shown in Figure 2-1. Additionally, the pumps purchased for the simulator were configured with outboard rolling element bearings to support the radially loaded pump shaft coupled to the belt drive system. As such, the vibration spectrum of the gear pumps is expected to exhibited discrete vibration components at the gear mesh and characteristic bearing frequencies.

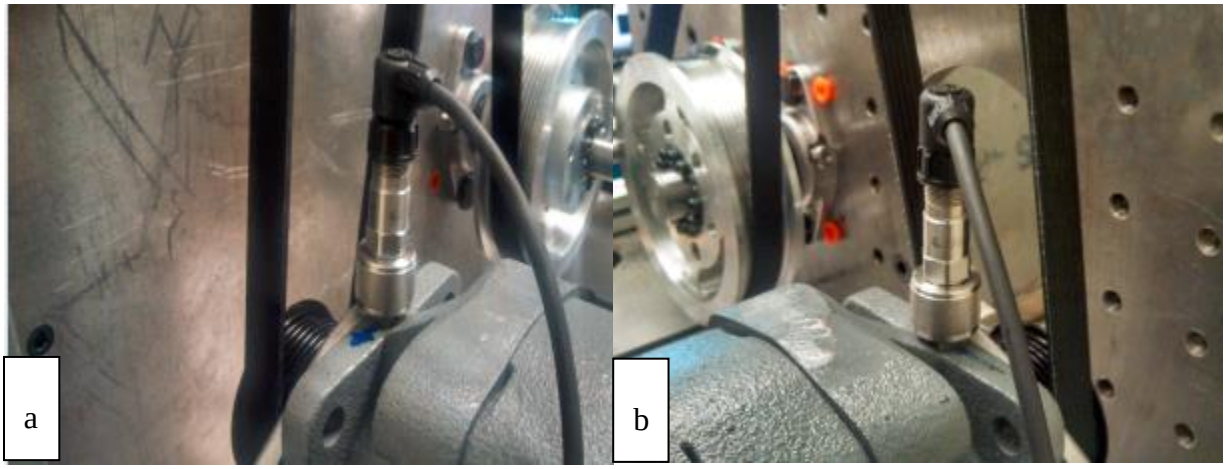

Figure 5-19: Instrumented Gear Pump; (a) left station, (b) right station

As shown in Figure 5-19, the vibration levels of both the simulator's pumps were instrumented using ICP accelerometers. Figure 5-20 presents the time waveform for the vibration signals collected at a motor speed of 500 RPM and load of 5%. Using the drive station's drive ratio, each pump's shaft speed was determined to be 375 RPM (6.25 Hz).

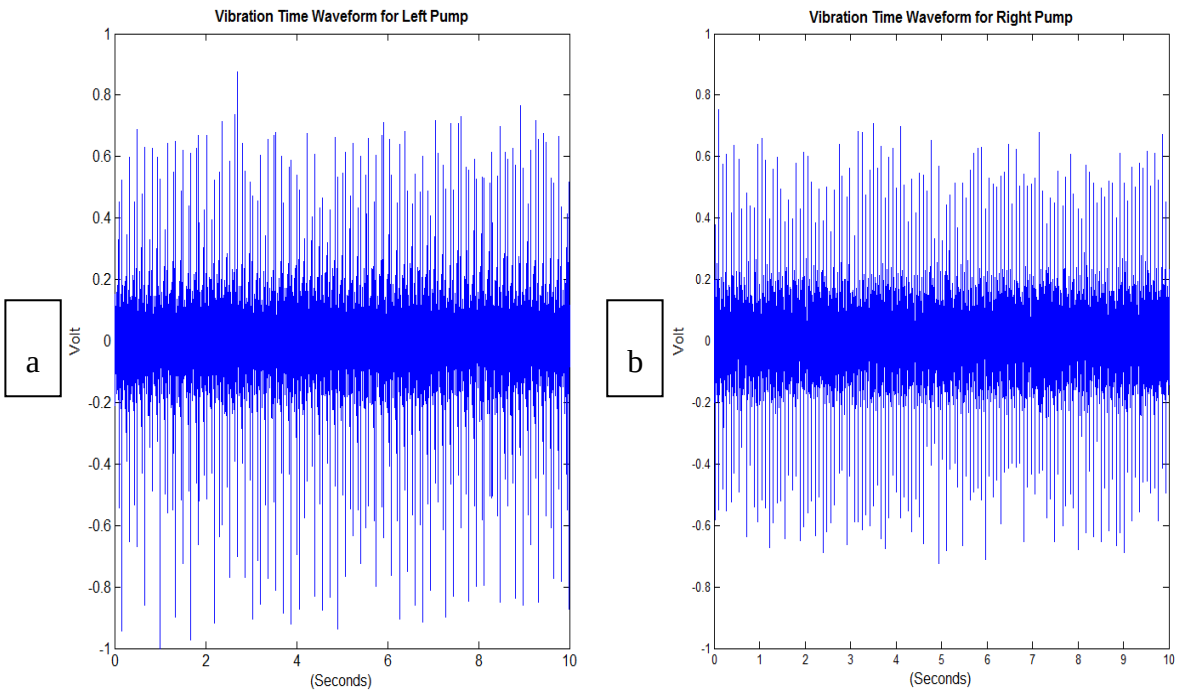

Figure 5-20: Time Wave Form for Pump Vibration at 500 RPM Motor Speed and 5% load; (a) left pump, (b) right pump

Amplitude modulation effects can be observed by comparing the vibration time waveform shown in Figure 5-20(b) for an operation speed of 500 RPM motor speed and 5% load to the vibration time waveform shown in Figure 5-21 for an operation speed of 500 RPM motor speed and 25% load. In order to appreciate the loading effect on the vibration signals, the RMS and the Peak-to-Peak values are calculated for both the signals shown in Figures 5-20(b) and 5-21. The calculated values are presented in Table 5-4. It should be noted that the signals shown in Figures 5-20 and 5-2 were instrumented using identical 500 mV/*g* ICP accelerometers. As such the aforementioned gain was used to determine the corresponding acceleration for the values as shown in Table 5-4.

Table 5-4: RMS and Peak-to-Peak Statistics for Pumps at Different Loads

Statistic	**Right Pump at 500 RPM Motor Speed and 5% Load**	**Right Pump at 500 RPM Motor Speed and 25% Load**
RMS	0.0459 V (0.92 m/s^2)	0.1166 V (2.28 m/s^2)
Peak to Peak	1.472 V (28.88 m/s^2)	3.753 V (73.63 m/s^2)

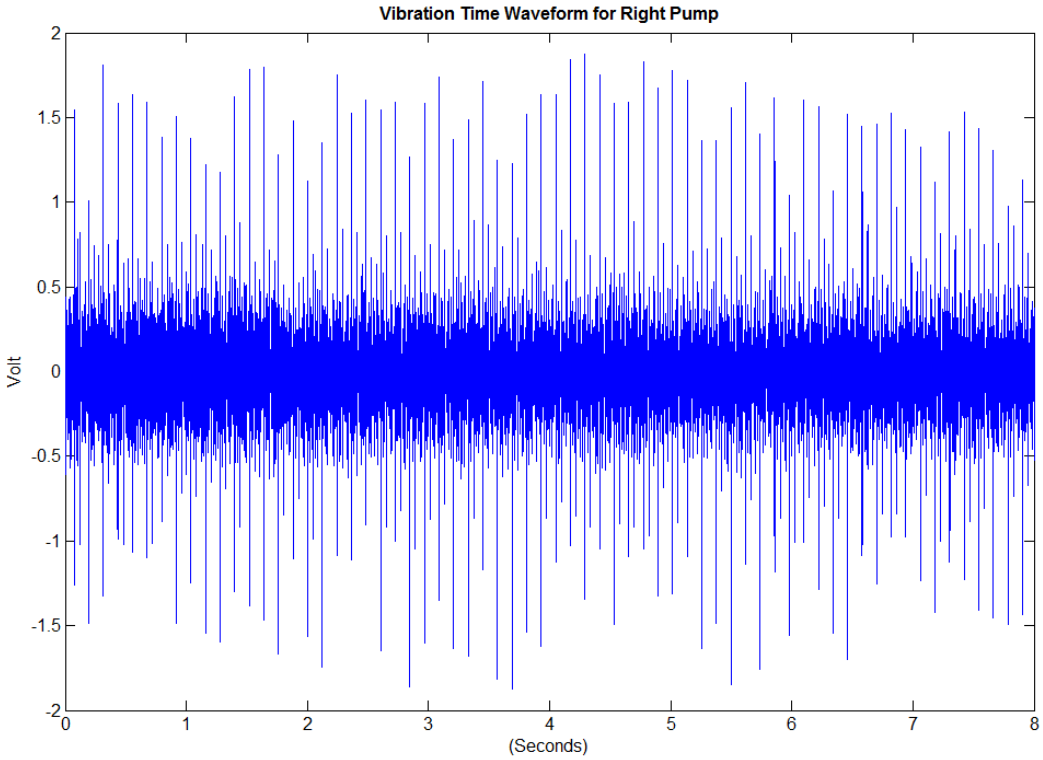

Figure 5-21: Time Wave Form for Pump Vibration at 500 RPM Motor Speed and 25% load

5.1.6 Speed Ramp Profile

As shown in Figure 3-7, the vibration signals acquired during the *in-situ* field data collection phase for the Rail-Veyor® drive stations exhibited the following duty cycle; a ramp up as the train engages to the drive stations followed by constant operation and then a ramp down as the train disengages from the stations. The speed component of the aforementioned duty cycle was replicated using the newly developed simulator. Figure 5-22 presents the vibration time-waveform for both RGFB_IN and LGFB_IN at a motor speed ramp from 0 to 700 RPM at a constant 5% load. From visual inspection, the vibration amplitude increases during the speed ramp up, stays uniform at constant speed and decreases during ramp down. It could be noticed that the left gearbox is slightly nosier than the right one.

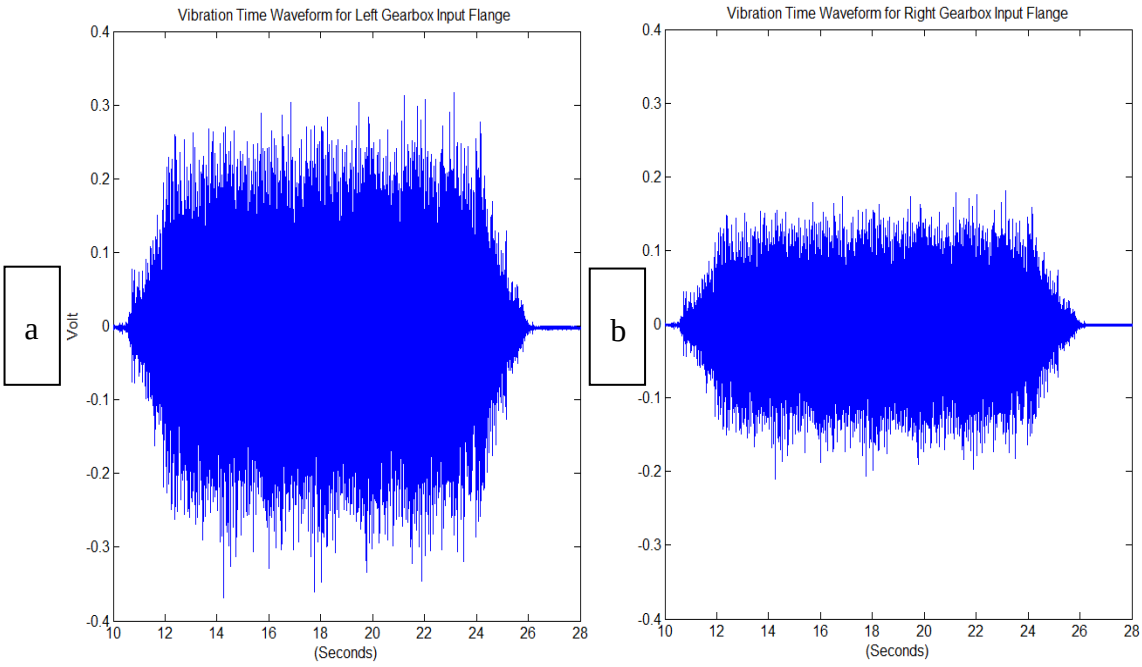

Figure 5-22: Time Wave Form for Gearbox Input Flange Bearing Vibration at 700 RPM Motor Speed Ramp and 5% load; (a) left gearbox, (b) right gearbox

The frequency modulation effect due to the variable speed cycle can be clearly seen using the Spectograms shown in Figure 5-23. As it can be seen, the gearbox charactersitc frequencies such as the gearmesh and bearing specific frequencies all shifed with the change of speed

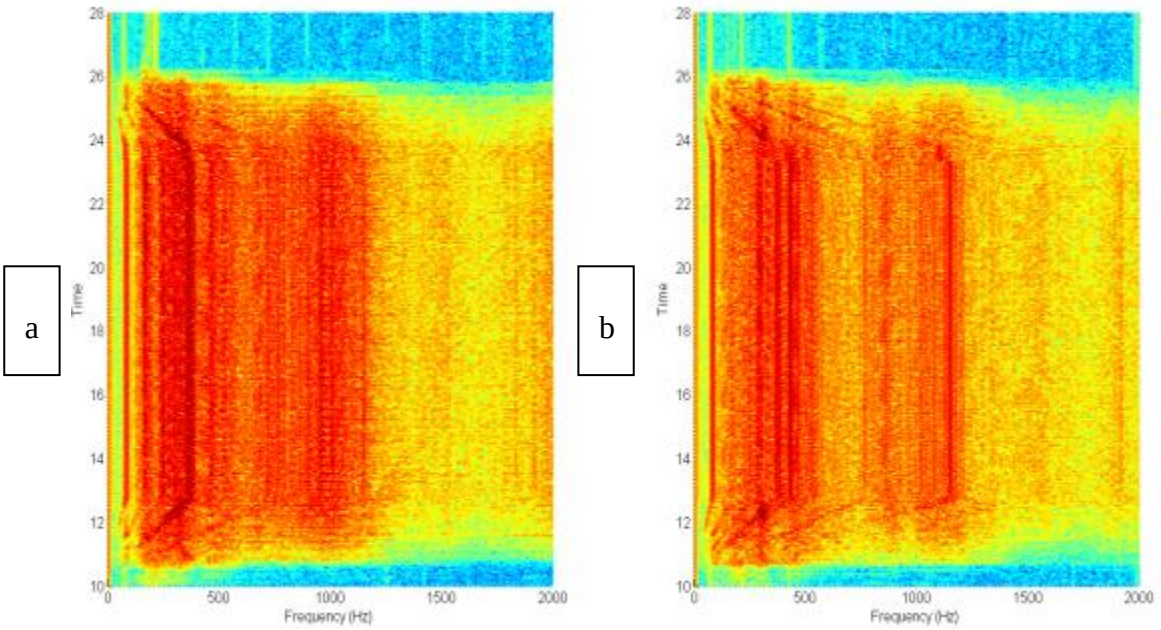

Figure 5-23: Spectrograms for Gearbox Input Flange Bearing Vibration at 700 RPM Motor Speed Ramp and 5% load; (a) left gearbox, (b) right gearbox

5.1.7 Load Ramp Profile

To further investigate the duty cycle observed for the Rail-Veyor® drive stations, the effects of load modulation were investigated using the new simulator. Using a data set representing a constant motor speed of 700 RPM and a load ramp from 5% to 50% load, the vibration amplitude modulation was demonstrated using Figure 5-24. As shown, the figure was divided into seven regions each specified with an alphabetic letter. For regions A and B, the motors speed was increased from 0 RPM to a constant speed of 700 RPM as it was done in Figure 5-

22(b). Region C represents the effect of increasing the reaction torque on the motors from 5% to 50%. Region D represents the uniform vibration signal at a constant motor load of 50% while region R shows the decrease in vibration amplitude associated with decreasing the motor load. Finally, regions F and G represent the decrease of the motor speeds from 700 to 0 RPM.

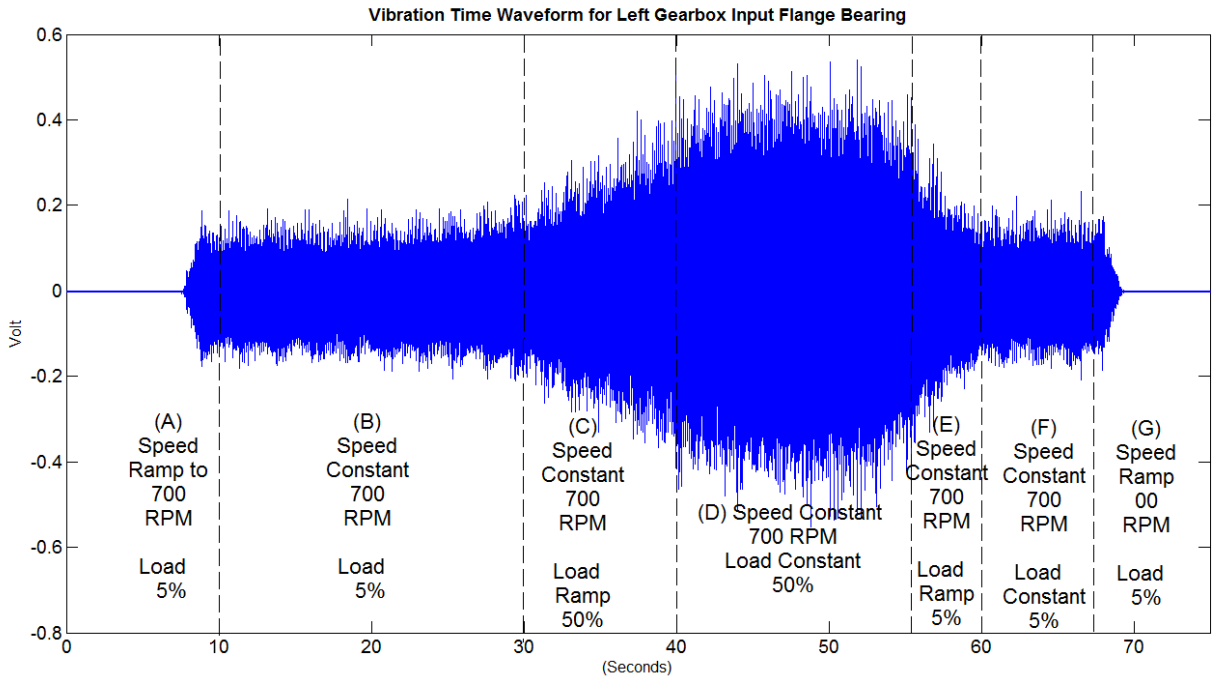

Figure 5-24: Vibration Time Waveform for the Right Gearbox Input Flange Bearing for a Variable Duty Cycle

The amplitude modulation effect for the previous duty cycle can also be seen in the Spectrogram presented in Figure 6-25. The load increase at the 30th second mark can be seen as an amplitude increase at the gear mesh frequency of 373 Hz (for shaft frequency of 11.67 Hz and 32 gear tooth). The amplitude increase in a Spectrogram is represented by a darker region.

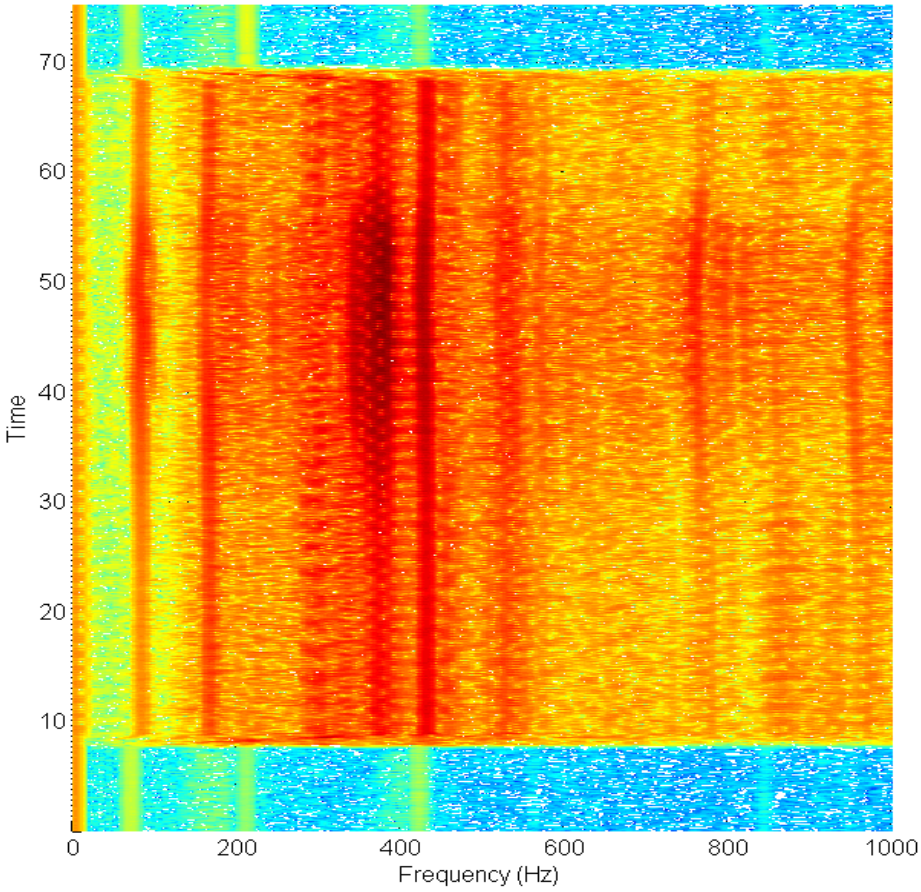

Figure 5-25: Vibration Spectrogram for the Right Gearbox Input Flange Bearing for a Variable Duty Cycle

5.2 Baselines Assessment

The main aim of this chapter was to evaluate the operational characteristics of the newly developed simulator to validate how well the new test rig can successfully replicates the loading similarity between the parallel simultaneously loaded drive stations. As a preliminary step, the mechanically response similarity was compared by visual evaluation of the time waveforms, spectrums and spectrograms of healthy and parallel components. Components investigated included both the gearbox input and output bearing flanges, the serpentine belt idlers, the AC prime movers and the loading hydraulic gear pumps.

Overall, the comparisons confirmed the following important points

- The amplitudes of the time waveforms for parallel components were generally similar and changed simultaneously with duty cycle variations
- The Spectrum of parallel components exhibited the same frequency components, yet with different levels. The degree of frequency similarity also varied between the components with spectrums of idlers representing a near match as shown in Figure 5-15 and an obvious difference as seen for the gear mesh frequencies shown in Figure 5-6
- The spectral shift caused by frequency modulation was very similar for both gearboxes as shown in Figure 5-23
- Overall it was seen that both the left gearbox and pump were slightly nosier than the right gearbox and pump as shown in Figure 5-5 and Figure 5-20
- The noisy nature of the left gearbox (compared to the right gearbox) can also be seen in Figure 5-22

The previous points represent promising preliminary results confirming that the design met the requirements of developing a simulator that can successfully reproduce the simultaneous loading experienced by parallel systems such as the Rail-Veyor® drive stations. As such, the new simulator can be successfully used in validating the statistical correlation algorithm as presented in the following chapter.

Chapter 6

6 Preliminary Implementation of the Statistical Correlation Algorithm Using the New Simulator

This chapter presents the use of the newly developed fault simulator in the validation of the Statistical Correlation fault detection algorithm previously presented earlier in this thesis. As discussed in Chapter 3, the proposed correlation-based fault detection technique was initially tested using vibration data sets generated by the SpectraQuest™ fault simulator and the results were promising. However, the limited capabilities of the SpectraQuest™ setup lacked a transmission system, variable duty cycle simulation and limited loading capabilities required to simulate industrial machinery.

After validating the performance of the newly developed fault simulator, the simulator was used to generate the vibration data sets presented in this chapter. In contrast to Chapter 5, this chapter presents vibration data sets for different faulted components obtained using the new simulator. Unlike the data sets obtained from the SpectraQuest™ simulator, the vibration data sets presented in this chapter were generated in the presence of a multi-stage transmission system under realistic speed and loading conditions.

In Section 6.1, this chapter discusses the test plan undertaken to generate the required vibration data sets. This is followed by Section 6.2 presenting the discrepancy scores obtained using healthy and faulted rolling element bearings (mounted in idlers) calculated at different load and speed profiles. Section 6.3 presents the discrepancy scores obtained for healthy and faulted gears also calculated at different duty points. Section 6.4 uses the results from sections 6.2 and 6.3 to

investigate the use of the discrepancy metric as a means for fault detection in non-stationary operation

6.1 Test Plan and Matrices

The main aim of the test plan presented here is to generate the vibration data sets required to validate the performance of the correlation-base fault detection algorithm proposed in this thesis. Data sets generated should represent the mechanical response of parallel components at different health states but for identical speed and load profiles.

It was demonstrated in Chapter 5 that the mechanical response of the belt idlers for both parallel drive stations was very similar. Given their distance from the gearboxes, the vibration signals for the belt idlers were not dominated by the noisy gear-meshing of the gearboxes and thus represented an ideal start to investigate the fault detection performance of the correlation-based algorithm.

Initially, it was required to confirm that the discrepancy metrics are insensitive to speed and load variations. As shown in Table 6-1, a test matrix developed to generate the required belt idler healthy vibration data sets collected over a range of speeds and loads. The following step was to investigate how the discrepancy metric distribution changes due to faults. Table 6-2 presents the test matrix followed to generate the required data sets.

Table 6-1 Test Matrix for Healthy Idler Bearings

Load (Percentage of Motor Rated Torque) / **Frequency (Hz)**	**5%**	**15%**	**25%**	**35%**
500	X	X	X	X
600	X	X	X	X
700	X	X	X	X
800	X	X	X	X
900	X	X	X	X

Table 6-2 Test Matrix for Faulted Idler Bearings

Load (Percentage of Motor Rated Torque) / **Frequency (Hz)**	**5%**	**35%**
500	X	X
700	X	X
900	X	X

In addition to bearing fault simulation, the newly developed fault simulator can be used to generate faulted gear vibration data sets. As it was done for the belt idlers, healthy gear data sets were collected at different speeds and loads as show in Table 6-3. Using the same speed and loading conditions, Table 6-4 presents the vibration data sets obtained for faulted gears required to investigate the fault detection capabilities of the newly developed algorithm.

Table 6-3 Test Matrix for Healthy Gears

Load (Percentage of Motor Rated Torque) / **Frequency (Hz)**	**5%**	**15%**	**25%**	**35%**
500	X	X	X	X
600	X	X	X	X
700	X	X	X	X
800	X	X	X	X
900	X	X	X	X

Table 6-4 Test Matrix for Faulted Gears

Load (Percentage of Motor Rated Torque) / **Frequency (Hz)**	**5%**	**35%**
500	X	X
700	X	X
900	X	X

The loading profiles presented in the test matrices were simulated using the control system presented in Chapter 4 and all vibration signals were collected using identical ICP accelerometers at a sample rate of 20 kHz.

The statistical correlation algorithm used to analyze the generated vibration data sets was identical to the one presented in Figure 3-10 from Chapter 3. Each vibration signal was divided into segments representing 10 complete revolutions. Using the statistical parameters listed in Equations 3-1 to 3-10, a feature vector of ten elements was calculated for each segment and used for the correlation algorithm proposed.

As presented later on in this chapter, the discrepancy score distribution for the faulted components was significantly different compared to the healthy ones suggesting that the proposed correlation-based algorithm could be used to monitor mechanical system health. Still, the evaluation process presented in this chapter is only a preliminary one given the time and space constraints of a Masters' Thesis.

6.2 Discrepancy Scores for Healthy and Faulted Idlers Bearings

7.2.1 Healthy Idlers Bearing

As it was shown in Figure 5-13, identical ICP accelerometers were used to instrument the vibration signals for both belt idlers simultaneously. Following the test matrix presented in Table 6-1, the statistical correlation algorithm was implemented for a total of 20 different data sets each collected at a different duty point for healthy idlers. As shown in Table 6-5, the discrepancy scores calculated for each data set ranged from 11 to 24. Remembering that the discrepancy

score represents the number of segments with correlation coefficient less than 5 and that each vibration data sets is divided into 390 equal segments, the results obtained for all 20 healthy shows that over the range of loads and speeds tested only 2.8% to 6.1% of data segments processed had a correlation score less than 5.

In contrast to the zero discrepancy scores calculated for the SpectraQuest healthy data sets, the scores for the new simulator idlers were non-zero. This can be explained by the same points mentioned in Section 5-2 including stochastic elements between different healthy bearing, non-identical alignment for both belt systems and differences in fits for the different pulleys used for each drive station.

Still, a general trend can be seen where the discrepancy sores slightly increase with the increase of load for a constant speed while the scores slightly decrease with the increase of speed for any given load. A possible explanation for this would be the fact that the increase of the reaction torque at the gear pump pulleys affects the belt tension and thus brings the pulleys further out of alignment. On the other hand the increase in motor speed generally increase the noise background common to both idlers vibration signal and thus increases the vibration signal similarity through cross talk which decreases the discrepancy metric.

Table 6-5 Discrepancy Scores for Healthy Idler Bearings

Load (Percentage of Motor Rated Torque) / **Frequency (Hz)**	**5%**	**15%**	**25%**	**35%**
500	18	17	20	24
600	18	18	22	21
700	13	14	19	20
800	14	12	16	20
900	11	14	15	19

Using the histogram distribution for the correlation coefficients generated for each data set, Table 6-6 presents the mode, range and standard deviation for each distribution. Overall, it can be seen that the correlation coefficient distribution was generally similar with minimal changes in distribution mean, range standard deviation seen over duty cycles representing 150% increase in speed and 600% increase in load which suggests the discrepancy metrics are generally insensitive to load and speed variations.

Table 6-6 Descriptive Statistics for Correlation Score Distribution Obtained for Healthy Bearings

Data Sets Motor Load (%) and Frequency (Hz)		**Min**	**Max**	**Mode**	**Standard Deviation**
5% Load	500	3.89	9.51	6.49	0.88
	600	3.90	9.53	6.50	0.85
	700	3.90	9.52	6.47	0.86
	800	3.89	9.58	6.52	0.83
	900	3.91	9.57	6.57	0.81
15% Load	500	3.88	9.52	6.47	0.92
	600	3.91	9.50	6.47	0.89
	700	3.89	9.51	6.49	0.88
	800	3.89	9.53	6.50	0.84
	900	3.89	9.54	6.52	0.86
25% Load	500	3.89	9.50	6.48	0.95
	600	3.88	9.48	6.45	0.92
	700	3.87	9.49	6.49	0.89
	800	3.91	9.53	6.47	0.91
	900	3.90	9.51	6.50	0.88
35% Load	500	3.87	9.47	6.46	0.96
	600	3.88	9.48	6.45	0.94
	700	3.89	9.46	6.47	0.91
	800	3.83	9.49	6.48	0.89
	900	3.87	9.48	6.51	0.9

6.2.2 Faulted Idler Bearings

After investigating the discrepancy score distribution for healthy idler bearings, the scores generated for faulted idlers are examined in this subsection in order to appreciate how mechanical faults can affect the discrepancy scores generated using the algorithm proposed in this thesis. As shown in Figure 6-1, a faulted bearing with extensive inner bearing damage was press fit into one of the belt idlers used in the simulator. After attaching the faulted idler to the left drive station, the test matrix shown in Table 6-2 was used to generate the required vibration data over a range of speeds and loads. It should be noted that the same test matrix was repeated after moving the faulted idler to the right drive station. This was done to investigate how that the structural differences between the two drive stations would affect the distribution of discrepancy metrics.

Figure 6-1: Faulted Bearing Press Fit into Belt System Idler

Tables 6-7 and 6-8 represent the discrepancy scores calculated using the faulted idler data sets obtained by attaching the faulted idler to the left drive station and right drive station,

respectively. As shown, the discrepancy metric calculated for all 12 data sets has ranged from 205 to 344. Remembering that each test signal was divided into 390 segments, the aforementioned discrepancy metrics express that 52.7% to 88.2% of the test segments processed had a correlation coefficient of less than 5.

Table 6-7 Discrepancy Scores for Faulted Idler Bearings Attached to Left Drive Station

Load (Percentage of Motor Rated Torque) / **Frequency (Hz)**	**5%**	**35%**
500	315	210
700	335	229
900	344	237

Table 6-8 Discrepancy Scores for Faulted Idler Bearings Attached to Right Drive Station

Load (Percentage of Rated Toque) / **Frequency (Hz)**	**5%**	**35%**
500	300	205
700	337	226
900	342	241

Direct comparison between the discrepancy scores obtained from the faulted idlers and the ones presented in Table 6-5 confirms that structural faults can significantly change the discrepancy metric calculated for parallel simultaneously loaded components. The introduction of a mechanical fault has skewed the correlation score distribution to the left thus increasing the discrepancy scores. This shift can be immediately seen by comparing the correlation coefficient distributions obtained for healthy and faulted idlers operating under the same speed and loading conditions as presented in Figure 6-2

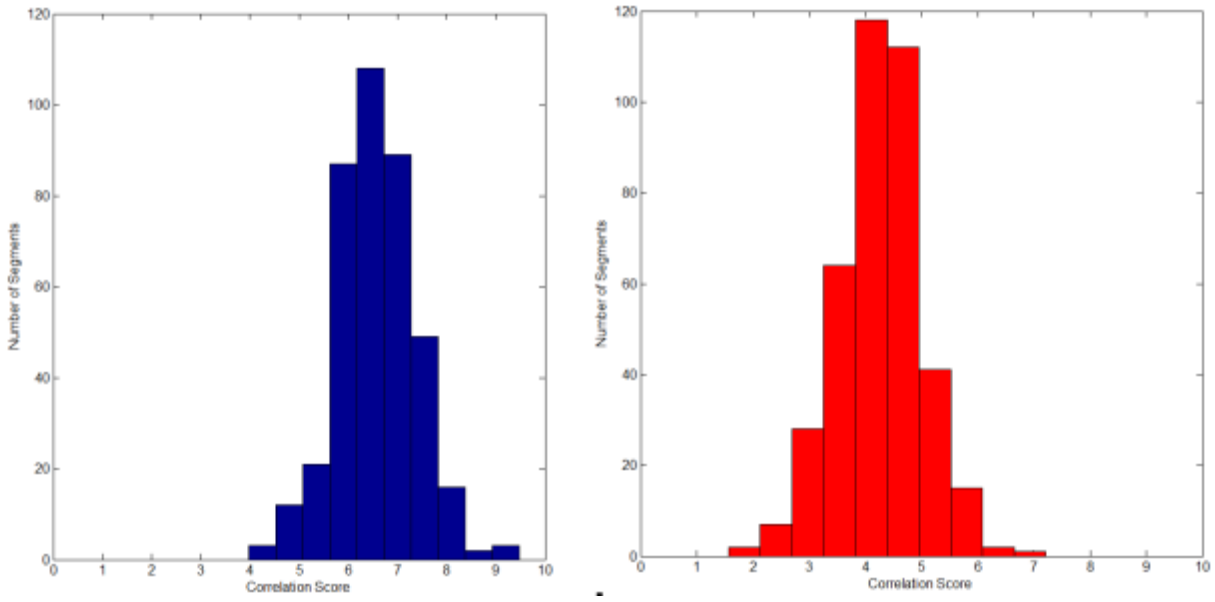

Figure 6-2 Correlation Scores Distribution Comparison at 700 RPM Motor Speed and 5% load; (a) healthy idler bearing, (b) faulted idler bearing

6.2.3 Further Discussion on Idler Bearing Fault Detection

As mentioned, the time and space constraints of this Masters' thesis did not permit for the exhaustive data collection and analysis process required to fully investigate the performance of the statistical correlation algorithm proposed. Extensive data collection using an array of identical healthy and faulted components is required to thoroughly understand the effects of load and speeds variations on the discrepancy metrics calculated.

In a general sense, it can be seen that the underlying stochastic nature of the machinery operation causes variance in the correlation scores measured resulting in a semi-normal score distribution as shown in Figure 6-2. On the other hand, it was noted for the 12 faulty data sets collected that the presence of a fault can significantly increase the discrepancy metrics calculated from the 2.8-6.1% range seen for healthy bearings to the 52.7-88.2% range seen for faulted idler bearings.

The need for extensive data collection is further stressed by the unexplainable discrepancy score trends caused by speed and loading variation. In contrast to the trends exhibited by the healthy idler bearings, the discrepancy scores presented in Tables 6-7 and 6-8 increase with speed and decrease with load. When the opposite was exhibited by the scores shown in Table 6-5, it was postulated that the increase in load affects the alignment of the belt system pulleys thus further changing the belt alignment for both idlers. It was expected that the same would happen for the faulted idlers causing the discrepancy scores to increase with load rather than decrease as shown in Table 6-7 and 6-8. A similar argument can be made for the effects of speed change.

Overall, the significant bias in the correlation scores exhibited for faulty data sets is promising feature of the proposed correlation algorithm. Before investigating how such a bias can be utilized for fault detection in non-stationary parallel operating machinery, the following section presents the discrepancy scores calculated for a different class of machine components; transmission system gears.

6.3 Discrepancy Scores for Healthy and Faulted Gears

6.3.1 Healthy Gears

Following the same investigation line used for belt idler bearings, this section examines the discrepancy scores generated using vibration data sets collected for both healthy gears over a range of operating speeds and loads. As shown in Figure 5-1 a pair of ICP accelerometers was used to instrument the input shaft bearing flanges. Following the test matrix developed in Table 6-3, a total of 20 vibration data sets were collected for different motor speeds and loads for healthy gearboxes.

Table 6-9 presents the discrepancy scores calculated for the healthy gear data sets. A quick examination of the discrepancy scores presented in the table reveal that the vibration signal discrepancy between the two gearboxes increase with speed and decreased with load. In this case, the explanation is fairly simple. The radial load transmitted to the instrumented bearing flanges is directly proportional to the torque loading experienced by the gearbox's output shaft. At low torque, the gear meshing is mainly dominated by the backlash present in the each gearbox. Increasing the torque, the gearbox meshing becomes more uniform translating into a more uniform radial loading experienced by the instrumented bearings. As such, the increase in load synchs the two gearboxes decreasing the discrepancy metric observed.

Table 6-9 Discrepancy Scores for Healthy Gears

Load (Percentage of Motor Rated Torque) / **Frequency (Hz)**	**5%**	**15%**	**25%**	**35%**
500	14	2	6	8
600	12	9	8	7
700	13	5	9	8
800	11	7	10	9
900	12	8	7	11

The discrepancy scores for the healthy gears presented in Table 6-9 showed a discrepancy score range of 2-14 over a wide operation range. Again with each vibration data set divided into 390

segments, the scores calculated shows that within each of vibration signals processed only 0.5% and 3.5% of the segments had a correlation score of less than 5. An indication that the correlation score distribution was highly skewed to the right as shown in Figure 7-3.

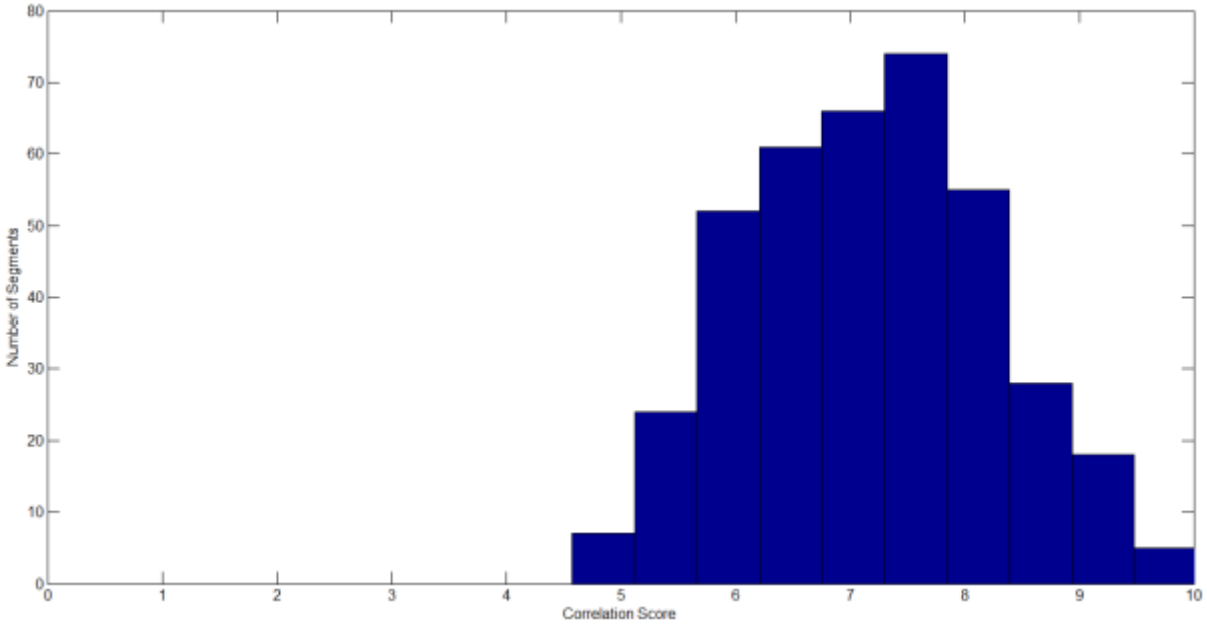

Figure 6-3 Correlation Scores Distribution for Healthy Gearbox at 500 RPM Motor Speed and 15% load

6.3.2 Faulted Gears

In this subsection, the discrepancy score for faulty gear are examined. Figure 6-4(a) presents the process used to fault a healthy 6'' (152 mm) 96 tooth steel gear. A Dremel™ tool with a stone grinder was used to grind three teeth off the steel gear. The faulted gear was installed at the left hand drive as shown in Figure 6-3(b).

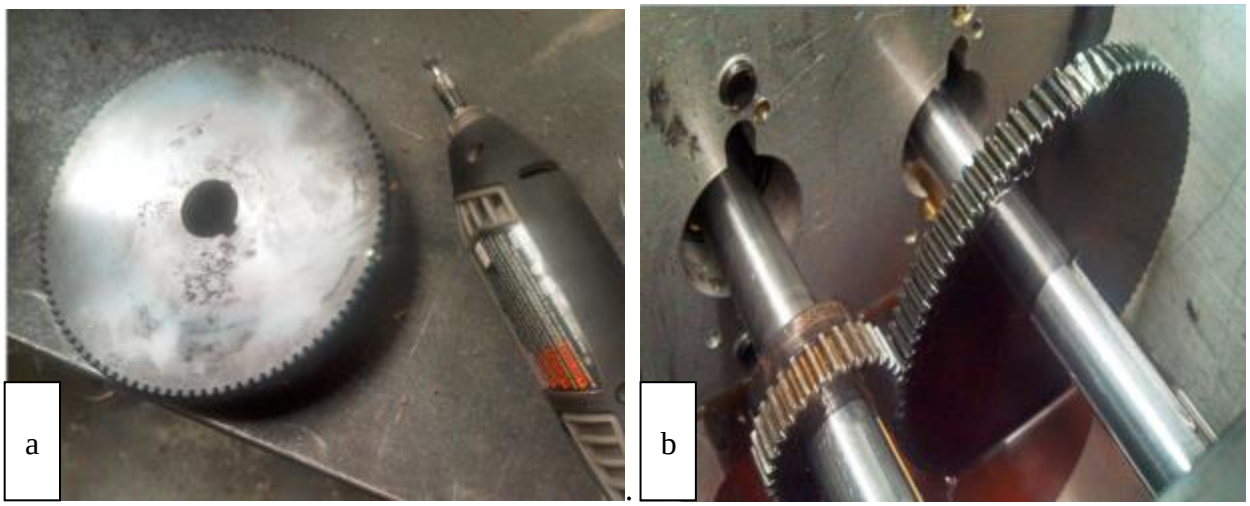

Figure 6-4 The Process of Faulting a Healthy Gear and Installing it in the Gearbox for Fault Detection; (a) the use of the Dremel™, (b) the faulted gear installed in the left gearbox

Using the test matrix presented in Table 6-4, a total of six vibration data sets were collected for both drive stations with the left drive station running a faulted gear. Table 6-10 presents the discrepancy scores calculated for the aforementioned six data sets. Compared to Table 6-9, the presence of the fault has significantly increased the discrepancy scores calculated indicating that the fault shifts correlation score distribution as was previously seen for idler bearing faults. For instance, at 500 RPM motor speed and 5% load, the presence of a gear fault has increased the percentage of segments with a score less than five from 3.5% for a healthy gear to 38.7% for a faulted gear. The distribution shift is clearly demonstrated in Figure 6-5 and agrees with the results seen in Figure 6-2 for the faulted bearings

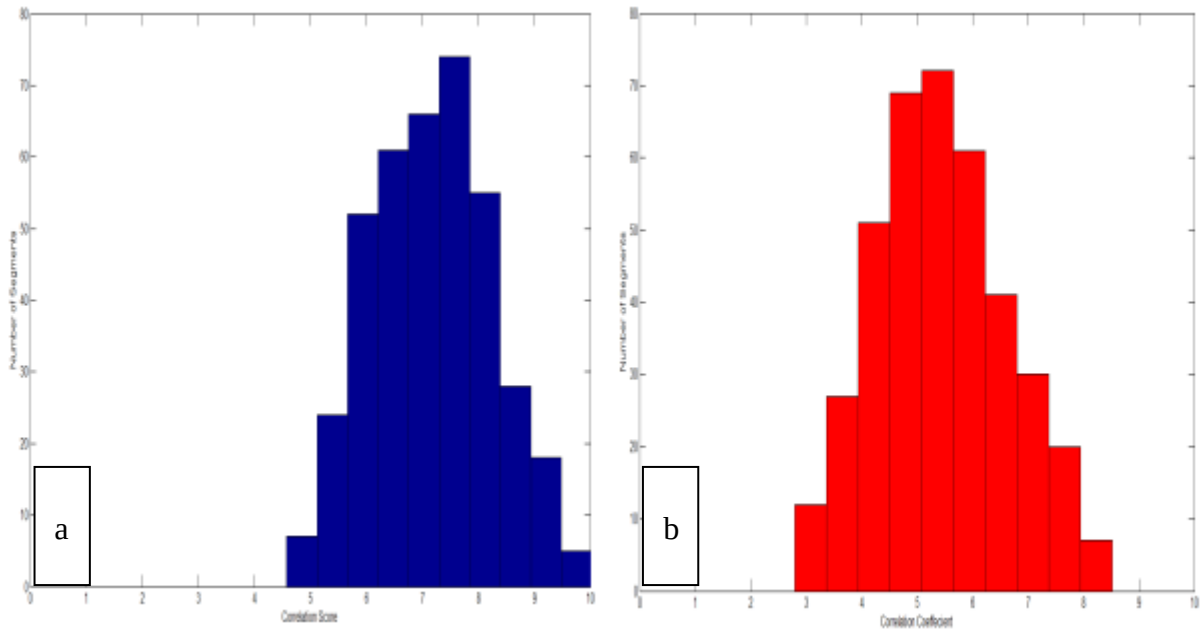

Figure 6-5 Correlation Scores Distribution Comparison at 500 RPM Motor Speed and 15% load; (a) healthy gear, (b) faulted gear

Table 6-10 Discrepancy Scores for Faulted the Gear Used in Left Drive Station

Load (Percentage of Motor Rated Torque) / **Frequency (Hz)**	**5%**	**35%**
500	151	99
700	104	72
900	63	45

As it was seen for the healthy bearings, the increase in load decreases the discrepancy metric for the same speed by minimizing the effects of backlash. However, unlike the healthy gears, the increase in motor speed also reduced the discrepancy metric measured for identical loading conditions. For the same reasons listed in subsection 6.2.3 an extended data collection and analysis process is required to fully understand the effects of speed and load variations on the discrepancy metrics calculated for gear systems.

6.4 Using the Statistical Correlation Algorithm for Fault detection

This chapter presented a preliminary study on the applicability of the statistical correlation algorithm for fault detection of machinery in non-stationary operation. By processing the vibration signals of identical simultaneously loaded components for parallel machinery, the proposed algorithm calculated the correlation of the two signals using a correlation vector based on 10 time-domain descriptive statists. Initially, the algorithm was implemented using the SpectraQuest™ simulator with promising results where a non-zero discrepancy metric was determined for healthy components irrespective of the operation cycle. In this chapter, the same algorithm was used to process the vibration signals from instrumented parallel components used in the new simulator. Unlike the results obtained for the SpectraQuest machine, the discrepancy scores proved to be non-zero for the tested healthy parallel components of the new simulator; idler bearings and gearbox gears. This was expected given the significantly more complex construction of the new simulator and the presence of a several transmission systems including gearboxes and belt drives in addition to a hydraulic loading system.

Even though extensive data collection and processing is needed to statistically study the underlying stochastic model generating the non-zero discrepancy metrics, the general results

obtained for faulted idler bearings and gearbox gear suggest that the increase in the discrepancy metric caused by a mechanical fault is significant enough that it can be differentiated from the variance caused by the underlying stochastic element of the vibration signals. Additionally, it was shown in Table 6-6 that the distribution of correlation scores was generally insensitive to duty cycle variations. The following subsection presents how the correlation coefficient can be used in fault detection

6.4.1 Modifying the Classical Alarm-based Fault Detection Approach for Simultaneously Loaded Non-Stationary Machinery

A typically monitored machinery vibration parameter such as the RMS is highly sensitive to load and speed variations. Figure 6-6 presents the changes seen the for the RMS values calculated for healthy idler bearings at a 500RPM motor speed and 5% load, 700 RPM motor speed and 35% load. As presented in Figure 3-13, a classical-alarm based system used to monitor the vibration signal RMS would issue a false alarm given that the RMS at the higher speed and load cycle surpassed the threshold

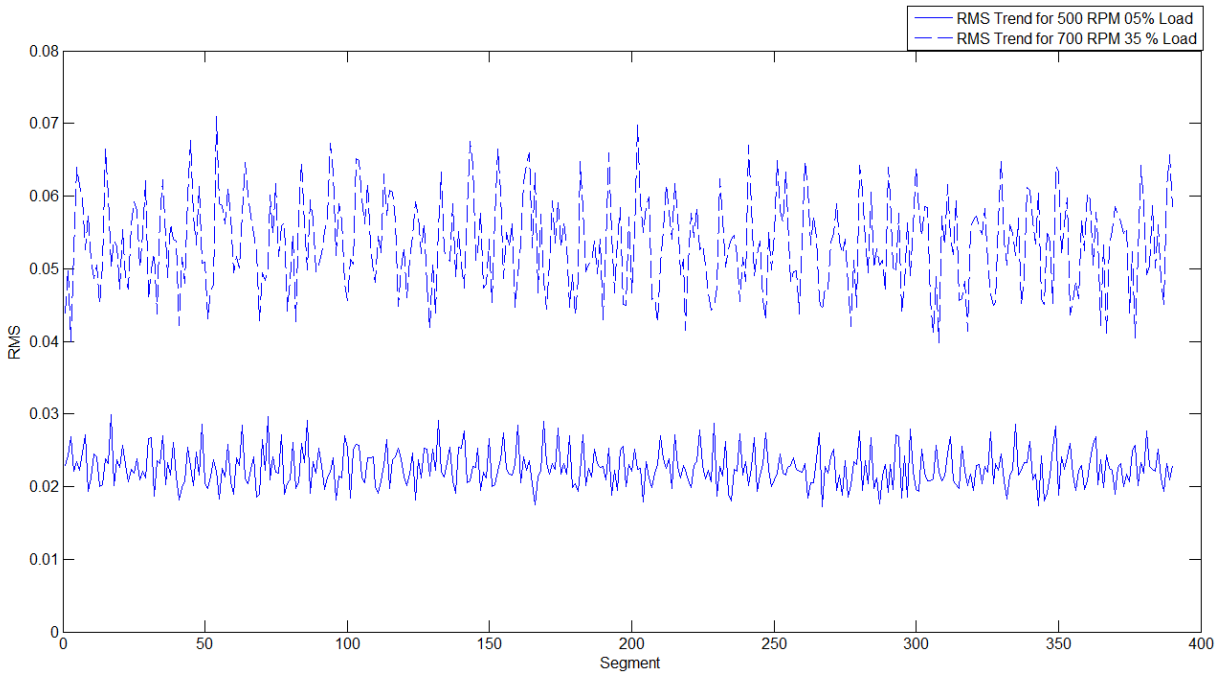

Figure 6-6 Comparison of RMS Trend for Different Load and Speed Profiles

On the other hand, Figure 6-7 presents the variance seen the correlation coefficients for the same idler bearings under the same loading conditions used for Figure 6-5. As it can visually be seen, the correlation coefficients for both exhibit a similar standard deviation a mean of 0.88 and 6.49 for the 500 RPM at 5% load data set and 0.91 and 6.47 for the 700 RPM at 35% load data set. As shown, the discrepancy metric had a minimal change even for a 140% increase in speed and 700% increase in load. Assuming that the same alarm-based approach was implemented using the correlation coefficient as a monitoring parameter, the end result is a simple alarm-based trend monitoring system that is insensitive to duty cycle variations and thus applicable to machinery in non-stationary operation

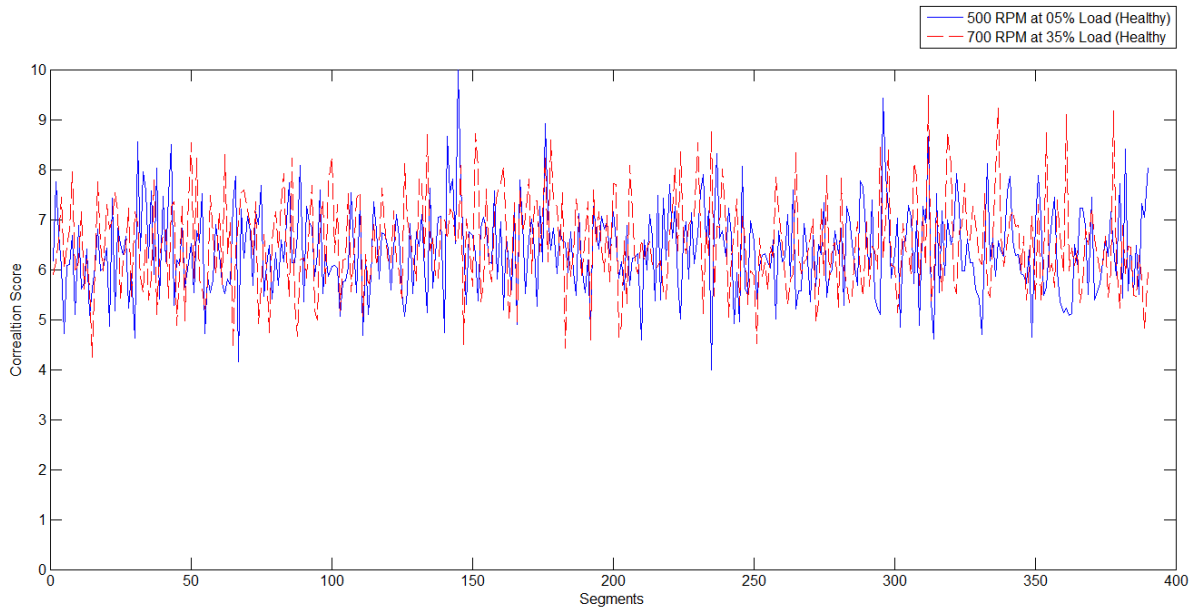

Figure 6-7 Comparison of Correlation Coefficients Trend for Different Load and Speed Profiles

To test the modified alarm system's fault detection capability, data sets for faulted idler bearings under the same operation conditions used for Figure 6-5 and 6-6 were used to show how the presence of a fault would successfully trigger an alarm for the new alarm system as shown in Figure 6-8

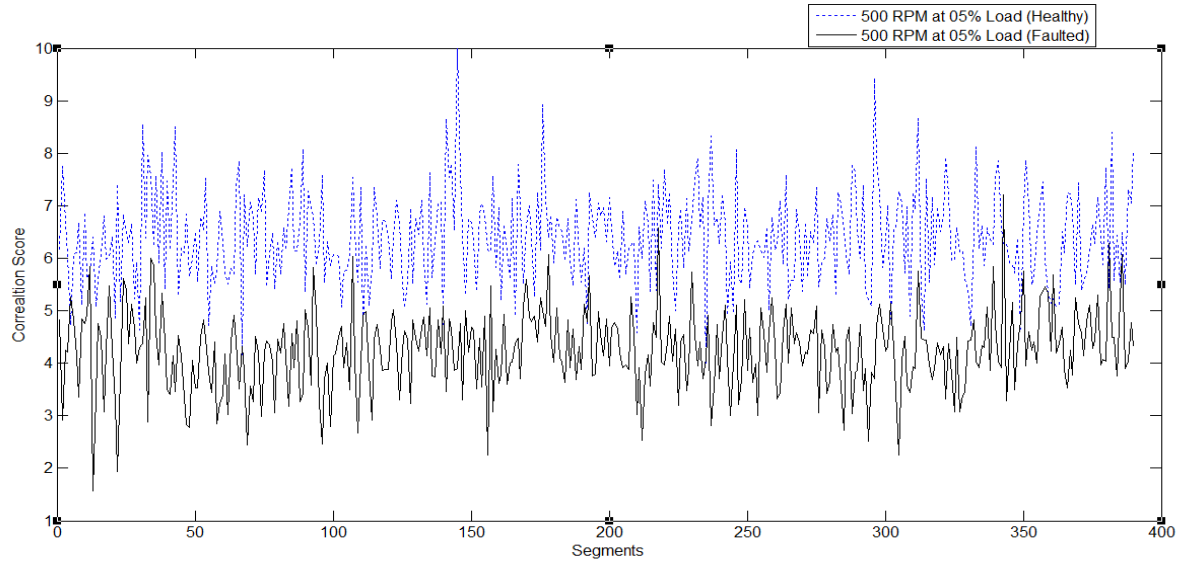

Figure 6-8 Comparison of Correlation Coefficients for Different Health Conditions Subjected to Same Loading

Chapter 7

7 Conclusions and Future Work

7.1 The Problem Identification

The problem of fault detection in non-stationary operation conditions was investigated for a particular class of machinery, simultaneously loaded parallel machinery. Existing monitoring solutions for variable duty machinery were examined and it was determined that their complexity and need for large training data limited their industrial application. This thesis proposed the use of the mechanical redundancy inherent to parallel machinery to facilitate the task of fault detection in non-stationary operation conditions. The proposed approach continuously monitors the degree of similarity between the two parallel machinery subsystems under the assumptions that simultaneously loaded healthy identical subsystems should exhibit similar mechanical response and that a change in the degree of similarity would indicate structural change.

7.2 Experimental Data Collection

7.2.1 In-Situ Data Collection

In order to validate the assumption that simultaneously-loaded identical subsystem would exhibit similar mechanical response, an *in-situ* field data collection was completed for a local novel material haulage solution that used a parallel drive station configuration to propel a passive, rail-based haulage system. The data collected included gearbox and motor vibration for both parallel drive stations simultaneously. Examination of the data, including current drawn by each drive

station's motor suggested that both parallel drive systems exhibited similar loading and vibration amplitude modulation when the train engaged into the drive station. Additionally, spectral comparison indicated that both drive systems exhibited similar characteristic frequencies including the bearing specific and the gear mesh frequencies.

7.2.2 Laboratory Data Collection

The effect of structural damage could not be investigated during the *in-situ* data collection phase. In order to avoid the financially unattractive route of seeding faults into healthy industrial machinery, a small table-top machinery simulator was used to investigate how the vibration signal of simultaneously-loaded identical bearings can be affected when one of the bearings is damaged. Using the SpectraQuest™ simulator, a set of 36 tests were completed using different types of bearing faults such as inner race, outer race and ball faults. The test matrix used to generate the data sets ensured that vibration data was collected for different loading and speed conditions. Given limited speed and loading capabilities of the SpectraQuest™ simulator, only three discrete loading conditions were examined each at three different speeds

A preliminary correlation-based statistical approach was developed with promising results. The encouraging initial results led to the development of new fault simulator that could reproduce the loading cycle seen for the Rail-Veyor® drive stations. In contrast to the SpectraQuest™ simulator, the new test-stand featured multi-stage transmission systems including reduction gearboxes, belt drive systems and hydraulic loading circuits. The new simulator allowed for continuous and repeatable simulation of realistic loading cycles and allowed us to investigate the performance of the proposed algorithm for complex machines. Before using the new machine to test faulted components, an extensive baseline data collection phase was completed for the

different parallel subsystems in the new simulator. This included the input and output bearing flanges for both gearboxes, the belt drive idlers for the two belt drive systems, the two AC motors and the two hydraulic gear pumps.

After validating the loading similarity experienced by the parallel components of the new machinery simulator, vibration data sets were collected for faulty components. Faulted components investigated included faulted idler bearings and faulted gears. A total of 20 data sets were collected for healthy idler bearings at speeds and loads ranging from 500 to 900 RPM and 5% to 35% motor load, respectively. That was followed by collecting six data sets for faulted bearings. The faulted idler bearing was switched to the other drive station and another six data sets were collected for the faulted bearings.

A total of 20 data sets were also collected for healthy gears over the same range of speed and loading used for healthy bearing data collection. Using a hand-held grinder three teeth from a healthy gear were chipped off and the faulted gear was installed in the left drive station. Only six data sets were collected for the faulted gear.

7.3 New Experimental Machine Conclusions

The design, development, validation and fabrication of the fully instrumented mechanical test stand with a mechatronically controlled loading system represents the significant contribution of this thesis. Given the complexity of the new machine and the precision fabrication required to ensure smooth baseline operation, the fabrication and set up of the new simulator took more than a year to finish. The main objectives of the new design were:

- True replication of the parallel system arrangement used in the Rail-Veyor™ drive station design.
- Capable of simulating repeatable different loading and speed profiles in a continuous manner
- Capable of simulating realistic speed and loading scenarios for target machinery
- High precision setup providing smooth repeatable baseline operation
- Modular design allowing for continuous modifications and upgrades
- A mechanical design that is highly accessible such that component replacement does not require disassembly
- Full instrumentation with data logging capabilities
- Highly flexible allowing for simulation of different faults whether individually or concurrently including bearing, gear, motor, hydraulic and belt drive faults

The data collection phase for the new machine represented an ideal opportunity to investigate the loading similarity for the new fault simulator. Overall, the vibration signals of parallel components were similar, but not identical. Additionally, the degree of similarity varied from one component to another with the idler bearings of both drive stations exhibiting the most similar vibration signal while the gearboxes exhibiting the least vibration similarity. Generally, this was expected given the underlying stochastic nature of mechanical system vibration, the differences in alignments and fits, cross-talk between the two drive stations and mechanical fabrication imperfections. Still, all the aforementioned points are valid for any industrial machine and as such the new simulator represents a valuable research tool for simulating the noisy vibration signal expected from industrial drive stations.

7.4 Experimental Data Analysis

7.4.1 SpectraQuest™ Data

Using the SpectraQuest™ generated bearing data sets, the implementation of the proposed correlation-based statistical algorithm presented very promising results. A zero discrepancy score was calculated for healthy bearings irrespective of their loading and speed cycle. These initial results suggested that a very simple monitoring solution could be developed for non-stationary operating parallel machinery where the discrepancy metrics of the vibration signals are calculated and a fixed threshold alarm system is used to indicate a fault when the discrepancy metric becomes non-zero. It was also noticed that the discrepancy metrics generally increased with load and speed for the SpectraQuest™ faulted bearing data. It should be noted that fault diagnosis was not investigated for the bearing data and that the discrepancy metrics values couldn't be used to indicate the bearing fault type.

Of course, the simple construction and high signal to noise ratio for the SpectraQuest™ machine were uncommon to actual industrial drive stations. As such, the new fault simulator was developed to investigate the discrepancy metrics generated for healthy components in complex noisy machinery.

7.4.2 New Simulator Data

Featuring a complex, multi stage transmission system and the capability to reproduce realistic loading profiles, the new simulator was used to investigate the performance of the proposed fault detection approach. As it was shown, non-zero discrepancy metrics were obtained for healthy components. Healthy idler bearings exhibited discrepancy metrics of 11 to 24 for the 20

vibration data sets collected over speeds and loads ranging from 500 to 900 RPM and 5% to 35% motor load. Even with a non-zero discrepancy metric the aforementioned scores showed that over the wide rand of duty cycles tested only 2.8% to 6.1% of the correlation scores calculated for each data set had a value less than five. Additionally, it was shown that range, mode and standard deviation for all 20 tests were very similar. Comparable results were obtained for the healthy gear data sets with discrepancy metrics ranging from 2 to 14 over the same range of duty cycles tested for the idler bearings.

To appreciate how the discrepancy metrics are mainly affected by structural health, the faulted data set collected using the new simulator were processed. As it was shown, the faulted bearing data sets had a significantly high discrepancy metric ranging from 344 to 205. As such, 52.7% to 88.2% of the correlation scores calculated for each data set had a correlation score less than a 5. Faulted gears also exhibited high discrepancy scores ranging from 151 to 45. The previous values present a clear indication that a mechanical fault can result in a considerable bias for the discrepancy score which can be seen as a left shift in the correlation score distribution towards the zero.

As it was stated previously, the data collection and analysis phase for the new simulator was a preliminary one given the time and space constraints for a Master's thesis. In order to fully understand the underlying stochastic processes resulting in non-zero discrepancy scores, extensive data collection and analysis is required for a range of components. Such analysis is also needed to investigate the statistical significance of the discrepancy scores calculated and to develop the thresholds needed for industrial implementation

7.5 Future Work

Overall, the results obtained for the new simulator suggest that the discrepancy scores can be used a monitored parameter that is generally insensitive to load and speed duty variations. By modifying a classical alarm-based fault detection system to monitor the discrepancy score trends for simultaneously-loaded parallel machinery, commercially available monitoring solutions would be able to discriminate vibration changes due to duty cycle variations from changes due to structural health problems. If successful, the simplicity of the proposed approach, compared to AI approaches used in variable duty fault detection, can be very attractive to the industry and might find applications in monitoring parallel pump and compressor stations used in the mining and process industry. However, the following points have to be addressed to fully validate the proposed approach

7.5.1 Modifications for the New Simulator

The new simulator represents a valuable research tool for validating the newly proposed correlation-based algorithm. By processing that vibration data collected for the new simulator it was found that the gearbox vibration similarity was not as expected. To enhance the gearbox similarity, the shaft alignment for both gearboxes has to be improved. Likewise, the vibration signal similarity for both output shaft bearing flanges could be improved by supporting the end shafts carrying the driver pulleys. Another important modification would be the installation of rotary torque sensors to instrument the loading for each drive stations.

To further investigate the loading similarity of parallel components, acoustic emission sensors can be used as a supplementary form of instrumentation to investigate the high frequency similarity of the two drive stations

7.5.2 Further Data Collection Using the New Simulator

As mentioned, extensive data collection is required to fully investigate how the discrepancy scores are affected by duty cycle variations. The non-zero discrepancy scores observed for healthy components necessitate the use of statistical analysis to develop the thresholds required for fault detection.

The data collection phase should include an array of identical components, should involve switching the components between the two drive stations and should cover a wider range of speeds and loads. Additionally, the data collection phase should involve the use of continuous variable duty cycles such as sinusoidal speed and load variations.

7.5.3 Modifications to the Proposed Statistical Correlation Algorithm

In this thesis, the statistical correlation algorithm measures the similarity between parallel components using time domain features only. Given how background noise can dominate the time domain representation of vibration signals, the use of frequency domain and time-frequency domain features should be investigated.

For instance, using a bank of band pass filters, the characteristic frequencies of gearbox vibration such as bearing specific and gear mesh frequencies can be separated for each signal. The power of corresponding bands can be compared for the two parallel components as a form of similarity

measure. Given that both components are sharing the same duty cycle, amplitude and frequency modulation due to duty cycle variations should be common to both spectrums and thus spectrum changes can be an indication of faults. This approach is very intuitive and very similar to the case when vibration specialists compare machinery spectra against a baseline. However, given the absence of an established baseline for variable duty machinery, the mechanical redundancy of parallel machinery can be capitalized such that parallel components can act as baselines for each other.

Another viable approach to signal comparison is the use of a geometrical distance measure between the features vectors calculated for the monitored vibration signals of parallel subsystems. A variety of distance measures can be investigated including measures implemented directly in the n-dimensional feature space such as the Euclidian, Manhattan, and Cosine distances between the feature vectors [74]. Alternatively, the distance measure can be calculated using only the linear predictive coefficients calculated for the vibration time signal of the two simultaneously loaded systems. This can be done by determining an autoregressive model for the signals monitored and then calculating the mean square error between the determined autoregressive matrices for each signal. A classical algorithm for this autoregressive distance measure is the Itakura distance used in biomedical seizure detection [75]. Together with the aforementioned feature-based distance measures, the performance of the Itakura distance measure should be investigated in future work. This would represent the first application of the Itakura distance in the literature of machinery fault detection.

References

[1] O. Krellis and T. Singleton. Mine maintenance-the cost of operation. 1998.

[2] Sandvik® Mining and Construction (2012, January 10). *Bucket Wheel Excavators for OpenPit Mining* [Online]. Available: http://www.miningandconstruction.sandvik.com

[3] Ackerman, A. (2005) 'Week 5: State Dependent Systems. ENGR4366 Reliability of Mining Equipment

[4] Currie, M. The new case for condition monitoring, *Energy Processing. Canada 30*, pp. 32-36. 2006.

[5] D. Sandy. Condition monitoring in the 21st century. 2000.

[6] Johnston, D. N. and Todd, C. (2010) Condition Monitoring of Aircraft Fuel Pumps using Pressure Ripple Measurements. In: Fluid Power and Motion Control, 2010-09-15 - 2010-09-17, Bath

[7] Tender® Lifts and Cranes (2010, August 14). *Gear Pumps* [Online]. Available: http://www.tenderliftsandcranes.co.uk

[8] Pagnutti, J. (2014) *In-situ railway track fault detection using railcar vibration*, master thesis, Laurentian University, Sudbury, Canada

[9] Rathbone, T.C, "Vibration Tolerances", *Power Plant Engineering 5*, 1939

[10] Mott, R.L.(2010). *Machine elements in Mechanical design* (4th ed.). Upper Saddle River, N.J.: Pearson/Merrill Prentice Hall

[11] Sakshat Virtual Labs. (2012). Diagnosis of Shaft Misalignment and its Effects [Online]. Available: http://iitkgp.vlab.co.in

[12] Randall, R.B.(2011). *Vibration-based condition monitoring* (1st ed.). Hoboken N.J.: Wiley & sons

[13] Bently Rotor Dynamics. (2001). Rolling element bearing defect detection [Online]. Available: http://bently.com

[14] Al-Arbi, Salem (2012) Condition Monitoring of Gear Systems using Vibration Analysis. Doctoral thesis, University of Huddersfield. UK

[15] McBain, Jordan (2012) Condition Monitoring of Machinery Subject to Variable States. Doctoral thesis, Laurentian University, Canada

[16] Slawomir Marian Zaremba, “Dynamical Signature of Gearbox Vibration”, United State – California: California Institute of Technology; 1997

[17] Randall, R.B, & Antoni, J. (2011). Rolling element bearing diagnostics-A tutorial. *Mechanical Systems and Signal Processing, 25, 485-520*

[18] Entek IRD International. (1998). The Time Waveform. [Online]. Available: http://irdmechanalysis.com

[19] Mechefske, C. (2010) 'Week 6: Machine Condition Monitoring and Fault Diagnosis. MECH826. Condition Monitoring

[20] Green Power Monitoring Systems (2009). A Quick Introduction to Bearing Envelope Analysis. [Online]. Available: www.mfpt.org

[21] Baydar, N., Ball, A., and Gu, F. - Detection of Gear Failures via Vibration and Acoustic Signals Using Wavelet Transform, Mechanical Systems and Signal Processing, 17(4).pp. 787-804 ,2003.

[22] Lee J. H., Kim J. and Kim H. J. - Development of Enhanced Wigner-Ville Distribution Function, Mechanical Systems and signal Processing 15(2) 367-398, 2001.

[23] Cohen L., Time-frequency distributions- a review, In Proceedings of the IEEE. Vol. 77/7. Page 941-981, 1989

[24] Ruqiang, Y. Base (2007) Wavelet Selection Criteria for Non-Stationary Vibration Analysis in Bearing Health Diagnosis. A Doctoral thesis Thesis, Birmingham University, UK

[25] Bollahbal, D., Golnaraghi, F., Ismail F., Amplitude and phase wavelet maps for the detection of cracks in geared system, Mechanical Systems and Signal Processing, 13(3), pp. 423-436. 1999.

[26] Worden, K., Staszewski, W., Hensman, J., Natural computing for mechanical system research: A tutorial overview, Mechanical Systems and Signal Processing, 25(1), pp. 4-111. 2010.

[27] Timusk, M. A.(2006) A unified method for anomaly detection in unsteady systems. A Doctoral thesis, Queen University, Canada

[28] Nandi, A.K, 2002. Vibration Based Fault Detection –Feature Classifiers and Novelty Detection. In: COMADEM, pp.23-36

[29] Fredrickson, Roberts, Townsend & Tarassenko, 1994. Speaker identification using

networks of radial-basis function. In: Proceedings of seventh European Signal Processing Conference, pp.812-815

[30] A. Nirac, T. Corbett-Clark, N. Townsend, L. Tarassenko, Choosing an appropriate model for novelty detection, in: Proceedings ofFifth IEE International Conference on Artificial Neural Networks,Cambridge, 1997

[31] Timusk, M. A.(2001) Autonomous Health Monitoring of a Hydraulic System. A Master's thesis, University of Western Ontario, Canada

[32] Bask, M. (2005) Dynamic Threshold Generators. A Doctoral thesis, Lulea University, Sweden

[33] Isermann, R. (2006) Fault-diagnosis systems – An introduction from fault detection to fault tolerance. Springer, Heidelberg,

[34] Rault, A et. al. (1971) Identification and modeling of a jet engine. IFAC Symposium on Digital Simulation of Continuous Processes, Gejor

[35] Willsky, A, A survey of Design Methods for Failure Detection in Dynamic Systems, Automatica, 12, pp. 601-611. 1976

[36] Walker, B.K, Huang, K.Y, FDI by Extended Kalman Filter Parameter Estimation for an Industrial Actuator Benchmark, Control Eng, 3, pp. 1769-1774. 1995

[37] Lee, J. 2007. Model-based fault detection and isolation for electric power steering system, ICCAS'07 2369:2374

[38] Chow, E., Willsky, A. Analytical Redundancy and the Design of Robust Failure Detection Systems, In Proceedings of the IEEE. Vol. 29/7. Page 603-615, 1984

[39] Deckert, J., Desal, M. F-8 DFBW Sensor Faliure Identification Using Analytic Redundancy, In Transactions of Automatic Control Vol. 22/5. Page 795-804, 1977

[40] Serdio, F., Lughofer, E., Pichler, K., Buchegger, T. and Efendic, H. (2014). Residual-based fault detection using soft computing techniques for condition monitoring at rolling mills. *Information Sciences*, 259, pp.304--320.

[41] Bachus, L. and Custodio, A. (2003). *Know and understand centrifugal pumps*. 1st ed. Oxford: Elsevier.

[42] Levitronix®. (2005) Redundency with Levitronix pump systems . [Online]. Available: www.levitronix.com/

[43] United States Army Aviation Warfighting Centre. (2008) UH-60A student handout.

[Online]. Available: www.aasf1-ny.org

[44] Japan Hamworth & Co., Ltd. (2010) Electro-hydraulic piston type steering gear. [Online]. Available: http://www.japanham.co.jp

[45] Girondin, V., Herv'e, M., Pekpe, K., Cassar, J. and others, (2012). Vibration-based monitoring of helicopter epicyclical gears. pp.669--683.

[46] Stack, J., Habetler, T. and Harley, R. (2003). Effects of machine speed on the development and detection of rolling element bearing faults. *Power Electronics Letters, IEEE*, 1(1), pp.19--21.

[47] Lyon, D. (2010). The discrete Fourier transform, part 6: Cross-correlation, *Journal of object technology*, *9*, pp.1--6

[48] Randall, R. (2004). State of the art in monitoring rotating machinery-part 2. *Sound and Vibration*, 38(5), pp.10--17.

[49] Rioul, O. and Vetterli, M. (1991). Wavelets and signal processing. *IEEE signal processing magazine*, 8(LCAV-ARTICLE-1991-005), pp.14--38.

[50] Hope, C. and Furlong, D. (1997). Time Frequency Distributions for Timbre Morphing: The Wigner Distribution versus the STFT.

[51] Burrus, C. S (2014, June 14). *Generalizations of the Basic Multi-resolution Wavelet System* [Online]. Available: http://www.cnx.org

[52] S. Sheng. (2012) Wind Turbine Gearbox Condition Monitoring Round Robin Study – Vibration Analysis. [Online]. Available: http://www.nrel.gov

[53] Hassan, M., Bayoumi, A. and Shin, Y. (2014). Quadratic-nonlinearity index based on bicoherence and its application in condition monitoring of drive-train components. *IEEE*.

[54] Coats, D., Cho, K., Shin, Y., Goodman, N., Blechertas, V. and Bayoumi, A. (2011). Advanced time--frequency mutual information measures for condition-based maintenance of helicopter drivetrains. *Instrumentation and Measurement, IEEE Transactions on*, 60(8), pp.2984--2994.

[55] Bayoumi, A., Ranson, W., Eisner, C. and Grant, C. (n.d.). On-Board Vibration and Health Monitoring Systems: An Approach to Achieve Condition-based Maintenance.

[56] Bayoumi, A., Ranson, W., Eisner, L. and Grant, L. (2005). Cost and effectiveness analysis of the AH-64 and UH-60 on-board vibrations monitoring system. pp.3921--3940.

[57] SpectraQuest™. (2012). Machinery Fault Simulator [Online]. Available:

http://spectraquest.com/machinery-fault-simulator/details/mfs/

[58] Zhang, S., Ma, L. and Mathew, J. (2005). Vibration feature analysis for rolling element bearing diagnosis using Bayesian neural networks

[59] Bozchalooi, I. and Liang, M. (2007). Identification of the high SNR frequency band for bearing fault signature enhancement. pp.39--43.

[60] Purvee, A., Banerjee, G. (2012). Dynamic Simulation and Experimental Results of Bearing Faults of Squirrel Cage Induction Motors. *Condition Monitoring and Diagnosis Conference , IEEE*

[61] Baldor Electric (2007). Product Information Packet – IDNRPM21104C.

[62] Cha-Cho Yeh, Gennadi Y.sizov, Ahmed Sayed-Ahmed, Nabeel A.O.Demerdash, Richard J.Ponivelli, Edwin E.YAz, Dam M.Ionel "A reconfigurable motor for experimental emulation of stator winding interturn and broken bar fault in polyphase induction machines",IEEE transaction on energy conversion, vol 23, Dec 2008.

[63] M. E. Benbouzid "A review of induction motor signature analysis as a medium for faults detection", IEEE, pp.l950 -1955 1998

[64] T. Breen and K. S. Patel "New developments in non-invasive online motor diagnosis", IEEE, pp.231 -236 1996

[65] McBain, J., Lakanen, G. and Timusk, M. (2013). Vibration-and acoustic-emissions based novelty detection of fretted bearings. *Journal of Quality in Maintenance Engineering*, 19(2), pp.181--198.

[66] McBain, J. and Timusk, M. (2011). Feature extraction for novelty detection as applied to fault detection in machinery. *Pattern Recognition Letters*, 32(7), pp.1054--1061.

[67] McBain, J. and Timusk, M. (2009). Fault detection in variable speed machinery: Statistical parameterization. *Journal of Sound and Vibration*, 327(3), pp.623--646.

[68] Hub City (2012). *Bevel Gear Drives* [Online]. Available: http://www.hubcityinc.com

[69] Adler, U. and Bauer, H. (1993). *Automotive handbook*. 1st ed. Stuttgart: Robert Bosch.

[70] Metaris™(2009). Hydraulic Gear Pumps Product Information.

[71] Vickers ™ (1989). *Industrial Hydraulic Manual*. 2st ed. Rochester Hills: Technical Training Center

[72] HydraForce™ (2012). *Proportional Relief Valve: TS12-26* [Online]. Available:

http://www.Hydraforce.com

[73] Esposito, A. (1980). *Fluid power with applications*. 1st ed. Englewood Cliffs, N.J.: Prentice-Hall.

[74] Xu, J., Bakardjian, H., Cichocki, A. and Principe, J. (2008). A new nonlinear similarity measure for multichannel signals. *Neural Networks*, 21(2), pp.222--231.

[75] Estrada, E., Nazeran, H., Nava, P., Behbehani, K., Burk, J. and Lucas, E. (2006). Itakura Distance: A useful similarity measure between EEG and EOG signals in computer-aided classification of sleep stages. pp.1189--1192

Appendix A – Additional Investigations

The following sections present a review on signal comparison techniques found in the biomedical signal processing literature.

Signal comparison is researched extensively in the fields of biomedical signal processing and speech recognition. In the biomedical domain, attempts have been made since the 1970's to develop automated diagnostic solutions to aid in detecting heart arrhythmias and epileptic seizures by applying signal comparison techniques to compare the patient's Electro-Cardiograph (ECG) and Electroencephalography (EEG) against healthy measurements. As such, this chapter presents the different signal comparison approaches used in biomedical signal analysis that can be adapted to the problem of fault detection in simultaneously-loaded machinery.

The term biomedical signal processing applies to the manipulation of biological data normally collected by medical devices. This processing step between the signal source and the final information assessment is instrumental in enhancing the information in the data, thus aiding physician in making their clinical assessments. Commonly processed biomedical data includes the electrical activity recording of vital human organs such as the heart and the brain. Non-invasive electrical measurement can be taken using electrodes attached to the chest or on the head such as the electrocardiogram (ECG) and electroencephalogram (EEG), respectively

In all cases, substantial signal processing is required to enhance the collected data through sampling, noise removal and signal construction. The quality of the output signal depends mainly on the reliability of the signal processing algorithm used. Biomedical signal processing converts

the input signal into a re-ordered form that best presents the content of the signal. For instance, EEG signal processing usually involves the application of FFT operations to convert the signal to the frequency domain. This is done since changes in EEG accompanying the different mental conditions such as sleep stages are better quantified using frequency domain features such as the power of specific frequency bands including; the delta (1–4 Hz), theta (4–8 Hz), beta (13–30 Hz) and gamma (30–70 Hz) frequency bands according to Rangayyan, R. (2002). [1]

Utilizing advancements in biomedical signal processing, the development of automated diagnostic tools can be of significant value to practitioners and patients alike. Medical Diagnostic Decision Support Systems (MDDSS) are currently widespread in the medical field accomplishing automatic diagnosis for a range of diseases including; cardiac arrhythmia, seizures and retinal disease. According to his review on MDDSS solutions, Miller (1994)[2] concluded that automated medical diagnosis is a highly complex problem requiring in some cases the use of various computing techniques including analytic functions; mathematical pathophysiological models; pattern recognition algorithms; Bayesian statistical systems; decision-analytical systems; and symbolic reasoning.

It is suggested here that the logic behind automated machinery fault detection and MDDSS is principally the same; a collection of measurements are used to infer the health status of a

[1] Rangayyan, R. (2002). *Biomedical signal analysis*. 1st ed. New York, NY: Wiley-Interscience

[2] Miller, R. (1994). Medical Diagnostic Decision Support Systems--Past, Present, And Future: A Threaded Bibliography and Brief Commentary. *Journal of the American Medical Informatics Association*, 1(1), pp.8-27.

machine and a patient, respectively. Analysis algorithms typically used in MDDSS systems focus on signal comparison methods including spectral, temporal and time-frequency domains.

Spectral Techniques

Spectral parameters of EEG are now routinely used in neurological signal analysis including intra-operative monitoring, sleep studies, seizure detection etc. Conventional FFT spectral estimation has several drawbacks including resolution, leakage effects, loss of time information and the fact that it assumes stationary signal content. The non-stationary nature of EEG signals is principally identical to the nature of the vibration signal measured of variable duty machinery. Therefore, the spectral techniques used for EEG processing can be adopted for the problem of fault detection in non-stationary operation.

The main theme of the spectral techniques utilized for a noise-filtered signal comparison in the biomedical domain is as follows: spectral estimation followed by spectral comparison.

Spectral Estimation

Spectral estimation involves the characterization of the signal's frequency content by estimating its spectral density. Depending on whether a model is used or not, spectral estimation can be done parametrically or non-parametrically. In the following paragraphs, the limitations of classical spectral estimation will be discussed and then the Welch Power Spectral Density and the Modified Covariance method will be presented as examples of non-parametric and parametric techniques, respectively.

Typically, the FFT is used to transform the time-domain signal into the frequency domain which is then graphically represented as the modulus-squared of the FFT; the periodogram. According to Equation A-1, the Periodogram is based on an autocorrelation sequence, which, in effect applies a rectangular window on the data set. Given that the FFT of a rectangular window is a sinc function, the periodogram suffers from bias and variance. Detailed analysis shows that the variance of the Periodogram is related to the sinc function as shown in Equation A-2.

$$R_{xx}(k) = \frac{1}{N}\sum_{n}^{\infty} x_N(n+k)x_N^*(n) = \frac{1}{N}x_N(k) * x_N^*(-k) \qquad \text{Eq. (A-1)}$$

$$Var\{P_{xx}\acute{}(w)\} \approx {P_{xx}}^2(w)\left[1 + \left(\frac{\sin(\frac{Nw}{2})}{Nsin(\frac{w}{2})}\right)^2\right] \qquad \text{Eq. (A-2)}$$

In order to improve the performance of a spectral estimator, the non-parametric Welch method is used as an overlapping modified periodogram. In this method, a sequence *N* points is divided into samples of size equal *L*, and offset by distance *D* points such that the sequence is divided into *K* segments as shown in Equation 3-3. Using a Bartlett window *w(n)* and a 50% overlap, the variance of the Welch methods can be computed as shown Equation A-4. Accordingly, the Welch method represents a consistent estimator where the spectral variance would decrease by increasing the sequence length *N*.

$$\{P_{xx}(w)\} = \frac{1}{K}\sum_{i=0}^{k=1} P_{xx}^{(\acute{m},\iota)}(w) \qquad \text{Eq. (A-3)}$$

$$Var\{P_{xx}\acute{}(w)\} \approx \frac{9}{16}\frac{L}{N}P_{xx}^2(w) \qquad \text{Eq. (A-4)}$$

Non-parametric spectral estimation methods neglect information that may be available about the underlying process generating the signal being studied. The incorporation of such information can significantly improve the spectral estimation's accuracy and resolution. In this approach, different modelling techniques such as Autoregressive (AR) modelling can be used to extract information regarding the underlying process.

For a conventional AR model the time series is modeled as show in Equation 3-5 with $x(n), a(n)$ and $e(n)$ representing the time series, the AR parameters and the prediction errors, respectively/

$$x(n) = e(n) - a(1)x(n-1) - a(2)x(n-2) - \cdots - a(n)x(n-p) \qquad \text{Eq. (A-5)}$$

By transforming to the z-transform, the representation in Equation A-5 can be summarized into the more compact form of Equation A-6 with *A* representing a polynomial of model parameters. The estimation of the model parameters can be accomplished using various algorithms including the autocorrelation, Burg and covariance methods.

$$Ax(n) = e(n) \qquad \text{Eq. (A-6)}$$

A good comparison on the performance of different AR techniques for spectral estimation of EEG signals for the detection of epileptic seizures can be found in Faust (2008)[3] where the author concluded that the spectral estimates obtained using the modified covariance AR

[3] Faust, O., Acharya, R., Allen, A. and Lin, C. (2008). Analysis of EEG signals during epileptic and alcoholic states using AR modeling techniques. *IRBM*, 29(1), pp.44--52.

modelling were the most accurate. Additionally, Wear (1995)[4] explained that the modified covariance method can produce higher resolution spectral estimates compared to the autocorrelation method since it requires no windowing and is based on a minimization algorithm for both the forward and backward prediction errors as shown in Equation A-7 rather than just the backward error minimization technique used in autocorrelation. Wear (1995) successfully used it to determine the AR model required for parametric spectral estimation of ultrasonic tissue characterization.

$$\begin{bmatrix} r_x(1,1) & \cdots & r_x(p,1) \\ \vdots & \ddots & \vdots \\ r_x(1,p) & \cdots & r_x(p,p) \end{bmatrix} \begin{bmatrix} a_1 \\ \vdots \\ a_p \end{bmatrix} = - \begin{bmatrix} r_x(0,1) \\ \vdots \\ r_x(0,p) \end{bmatrix}$$

$$r(k,l) = \sum_{N=p}^{N-1} [x_{n-l} x_{n-k}^* + x_{n-p+l} x_{n-p+k}^*] \qquad \text{Eq. (A-7)}$$

After obtaining the spectral estimates of the signals of interest, their similarity can be determined by comparing their spectral content. The spectrum of both signals can be compared either using an inner product operation such as Coherence or a form of distance measure such as the Itakura distance.

Based on Fourier transform, the spectral coherence of two signals as shown in Figure A-1 from Faust (2008) specifies the linear associations in the frequency domain as the ratio of squares of cross spectral densities divided by the products of two-auto spectra as presented in Equation A-8. If the amplitude of a certain frequency band is identical in both signals, a coherence score of 1 is

[4] Wear, K., Wagner, R. and Garra, B. (1995). A comparison of autoregressive spectral estimation algorithms and order determination methods in ultrasonic tissue characterization. *Ultrasonics, Ferroelectrics and Frequency Control, IEEE Transactions on*, 42(4), pp.709--716.

measured while a score of 0 is measured when for frequency bands are absent from either the two signals. Coherence function is widely applied in biomedical signal analysis for EEG, agood review on the use of coherence in the applications of coherence for Neurology, Cardiology and Gynecology can be found in Golinski (2011)[5]

$$C_{xy}(w) = \frac{P_{xy}(w)}{\sqrt{P_{xx}(w)P_{yy}(w)}} \qquad \text{Eq. (A-8)}$$

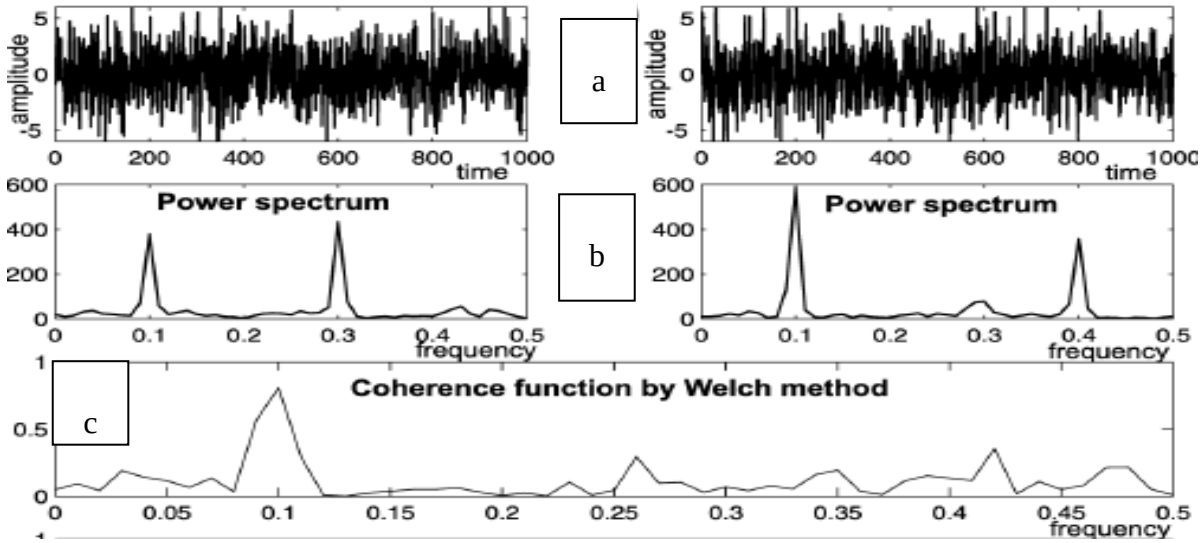

Figure A-1: Application of Spectral Coherence for two EEG signals; (a) time waveform of two signals, (b) power spectrum, (c) welch method coherence Golinski (2011)

[5] Goli\'nska, A. (2011). Coherence function in biomedical signal processing: a short review of applications in Neurology, Cardiology and Gynecology. *Studies in Logic, Grammar and Rhetoric*, 25.

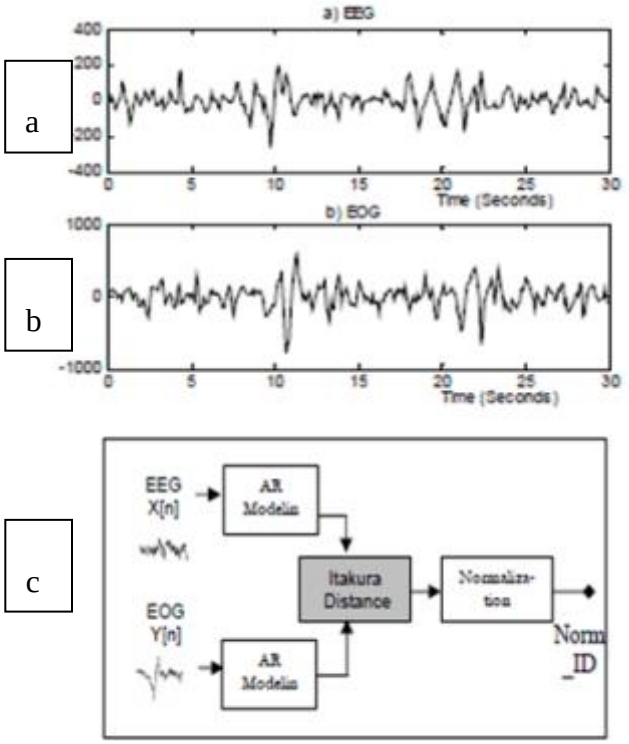

Figure A-2: Similarity Measurement between (a) EEG and (b) EOG Using Itakura Distance Approach (c)

The spectral content of two signals can also be compared indirectly by calculating the distance between the AR vectors determined during the spectral estimation step. Itakura Distance (ID) is a widely used speech-processing tool that measures the distance between sets of Linear Predictor Coefficients (LPC). Recently, ID has been adopted in the biomedical processing domain as an important feature for sleep classification approaches. Moreover, pilot studies such as the one reviewed in Estarda (2006)[6] utilised the ID as measure of similarity between EEG and EOG and at different sleep stages. In their study, ID was used to confirm the observation that both the EEG and ECOG of healthy adults synchronize during the 4th stage of sleep with the aim of developing an automated sleep stage classifier for sleep studies. Their approach is shown in Figure A-2

[6] Estrada, E., Nazeran, H., Nava, P., Behbehani, K., Burk, J. and Lucas, E. (2006). Itakura Distance: A useful similarity measure between EEG and EOG signals in computer-aided classification of sleep stages. pp.1189--1192.

where AR models are determined for both signals and then the ID is used to determine the similarity between the two sets of LPCs.

For two linear predictor coefficient vectors a_x and a_y determined using an AR model, the optimality of the coefficients in modelling the process is measured using the mean square distance (MSE) from the actual process as in Equation A-9 with $R_x(p)$ and $R_y(p)$ representing the autocorrelation matrix for $x[n]$ and $y[n]$, respectively. Then the ID for the two signals $x[n]$ and $y[n]$ is the average of $d_{I_{x,y}}$ and $d_{y,x}$ shown in Equation A-10.

$$MSE_{x.x} = a_x^T R_x(p) a_x \quad with \quad R_x(p) = E\{x[n]x[n]^H\}$$

$$MSE_{x.y} = a_y^T R_x(p) a_y \quad with \quad R_y(p) = E\{y[n]y[n]^H\} \qquad \text{Eq. (A-9)}$$

$$d_{I_{y,x}} = \log\left(\frac{MSE_{x,y}}{MSE_{x,x}}\right) = \log\left(\frac{a_y^T R_x(p) a_y}{a_x R_x(p) a_x}\right)$$

$$d_{I_{x,y}} = \log\left(\frac{MSE_{y,x}}{MSE_{y,y}}\right) = \log\left(\frac{a_x^T R_y(p) a_x}{a_y R_y(p) a_y}\right) \qquad \text{Eq. (A-10)}$$

Temporal Techniques

In addition to frequency techniques, signal similarity can also be assessed in the time domain and depending on the complexity of the signals to be compared, temporal techniques can range from simple time waveform subtraction, to more advanced methods comparing the entropy of the signals analysed.

A common technique to compare two time waveforms is the use of a linear inner product operation such as cross-correlation. For instance consider r_{12} in Equation A-11 representing the simple correlation between two time series x_1 and x_2. Intuitively, if both time series are pure noise with equal probability of having positive or negative values, it would be expected that the summation in Equation A-11 will include positive and negative numbers that would cancel out (on average) and thus a low r_{12} would be calculated confirming the low correlation between the two random noise signals. On the other hand, if the two signals are identical, the summation in the r_{12} equation will result in a high correlation coefficient. Even though the division by *N* in Equation A-8 serves to prevent the r_{12} from growing due to signal length, it would be advantageous to modify the simple cross-correlation with a standardizing factor to get values between (-1) and (1). This is achieved in the normalized cross-correlation presented in Equation A-12 adapted from Lyon (2010)[7].

$$r_{12} = \frac{1}{N}\sum_{n=0}^{N-1} x_1[n]x_2[n] \qquad \text{Eq. (3-11)}$$

$$r_n = \frac{\sum_i [x[i]-\bar{x})\cdot(y_1[i-d]-\bar{y})]}{\sqrt{\sum_i (x[i]-\bar{x})^2}\cdot\sqrt{(y_1[i-d]-\bar{y})^2}} \qquad \text{Eq. (3-12)}$$

Normalized cross-correlation is typically used template matching for the detection of abnormalities in EEG signals. Assuming that a representative time segment exists for the abnormality investigated, normalized cross-correlation is used to detect the presence of the known abnormality in the EEG waveform such as presented in Rangayyan, R. (2002).

[7] Lyon, D. (2010). The discrete Fourier transform, part 6: Cross-correlation, *Journal of object technology, 9,* pp.1--6

Despite the wide application of the correlation function as presented in the previous paragraph, correlation is still a linear function, and as such cannot detect the non-linear interdependencies between the underlying dynamic systems generating the signals under observation. In his paper Xu (2008)[8] suggested a new nonlinear similarity measure for multichannel biological signals; the Correntropy coefficient. This new method characterizes the interdependencies between two systems by using a nonlinear transform to map the process under observation into a reproducing kernel Hilbert space (RKHS). In this higher dimensional RKHS, cross-correlation is performed generating a similarity metrics called correntropy coefficient. In addition to being a non-linear operation, the correntropy coefficient produced by this method is directional, where a coefficient of 1 indicates identical signals and -1 indicates opposite signals.

According to the same paper, the novel crosscorrentropy approach outperformed the conventional correlation methods in EEG synchronization detection due to its sensitivity and ability to extract more information. The generalized crosscorrentropy is presented in Equation A-13 with $\mathcal{K}(\cdot,\cdot)$ representing a symmetric positive definite kernel function. Xu *et al.* used the Gaussian kernel presented in Equation A-14 with σ representing kernel width. Substituting Equation A-14 into Equation A-13, the centred crosscorrentropy is calculated using Equation A-15. Finally, the crosscorrentropy coefficients are calculated by normalizing the centred crosscorrentropy as shown in Equation A-16 with $U(x,x)$ and $U(y,y)$ representing the centred autocorrentropy.

[8] Xu, J., Bakardjian, H., Cichocki, A. and Principe, J. (2008). A new nonlinear similarity measure for multichannel signals. *Neural Networks*, 21(2), pp.222--231

$$V(x,y) = E[\mathcal{K}(x,y)] \quad \text{Eq. (A-13)}$$

$$\mathcal{K}(x,y) = \frac{1}{\sqrt{2\pi}\sigma} exp\left\{-\frac{(x-y)^2}{2\sigma^2}\right\} \quad \text{Eq. (A-14)}$$

$$U(x,y) = E[\mathcal{K}(x,y)] - E_x E_y[\mathcal{K}(x,y)] \quad \text{Eq. (A-15)}$$

$$\eta = \frac{U(x,y)}{\sqrt{U(x,x)U(y,y)}} \quad \text{Eq. (A-16)}$$

Application of Spectral Comparison Techniques

The application of the different similarity measurements discussed in the previous subsection will be presented here using MATLAB™ environment. First, the following two signals were generated to test the different comparison methods:

$$x(t) = \sin(2\pi(20)t) + \sin(2\pi(50)t) + \sin(2\pi(65)t) + \varepsilon(t) \quad \text{Eq. (A-17)}$$

$$y(t) = \sin(2\pi(10)t) + 2\sin(2\pi(50)t) + \sin(2\pi(90)t) + \varepsilon(t) \quad \text{Eq. (A-18)}$$

As it can be seen, the two signals share a common frequency at 50 Hz buried in white noise $\varepsilon(t)$. The task of the comparison methods previously discussed is to present a measure of how similar the two signals are, and show the common frequency. First, non-parametric spectral estimation using the regular periodogram will be compared against the one obtained using the Welch method. Next, the modified Covariance method will be used as an example of parametric spectral estimation.

Spectral estimation: periodogram and Welch method

At a sample rate of 1000 Hz and 4096 frequency lines, the periodogram of both signals $x(t)$ and $y(t)$ are presented in Figure A-3. The periodogram was able to detect the characteristic frequencies for both signals. However, as discussed previoulsy, the periodogram suffers from high variance given that the rectangular window used is transformed into a Sinc function in the frequency domain. To overcome this variance, the Welch method is used for spectral estimation where the use of an averaging algorithm reduces the variance significantly in Figure A-4.

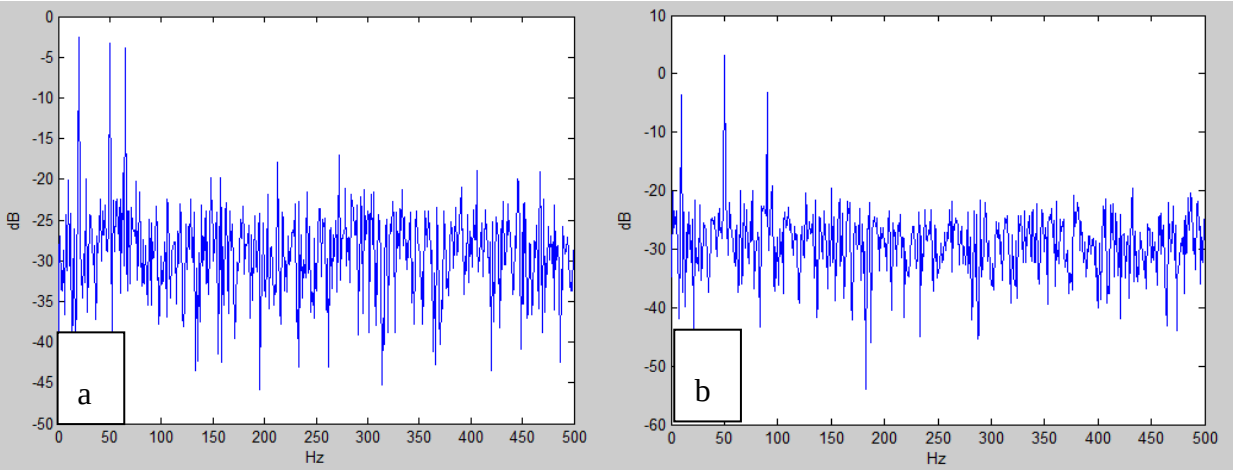

Figure A-3: Periodogram for Signals (a) $x(t)$ and (b) $y(t)$

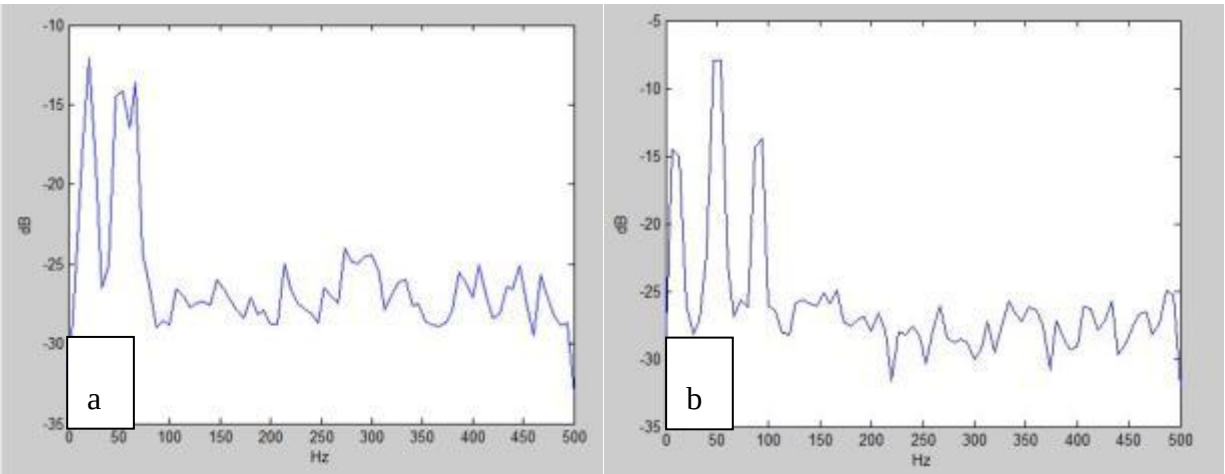

Figure A-4: Welch periodogram for Signals (a) $x(t)$ and (b) $y(t)$

As discussed earlier, spectral estimation can also be done using parametric methods. The method involves the use of an AR algorithm to model the process generating the signal. The main advantage of the use of this parametric method is that it reduces the high dimensionality of the signal; especially for signals processed at a high sampling rate, to a more concise feature represented by an AR model of order p. The modified covariance method was used to generate the spectral estimates presented in Figure A-5

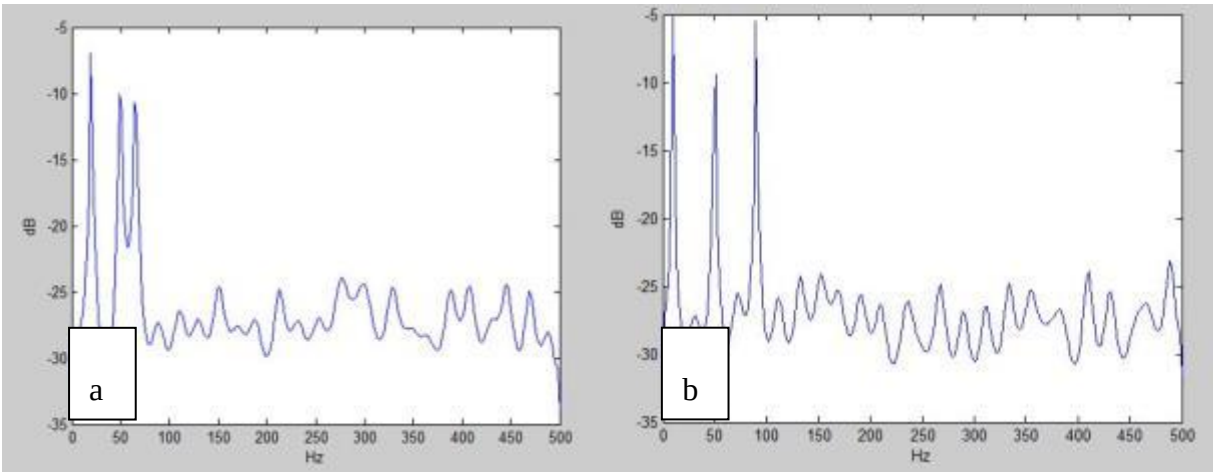

Figure A-5: Modified Covariance Spectrum for Signals (a) $x(t)$ and (b) $y(t)$

Spectral comparison: Coherence and Itakura distance

Now that the spectral contents have been estimated for the two signals considered, the task of determining the similarity between the two spectra can be accomplished using spectral comparison. The coherence function discussed previously can be used to determine the common frequencies between two spectrums as shown in Figure A-6. In the standardized form, the coherence for each frequency band is a ratio between 0 and 1. As shown in the figure, a coherence of 1 was observed for the 50 Hz frequency common to both signals.

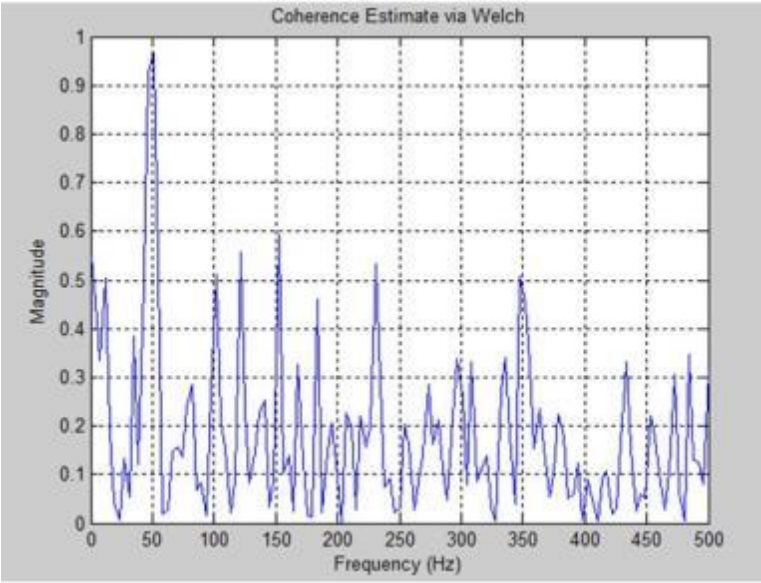

Figure A-6: Spectral Coherence for Signals $x(t)$ and $y(t)$

A different way to compare the spectral estimates of the signal is to measure the distance between the LPC used to in the parametric spectral estimation discussed previously. Using the Itakura distance measure, the similarity between the spectral content of two waveforms can be estimated. Consider Figures A-7 and A-8 representing recorded sentences “way in” and “way out”, respectively. Intuitively, given that the two sentences share the common word ‘way’, the

Itakura distance of this part of the sentence should be small compared to the second part of the sentences. Using MATLAB™, the two waveforms were recorded at a rate of 7418Hz for 0.53 seconds each. Each signal then is segmented into 10 windows of 400 points and the ID calculated for each window. As shown in Figure A-9, the ID is initially between zero and 0.5 for the two segments before the words are uttered and increases slightly to 0.6 when the word "way" is said in both signals; segment number three. Now the rest of the segments where the words "in" and "out" are said, the ID distance grow as expected.

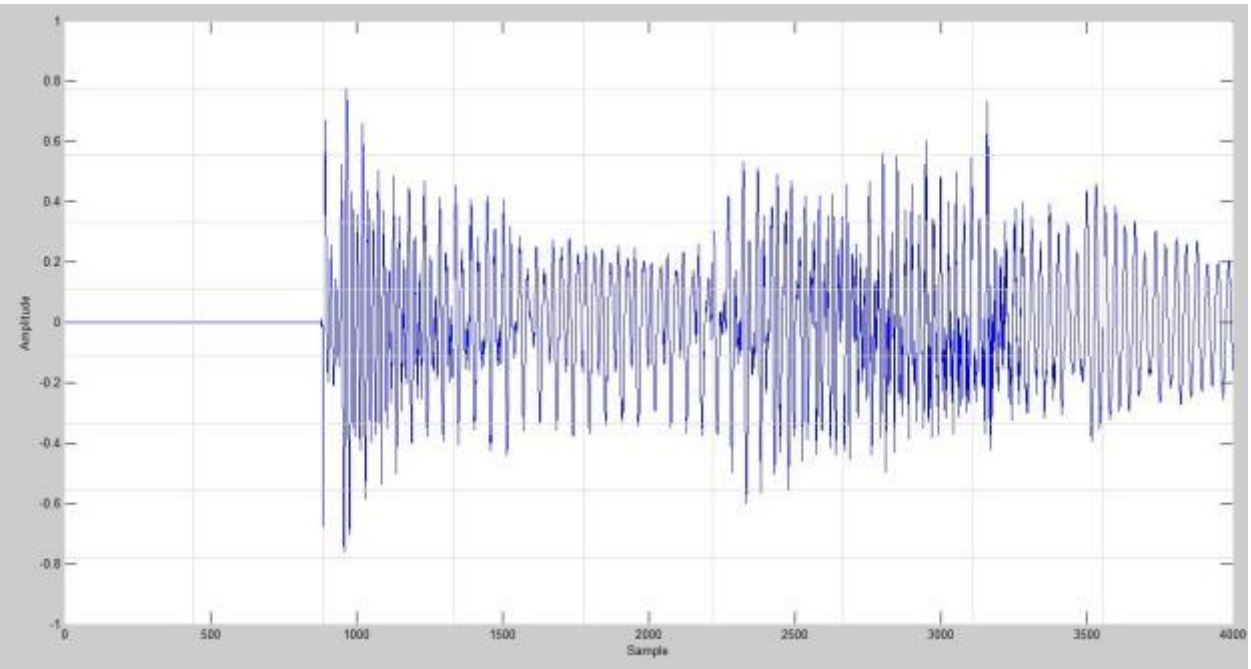

Figure A-7: Recorded Waveform for "Way In"

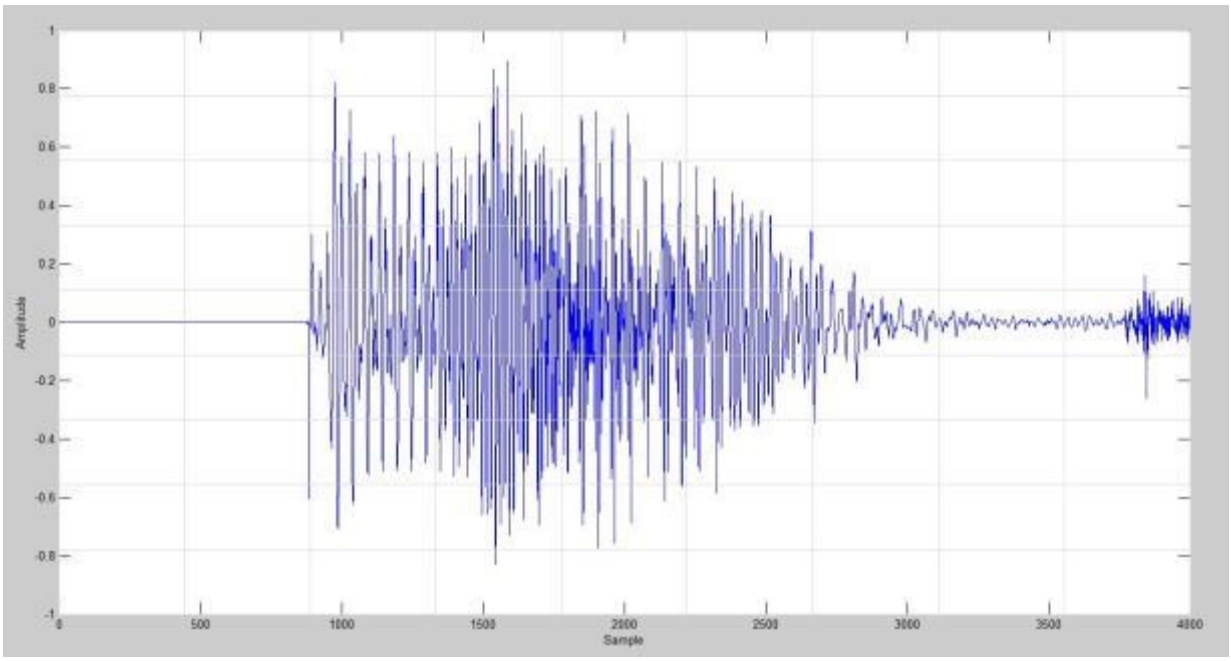

Figure A-8: Recorded Waveform for “Way Out”

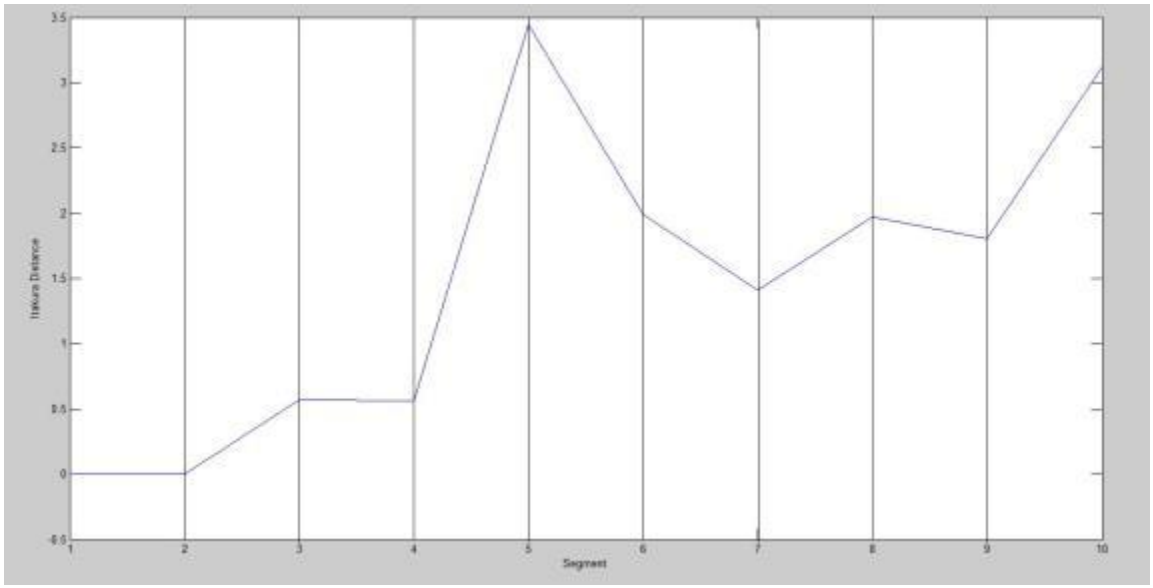

Figure A-9: Itakura Distance